

Tissue Structure Analysis in Urological Dysfunctions

Bas de Jong

ISBN 978-90-9022917-1

The studies described in this thesis were done at the sector Pediatric Urology, the sector Experimental Urology and the sector Physics of the Urinary Tract of the department of Urology and the sector Raman spectroscopy of the Center of Optical Diagnostics and Therapy of the department of Dermatology, Erasmus MC.

Financial support was obtained from the Dutch Kidney Foundation (NSN) and the Stichting Urologisch Wetenschappelijk Onderzoek.

Publication of this thesis was financially supported by the Dutch Kidney Foundation (NSN), the Stichting Urologisch Wetenschappelijk Onderzoek and the Erasmus Universiteit Rotterdam.

Cover: 'Harry' by Margriet Steenbergen, 2008 (acrylic painting on linen).

Cover photography: Frans van den Brink.

Layout: Bas de Jong.

Printed by PrintPartners Ipskamp, Enschede.

© 2008 B.W.D. de Jong

No part of this thesis may be reproduced, stored in a retrieval system or transmitted in any form or by any means, electronical, mechanical, photocopying, recording or otherwise, without written permission of the author. Several chapters are based on published papers. Copyright of these papers remains with the publisher.

Tissue Structure Analysis in Urological Dysfunctions

Weefselstructuur analyse in urologische dysfuncties

Proefschrift

ter verkrijging van de graad van doctor aan de
Erasmus Universiteit Rotterdam
op gezag van de
rector magnificus

Prof.dr. S.W.J. Lamberts

en volgens besluit van het College voor Promoties.
De openbare verdediging zal plaatsvinden op

woensdag 7 mei 2008 om 11.45 uur

door

Bas Willem Dirk de Jong

geboren te 's Hertogenbosch



Promotiecommissie

Promotor: Prof.dr.ir. R. van Mastrigt

Overige leden: Prof.dr.ir. A.F.W. van der Steen
Prof.dr. R.J.M. Nijman
Prof.dr. T.H. van der Kwast

Copromotoren: Dr. D.J. Kok
Dr.ir. G.J. Puppels

**SMILES HAVE
BOOMERANG EFFECT**

Loesje

P.O.-BOX 1045 6801 BA ARNHEM HOLLAND

Voor mijn ouders en zus

Contents

	List of abbreviations	9
Chapter 1	Introduction	11
Chapter 2	Detrusor glycogen reflects the functional history of bladders with partial outlet obstruction	31
Chapter 3	The detrusor glycogen content of a de-obstructed bladder reflects the functional history of that bladder during PBOO	45
Chapter 4	The effect of Oxybutynin on structural changes of the obstructed guinea pig bladder	59
Chapter 5	Prevention of obstruction induced bladder damage by Acetylsalicylic acid	71
Chapter 6	Ischemia in the bladder upon PBOO: the role of voiding pressure, contractility, detrusor overactivity and compliance	83
Chapter 7	Identification of bladder wall layers by Raman spectroscopy	97
Chapter 8	Raman spectroscopic detection of changes in molecular composition of bladder muscle tissue caused by outlet obstruction	113
Chapter 9	Discrimination between nontumor bladder tissue and tumor by Raman spectroscopy	125
Chapter 10	General discussion	143
Chapter 11	Summary	153
	Samenvatting	
	Dankwoord	
	Curriculum Vitae	
	List of publications	
Appendix		172

List of abbreviations

BPE	Benign Prostatic Enlargement
PUV	Posterior Urethral Valves
IPSS	International Prostate Symptom Score
CIC	Clean intermittent catheterisation
PBOO	Partial Bladder Outlet Obstruction
VUDS	Video Urodynamic Study
BOO	Bladder Outlet Obstruction
SEM	Scanning Electron Microscopy
	Standard Error of the Mean
PAS	Periodic Acid Schiff's stain
IR	Infrared
AU	Arbitrary Units
CCD	Charged Coupled Device camera
S/N	Signal-to-Noise ratio
NUC	Number of Unstable Contractions
SD	Standard Deviation
TGF- β	Transforming Growth Factor beta
DO	Detrusor Overactivity
EVG	Elastic Von Gieson stain
ASA	Acetylsalicylic Acid (aspirin)
GS	Glycogen Score
ATO	Aspirin Treated and Obstructed animal
OTO	Oxybutynin Treated and Obstructed animal
NNLS	Non-Negative Least Squares fit procedure
KMC	K-means Clustering
PC	Principal Component
PCA	Principal Component Analysis
HCA	Hierarchical Cluster Analysis
LDA	Linear Discriminant Analysis
CAS	Cluster Averaged Spectrum
CIS	Carcinoma In Situ
CT	Computed Tomography
MRI	Magnetic Resonance Imaging
ROC	Receiver Operator Characteristics curve
WHO/ISUP	World Health Organisation / International Society of Urological Pathology
HE	Haematoxylin Eosin stain



Introduction

Chapter

1

Urinary bladder function and dysfunction

The urinary bladder serves as storage for the urine that is continuously produced in the kidneys. A well-functioning bladder can store urine by elastic expansion. The bladder registers when the maximum filling capacity is reached and sends this information to the pontine miction centre in the brain stem [1]. Here the decision is made whether emptying the bladder at that time is appropriate. If so, this center sends signals to relax the sphincter, which opens up the bladder outlet (urethra), and to contract the bladder muscle (detrusor), which forces the urine out of the bladder. Adult men and women urinate on average 4 – 7 times a day. For most of us urination is intuitive. For an increasing number of people, however, urination becomes an everyday, and even painful, problem as a consequence of inadequate bladder function. In adults examples of causes of improper bladder function are trauma (spinal cord injury), bladder cancer, low bladder contractility and (only in men) Benign Prostatic Enlargement (BPE). In children improper bladder function is related to an improper sphincter relaxation due to congenital (spina bifida) or acquired spinal cord lesions and to obstruction of the urine flow by Posterior Urethral Valves (PUV).

Loss of bladder function

Problems with bladder emptying are often related to increased urethral resistance. The cause of the increased urethral resistance can be structural or functional. In structural obstruction such as BPE, the urethra may be compressed by the surrounding prostate mass. Boys can be born with structures inside the urethra, urethral valves, which have failed to disappear during fetal development and partially obstruct the internal urethra. In general, functional obstruction is the result of acquired or inborn damage to the nerves that transmit signals between the bladder, urethra and pontine miction centre. In a later stage psychological factors may also play a role. As a result the co-operation between opening of the urethra and contraction of the bladder is disturbed and the bladder has to empty through a partially closed urethra. Irrespective of the cause of obstruction, the result is that the pressure inside the bladder during voiding is abnormally high and that the bladder muscle must work harder to produce this pressure. Recurring episodes of higher pressure may progressively damage the bladder tissue. Furthermore at some point the pressure may reach a level where urine flows back from the bladder to the kidney (reflux) [2]. This can ultimately damage the kidney, directly by exposure to high pressure and indirectly by increasing the risk of renal infection because the normal defence mechanism of the ureteral lining is by-passed [3]. In the days when treatment options for pediatric patients with outlet obstruction were scarce or facilities for

proper treatment were limited, the worst-case scenario of complete kidney failure was not uncommon [4] (figure 1).

In response to both the damage and the requirement of more force production the bladder changes in structure. It is strengthened to withstand the higher pressures and the muscle mass increases. Unfortunately, although these changes may serve the purpose of ensuring good bladder emptying, they negatively effect the elastic properties of the bladder and thereby its storage function.

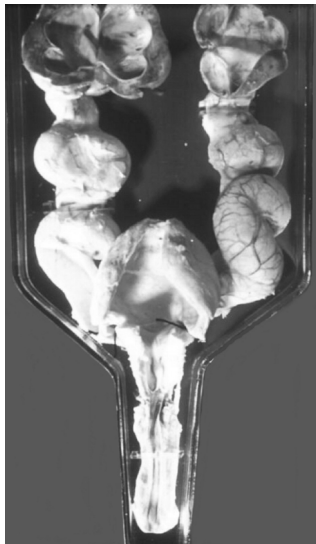


Figure 1

The urological system of a patient suffering from partial obstruction. Note the large calyces in the kidneys and the widened ureters as a consequence of reflux and a thick bladder wall layer.

Overall, urethral obstruction causes the bladder to migrate from elastic tissue and low voiding pressure to thickened in-elastic tissue and high voiding pressure. A major challenge in the treatment of these patients is to establish the condition of the bladder, to maintain it and to preferably restore function and structure.

Diagnosis of bladder dysfunction

In BPE patients, bladder dysfunction is assessed from specific symptoms using the international prostate symptom score (IPSS) questionnaire [5], followed by urodynamic measurements. The presence of bladder dysfunction may indicate acquired or congenital spinal nerve damage (spina bifida). In unborn children with outlet obstruction bladder dysfunction is in most cases revealed by widened ureters, observed with prenatal echography [6]. Intervention by cystoscopic valve ablation is then performed early after birth. Especially in children, quick and appropriate treatment is of importance because the bladder is still developing.

Urodynamic measurements are used to determine the initial severity of bladder dysfunction and during follow-up (see next section). These diagnostic modalities used in conjunction with medicines that relax the bladder muscle (anticholinergics) and the application of clean intermittent catheterisation (CIC) are in general the treatment of

choice in pediatric patients. In spina bifida and PUV patients this approach has significantly increased the success of maintaining bladder and kidney function.

Unfortunately, a permanent loss of bladder and kidney function still occurs in some patients. There may be several causes for this. The main cause is the problem of irreversible bladder structural damage. Even when an obstruction is removed, the changes in structure are so severe that the bladder is now fighting against its own incapability to extend upon filling and to properly empty upon voiding. Bladder function will only deteriorate further until the bladder has become no more than a complete non-compliant bag mainly consisting of collagen. But before this end-stage scenario is reached the kidneys may very likely be damaged as well because of reflux. Because there is still a poor insight in the relation between functional and structural changes in the bladder upon partial bladder outlet obstruction (PBOO), it is not (yet) possible to determine a definite point of damage becoming irreversible in both functional and structural analysis. This emphasizes the need for accurate treatment. Furthermore, specifically in PUV patients it is a problem to correctly diagnose the onset of bladder dysfunction. Urodynamic measurements cannot be done prenatally. In addition, immediately after birth the urine flow is diverted through a catheter, which bypasses the bladder function. This catheter is kept in place until some time after the valves have been removed. Thus, at present there is no insight into the severity of changes in function of these bladders during the obstructive period. The first urodynamic measurement, which serves as the reference point for future changes in bladder function, is usually obtained some time after the valve ablation. Also in patients with functional obstruction caused by e.g. spina bifida, permanent loss of bladder function and kidney function still occurs. The current approach is therefore inadequate.

In summary the problem is twofold: the follow-up methods used do not timely register changes in bladder function and the exact mechanism of bladder function deterioration is not completely clear. For these reasons possibly current treatment may not be targeted correctly.

Urodynamic measurements

The variables most often used in pediatric urodynamic measurements are bladder pressure and urine flow rate. Monitoring these variables may reveal higher pressures than normal, urine flow rate changes and involuntary detrusor contractions (detrusor overactivity). Bladder residue after urination is measured by echography. After calculations using pressure and flow rate data as input, the compliance and contractility can be obtained. Compliance is a variable that gives insight into the elasticity of the bladder wall. The more compliant, the easier for the bladder it is to expand during filling, thus pressure remains low. In clinical practice compliance is

determined mostly quantitative as 'good' or 'bad' according to the shape of the pressure/volume relation. Quantitative calculations for compliance are seldom performed. Contractility quantifies the ability of the bladder to contract. Force is one aspect of contractility, the other one is contraction velocity. An outflow obstruction may suppress this velocity while force is high. Contractility is rarely used in clinical decisions, as its relevance in the diagnosis of obstructive bladder disease is not yet clear.

Video urodynamic studies (VUDS) in young children mostly include pressure and flow rate data. Upon instillation of contrast agents, X-ray diffraction video-images of the whole urinary tract give insight into sites of obstruction (figure 2). The majority of

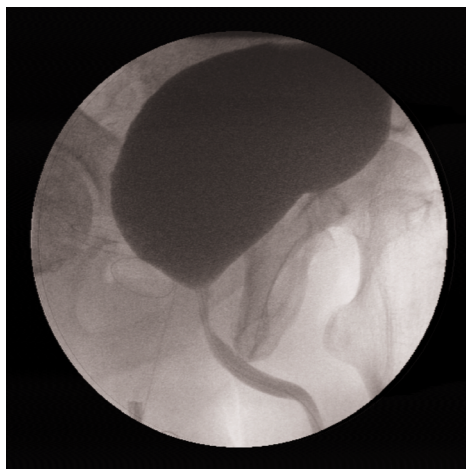


Figure 2

X-ray image of a video urodynamic study using a contrast agent. The dark spot in the upper half is the bladder, the urethra with a clearly visible catheter goes down from the bladder.

VUDS are performed in patients with spina bifida, chronic inflammatory urinary tracts and with suspicion of reflux and obstruction. VUDS is often used in follow-up studies to monitor bladder function during and some time after treatment of the disease. All in all these diagnostic modalities can give a good assessment of bladder function at a specific time point. This has greatly improved the follow-up of patients with obstructive bladder disease. Unfortunately they do not tell what happened to the bladder before the time of assessment. The question, what route of deterioration did the bladder follow, remains unanswered. In addition they give no direct insight into the structural changes in the bladder wall. The course of the changes may be guessed from changes between the first time point and repeat measurements. Indirect conclusions about changes in bladder structure might be drawn from changes in bladder compliance. For instance, a loss in compliance could point to thickening of the bladder wall. There remains a desire to gain more insight into what happened to a bladder before the first time it was studied.

Our working hypothesis is that at any given time the bladder structure will reveal adaptation to the urodynamic history. Structural analysis of the bladder wall may be the key factor that could provide insight into this history. To test this hypothesis and to enable the use of structural analysis for determining historic bladder function we need to examine tissue from bladders of which the complete urodynamic

development is known at multiple time points from the start of bladder outlet obstruction (BOO) up to the point that structural analysis is performed. Since such data are not available clinically, we used an animal model for partial BOO.

Urodynamic model

Of all rodents, the anatomy and nervous system of the guinea pig bladder most resemble those of the human bladder [7]. Hence the choice of this animal for the PBOO model, besides the fact that the guinea pig is easy to handle in terms of size and character. This model was developed to perform single urodynamic measurements with pressure monitoring [8]. Later, this model was adapted to include also flow rate measurements and to allow for repeat measurements in each animal. The developments and findings of this evolved model are described in detail in previous work [9,10]. Here, this model and the urodynamic measurements are explained briefly.

A PBOO was created in immature guinea pigs (approximately 300 grams) by surgically placing a silver jeweller's ring (inner diameter 2.2 mm) loosely around the urethra. The presence of this ring caused fibrosis on the outer side that partially compressed the inner side of the urethra.

The PBOO model allowed for controlled filling of the bladder and continuous monitoring of bladder pressure and urine flow rate. Animals were anaesthetized and the bladder was filled with sterile saline through a suprapubic catheter. Via this catheter bladder pressure was also measured. The urine flow rate was measured simultaneously with an ultrasound transducer around the penis as shown in figure 3. During measurement, pressure and flow rate were monitored continuously, so that unstable contractions could be observed and compliance and contractility could be calculated.

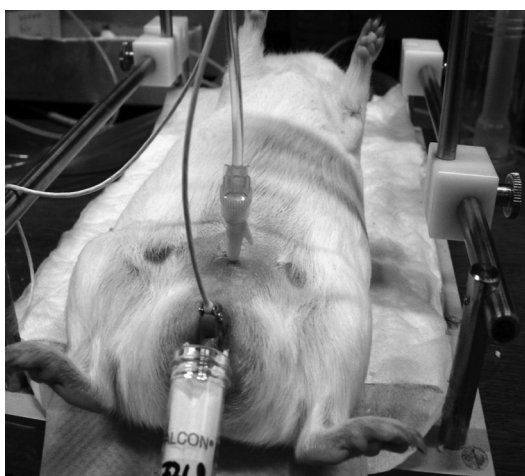
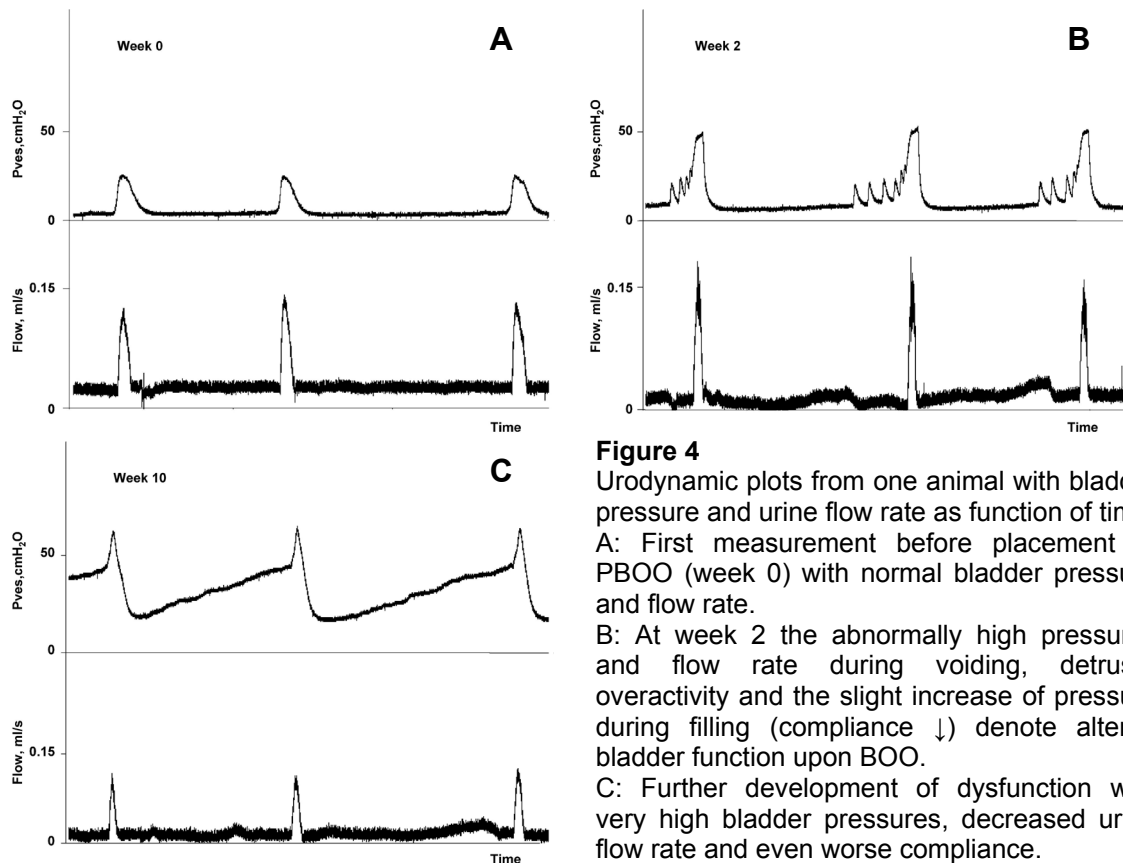


Figure 3

A urodynamic measurement in a sedated guinea pig. The catheter enables filling of the bladder with saline and measuring of intra-vesical pressure simultaneously. Around the penis is a very sensitive ultrasound flow probe to measure urine flow rate upon voiding.

**Figure 4**

Urodynamic plots from one animal with bladder pressure and urine flow rate as function of time. A: First measurement before placement of PBOO (week 0) with normal bladder pressure and flow rate.

B: At week 2 the abnormally high pressures and flow rate during voiding, detrusor overactivity and the slight increase of pressure during filling (compliance ↓) denote altered bladder function upon BOO.

C: Further development of dysfunction with very high bladder pressures, decreased urine flow rate and even worse compliance.

Just before the induction of PBOO, all animals were urodynamically measured for the first time (week 0). After PBOO, each animal was urodynamically measured once a week, thereby creating an individual time series of urodynamic measurements that reflected the development of bladder dysfunction. Figure 4 shows examples of urodynamic measurements in one animal just before placement of PBOO, at 2 weeks and at 10 weeks of obstruction. Directly after the last urodynamic measurement the animals were sacrificed and tissue was harvested to perform structural analysis by histochemistry. To study multiple stages in urodynamic changes correlated with structural changes, animals were sacrificed after different times of exposure to PBOO, ranging from 2 to 11 weeks. An important finding was that functional and structural changes did not develop synchronously. Therefore a correlation between function and structure but not between duration of obstruction and structural changes was found. The model also allowed for monitoring the course of bladder function changes after removal of the obstruction. At different degrees of bladder dysfunction the silver ring was surgically removed and urodynamic measurements were conducted for several weeks. By observing if the bladder would further deteriorate or regain normal function, we determined at which level of dysfunction the structural damage would become irreversible.

Medical intervention is presently used in the clinic to suppress detrusor overactivity. We studied if medical intervention could also prevent deterioration of bladder

function and structure upon BOO. Orally administered oxybutynin and aspirin in our animal model were tested for their effects on function and structure.

The bladder

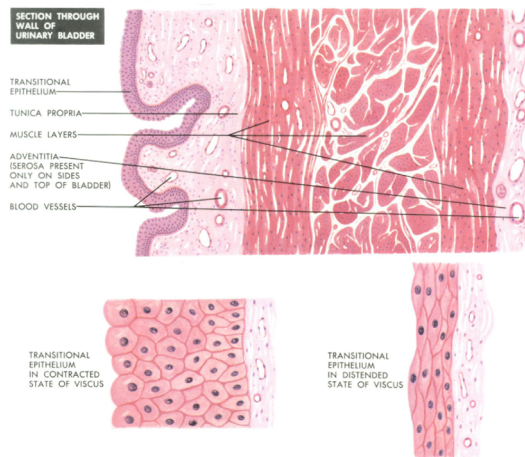


Figure 5

A schematic cross section of the bladder wall showing the different layers: transitional epithelium (better known as urothelium), tunica (lamina) propria, the three muscle layers (detrusor) and the adventitium.

The human bladder consists of three main layers, from the lumen outwards: The urothelium, the lamina propria and the detrusor muscle (Figure 5). The outside of the bladder is covered with a thin layer of connective tissue, called the serosa, which holds some blood vessels. The urothelium in both humans and guinea pigs consists of 5 to 7 cell layers. At the basement membrane, which lies between the urothelium and the lamina propria and largely consists of collagen type IV, the undifferentiated basal

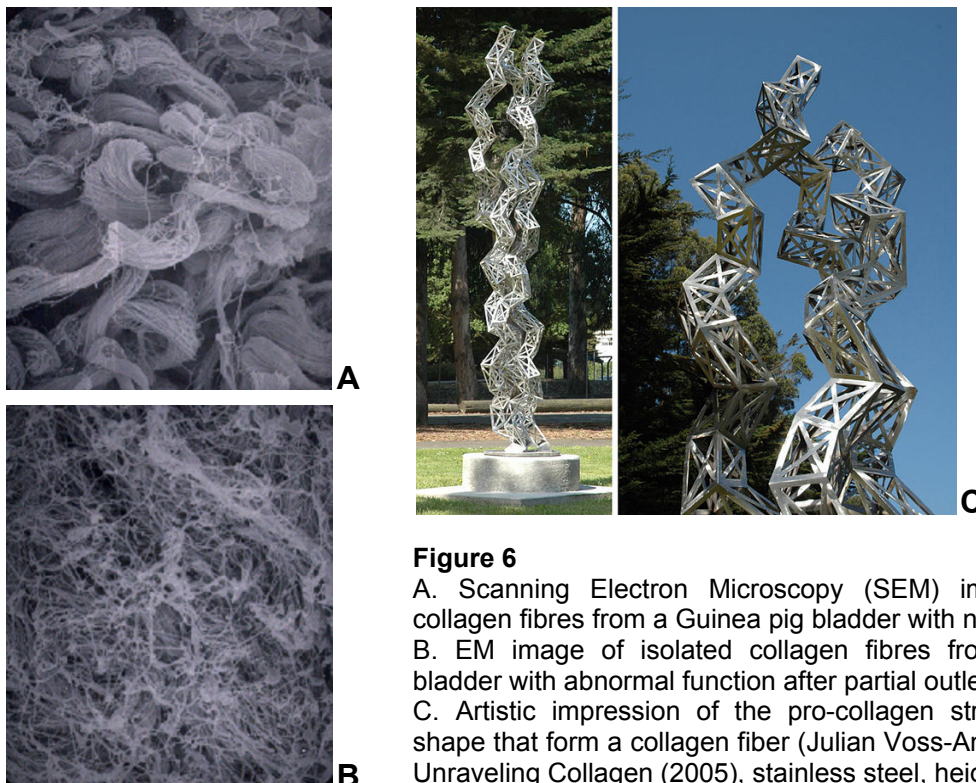


Figure 6

A. Scanning Electron Microscopy (SEM) image of isolated collagen fibres from a Guinea pig bladder with normal function.
 B. EM image of isolated collagen fibres from a Guinea pig bladder with abnormal function after partial outlet obstruction.
 C. Artistic impression of the pro-collagen strings in a helical shape that form a collagen fiber (Julian Voss-Andreae's sculpture *Unraveling Collagen* (2005), stainless steel, height 3.40 m).

urothelium cells are located. At the luminal side the urothelium is covered by large umbrella cells that form the barrier between the bladder tissue and urine. Urothelium cells are strongly distended when the bladder is filled. The lamina propria mainly consists of thick collagen fibres of types I and III. They have a helical form to allow for large distension (figure 6a&b). Furthermore, this layer accommodates the main blood vessels and nervous fibres that branch off to all areas of the bladder. The detrusor layer is built up from three sub-layers of smooth muscle: two layers with longitudinally arranged muscle fibres and in between these a layer with circularly arranged muscle fibres, though it often is difficult to clearly distinguish these layers. Blood vessels for oxygen supply and collagen fibres that provide strength are located in between the muscle fibres throughout the bladder.

Upon PBOO, various changes in bladder wall structure occur that have been described in many studies. These changes include extra- and intra-muscle fibre collagen deposition [11, 12], changes in the ratio of collagen types I/III [13, 14], changes in myosin subtypes SM1/SM2 within muscle cells [15,16,17], changes in neuronal control of the bladder [18-20], changes in vascular density [21-23] and several molecular changes involving membrane and cytoskeleton proteins, ion channels, growth factors, enzyme activity and mitochondrial function [24-26]. In this thesis the role of total collagen deposition and invasion of collagen into the muscle layer correlated to loss of bladder function is briefly addressed.

A second focus is put on the possible role of ischemia in the bladder wall as a mediator between the mechanical changes, high bladder pressure and low compliance, and damage to the bladder structure. It has been shown that ischemia may already occur when blood flow is (partially) blocked. In a normal bladder blood flow decreases transiently when the bladder pressure increases during voiding. In a low compliant bladder the arteries are compressed already by increased pressure during the filling phase [27]. The reduction in blood flow means a reduction in supply of oxygen. As the muscle cells exert force they will deplete the available oxygen and subsequently must resort to anaerobic action. This anaerobic action requires an alternative energy source, glycogen. With frequent recurrence of ischemic periods,

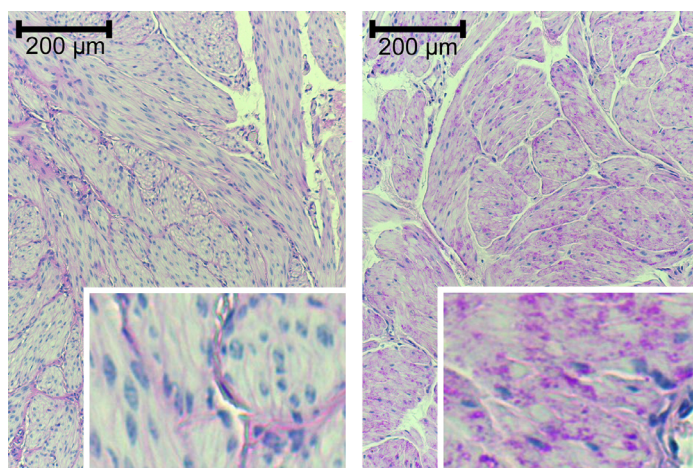


Figure 7

Left: PAS stain of bladder tissue without glycogen granules (score 0), note the light magenta staining of membranes. Right: PAS stain of bladder tissue with glycogen granules stained as dark magenta spots all over the detrusor (score 3), more clearly seen in the enlargements (5x) of the image in the right bottom corner.

both during filling and urination, the bladder adapts to this by accumulation of intracellular glycogen granule deposits. In the presence of such glycogen deposits, ischemic damage to nerve fibres seems to be reduced [28]. These glycogen granules are clearly visible in standard histochemical stains such as the periodic acid Schiff's (PAS) stain (figure 7). Analysing glycogen content in bladder wall tissue with a history of PBOO will therefore be a useful tool for the determination of ischemic conditions.

Determination of bladder structural changes

The question of course is; what is lacking? One feature that has not been included in the current approach to diagnosis and treatment is the role of changes in bladder structure. Even though these changes are mostly obvious, there is insufficient knowledge of the relationship between specific changes in bladder structure and specific changes in bladder function, the risk of further loss in bladder function or the potential for reversal of bladder deterioration. This lack of knowledge is also due to the lack of proper methods and models to study these relationships.

This thesis describes relationships between bladder structure and bladder function. In addition methods that may allow measurement of bladder structure *in vivo* in a non-destructive manner that would enable follow-up of changes in bladder structure are explored.

Relations between bladder function and bladder structure were studied by other groups using bladder material from an animal model in which obstruction was induced and removed and bladder function was followed weekly by urodynamic measurements (for details see 'Urodynamic measurements'). Their focus was put on changes that related to bladder elasticity, like collagen content, and changes that may be connected to mechanisms of tissue damage and markers of ischemia. In many studies morphological changes in the nervous system, muscle cells and collagen composition and deposition have been described [11-17,24,25,29-36]. More recent studies reveal a role of ischemia, either as initiator or as a consequence, in many of these structural changes [27,37-41]. The latter represent adaptations of the bladder to its time span of changes in function. Analysis of bladder structure therefore deserves a place in clinical practice. But to make this practical, two requirements must be met. As stated above the relation between bladder structure and bladder function must be clear. But in addition the clinical burden posed by analysing bladder structure must be outweighed by the potential benefit derived from the information obtained. At present the latter requirement is not met, as current analysis techniques require obtaining bladder tissue from biopsy samples.

With the ultimate goal of excluding the need for biopsies, we therefore explored the possibilities of Raman spectroscopy, a non-destructive optical technique to analyse the

biochemical composition of tissues. In this technique the tissue is illuminated with low-power monochromatic light and changes in colour of the scattered light are analysed. This can be done *in vitro* and *in vivo*. The details of this approach are explained hereafter. First it was determined if Raman spectroscopy could distinguish structural changes in bladder tissue based on biochemical information derived from the spectra. Then a study was performed on bladder tumor tissue, to further test the abilities of this technique. A significant advantage is that the technique requires no pre-treatment of the tissue. With the application of fibre optics this could enable *in vivo* biochemical analysis. This approach, however, is outside the scope of this thesis. The *in vitro* application proved its value as it revealed specific markers in the bladder wall that point to a role of ischemia in Bladder Outlet Obstruction (BOO). Since changes in bladder tissue structure reflect adaptation to a previous period of dysfunction we explored the specific role of bladder structure analysis to assess changes that occurred during a period that could not be monitored, e.g. prenatally. As mentioned earlier, ischemia caused by insufficient blood perfusion may occur at the very beginning of structural changes in the bladder upon BOO. Structural changes, for which the biochemical changes measured with Raman spectroscopy are markers, are secondary to this ischemia caused by reduced blood flow. Therefore the thesis ends with the recommendation to explore a technique that can monitor blood saturation *in vivo* using a minimally invasive and non-destructive technique during bladder filling and emptying.

Raman spectroscopy

The term 'Raman spectroscopy' is derived from its discoverer, the Indian physicist Chandrasekhara Venkata Raman (figure 8).



Figure 8
Chandrasekhara Venkata Raman (1888-1970)

Although Raman, together with co-worker K.S. Krishnan, was the first to demonstrate the principles behind this type of light scattering in 1928 [42], G.A. Smekal predicted the 'Raman' effect in 1923 on theoretical grounds [43]. Raman was awarded the Nobel

Prize for physics in 1930 for describing the Raman scattering. The complete story of achieving the Nobel prize was published by Singh et al. [44]. It was only a matter of time or this effect would have had another name since two other physicists, G.S. Landsberg and L.I. Mandelshtam [45], were also trying to prove Smekal's theory independently from Raman. They published their work just a few months later.

Technical background

The atoms in a molecule consist of an inner nucleus of protons and neutrons and one or more outer shells of electrons. The bonds between atoms allow them to vibrate and rotate within the molecule. Light can be interpreted as a wave pattern of almost weightless electromagnetic energy carriers, photons. When a light beam is incident on a sample, the photons interact with the molecules of that sample and are scattered. There are three types of scattering: elastic Raleigh scattering, and inelastic Stokes and anti-Stokes Raman scattering. With Raleigh scattering there is no transfer of energy from the photon to the molecules in the sample. The equilibrium vibrational level of

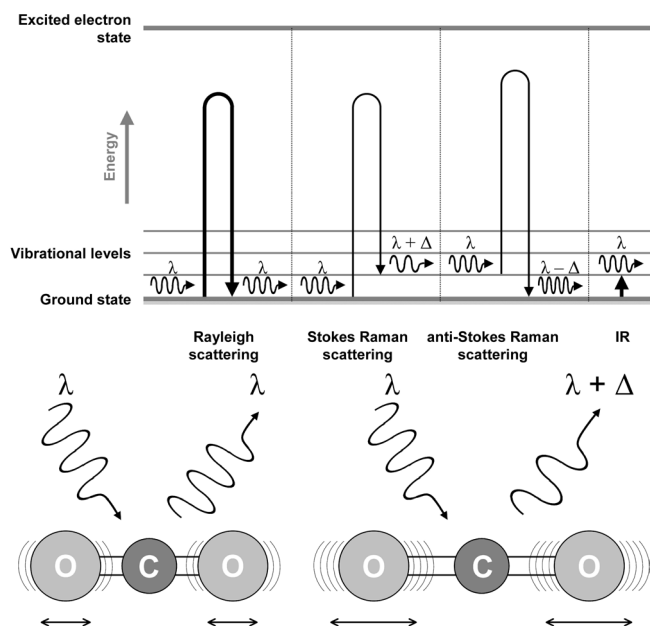


Figure 9

A. Energy diagrams of Raleigh scattering, Stokes Raman scattering, anti-Stokes Raman scattering and infrared (IR) absorption. λ is the wavelength of the incoming photon, $\lambda + \Delta$ is the increased wavelength due to reduction of energy, $\lambda - \Delta$ is the decreased wavelength due to input of energy.

B. Schematic representation of a CO₂ molecule that undergoes Raleigh scattering (left) and Stokes Raman scattering.

atoms in the molecule is unaffected and the scattered light has the same energy as the incoming light with the same wavelength (figure 9 a&b). Most scattering of light is Raleigh scattering; only 1 in 10⁶ to 1 in 10⁸ of the photons exhibit a change in energy. With Stokes Raman scattering a small part of the energy from the photon is transferred to the molecule and changes the vibrational level of the atoms. The energy of the scattered photon is reduced by the amount of energy received by the molecule, resulting in a lower frequency and thus a longer wavelength. Anti-Stokes Raman scattering is the opposite of Stokes Raman. Atoms in a molecule that are already in a higher vibrational level transfer energy to the photon, which is then scattered with a higher frequency, thus a shorter wavelength.

When using a monochromatic light source, the wavelengths shifts in Raman scattering from a molecule can be detected. The magnitude of the wavelength shift depends on the type and strength of a bond between two specific atoms. Every molecule is a unique composition of atoms and therefore each molecule has a specific range of wavelength shifts. In theory a molecule can have $3N-6$ vibrational levels, in which N is the number of atoms. But only when a bond between atoms in a molecule can form a dipole moment, a Raman effect occurs. This is expressed in the ability for polarization. Larger molecules usually have a larger polarization than smaller ones, hence more wavelength shifts. In a Raman spectrum the range of shifts from the incident monochromatic light is plotted along the x-axis and the intensity of each shift along the y-axis. Relative Raman shifts are calculated according to the formula:

$$\Delta\text{cm}^{-1} = \left(\frac{1}{\lambda_o} - \frac{1}{\lambda_s} \right) * 10^{-2}$$

where λ_o = wavelength of incident light (in meters), λ_s = wavelength of scattered light and Δcm^{-1} the Raman shift from the incident light. The Stokes and anti-Stokes parts of the Raman spectrum on both sides of the Raleigh scattering are symmetrical. But the intensity of Stokes Raman is higher than that of anti-Stokes Raman because at room temperature more molecules are at the ground (equilibrium) vibrational level than at a higher vibrational level. Therefore only the Stokes Raman part of the spectrum is used in the work described in this thesis and is henceforward referred to as 'Raman spectrum'.

In a Raman spectrum from a single molecule the intensity of bands depends on the ability for polarization of each atom bond. But in a Raman spectrum of a sample with a variety of molecules the intensity of bands also depends on the concentration of each molecule, the chemical bonds between them and environmental influences (temperature, acidity, etc.). From relatively simple molecules as urea and organic solvents up to large proteins and even complete parts of tissue, the complexity of a

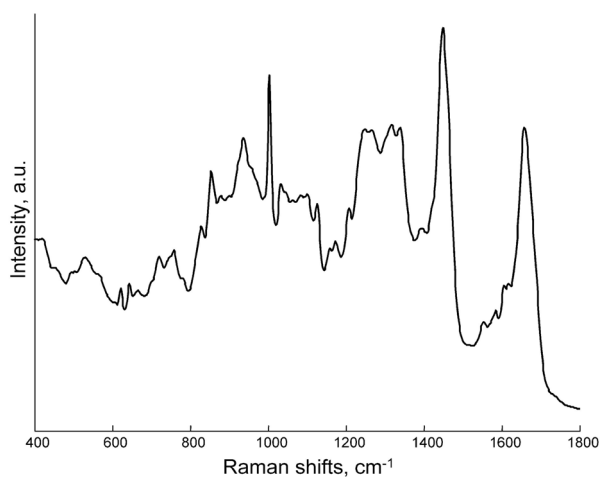


Figure 10

Raman spectrum measured on a frozen section of bladder wall tissue (a.u. = arbitrary units). Most tissues are composed of a wide variety of different molecules. Therefore a spectrum from tissue contains a large number of bands that may overlap. Comparison of spectra from slightly different tissues (e.g. 'normal' and 'diseased') require computer controlled analysis.

Raman spectrum with more and more specific Raman shift bands increases (figure 10). Since each type of tissue consists of a large specific range and concentration of molecules, a Raman spectrum from that tissue will also be very specific. For this reason the term 'Raman fingerprint' is often used.

Instrumentation

The instrumentation for Raman spectroscopic measurements is continuously evolving. When C.V. Raman discovered the 'Raman' effect, he used filtered sunlight as a monochromatic light source and the human eye as a detector. Much later a mercury arc lamp was applied but only when lasers as a powerful monochromatic light source became available in the nineteen sixties, the collection time of Raman spectra could be greatly shortened. Also in the detection path some major developments have taken place. Starting from the human eye, to photographic film and photo multipliers, nowadays charge coupled device (CCD) cameras are the standard. These developments reduced collection times but moreover improved accuracy and the convenience of this technique. Where measurement of a single



Figure 11

Photo-image of the Raman microspectrometer that was used for the measurements in all studies in this thesis.

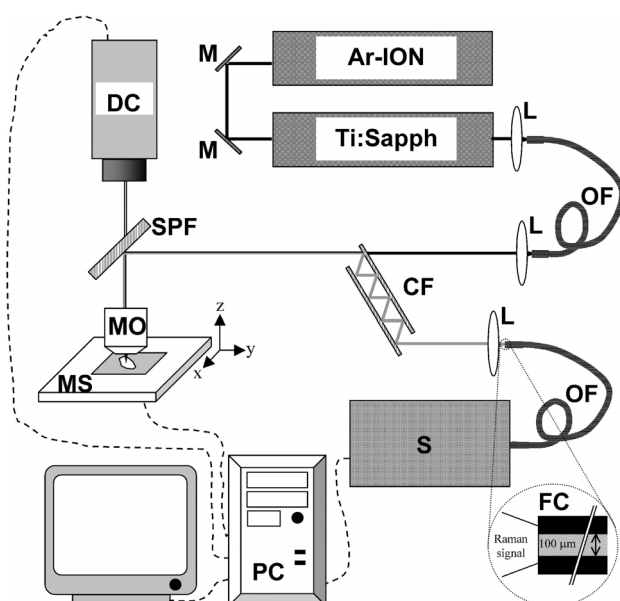


Figure 12

Schematic overview of the Raman microspectrometer. Ar-ION = Argon-ionised laser, Ti:sapph = tunable titanium sapphire laser powered by the Argon-ionised laser, L = lenses, OF = optical fibres, CF = Chevron filter set, DC = digital video camera, SPF = short pass filter, MO = microscope objective (80x, NA 0.75, NIR) MS computer controlled x-y-z microscope stage, FC = detailed enlargement of coupling of Raman scatter signal into fibre optic core (volume of beam that covers the inner core determines confocality), S = spectrometer, PC = computer.

Raman spectrum initially took up to several hours or even days, nowadays (diode) lasers and CCD cameras allow for high signal to noise ratio (S/N) Raman spectra to be measured in the order of seconds or even less (figure 11).

The instrument used in the Raman studies presented in this thesis consisted of an argon pumped tunable titanium-sapphire laser and a microscope that was attached to a spectrometer, a so-called microspectrometer. Laser light with a wavelength of around 845 nm was focused onto the sample through an infrared-optimized microscope objective. The Raman scattering was collected through the same objective, separated from the incident light by optical filters and guided to a spectrometer with a confocal signal collection geometry as displayed in figure 12. In this way only Raman signals from very small sample volumes could be obtained. The measurement volume of a confocal Raman set-up is dependent on the microscope objective and the coupling of guiding fibres to the spectrometer. In the set-up used in this thesis the measurement volume was shaped as a vertical cylindrical form with about 2-3 μm in lateral direction and 1 μm in diameter. This enabled accurate positioned signal collection from frozen tissue sections, a key feature for Raman spectroscopic mapping.

Raman mapping was done on frozen sections of bladder tissue without pre-treatment of any kind other than freezing and cutting. With the use of an automated sample stage on the microscope a rectangular measurement area (grid) was selected that comprised all tissue slide sections of interest. This grid was then divided in small squares, called grid elements. In each of these grid elements one Raman spectrum was

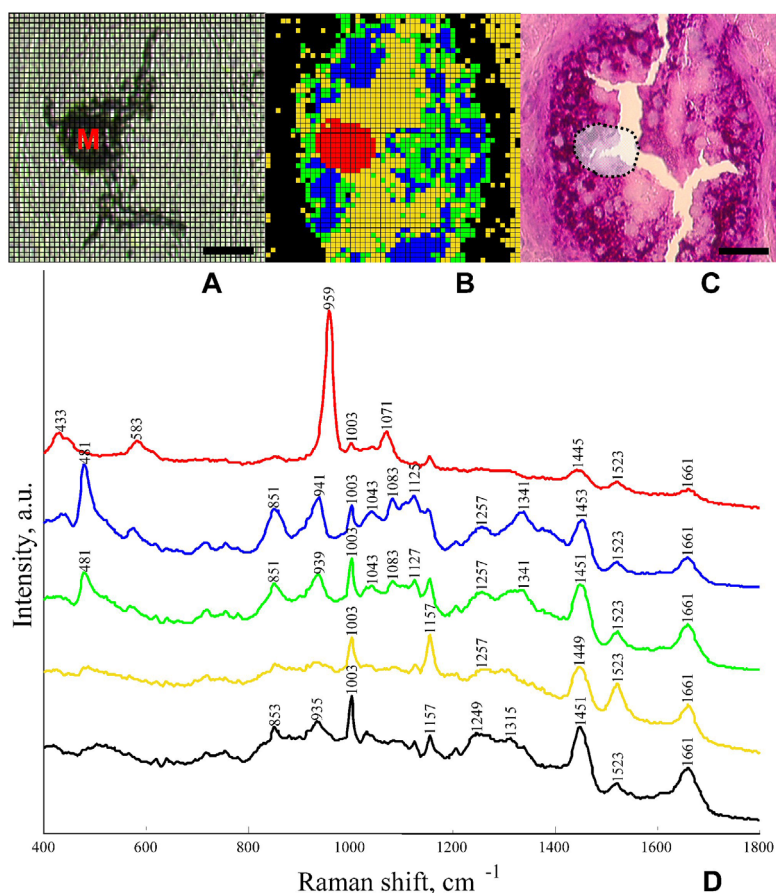


Figure 13

Typical result of a Raman spectroscopic map, with a photo-image of the exact tissue area being measured (A), color labelling from each cluster on the original location of each spectra belonging to a cluster in the grid, resulting in a Raman spectroscopic map (b), the same tissue as photographed in 'a' but now stained with a PAS stain (c) and cluster averaged spectra (d).

measured. Figure 13a shows a grid with grid elements displayed on an untreated 20 μm thick frozen section of testis tissue.

After Raman shift calibration and background signal correction, the Raman spectral data was interpreted using clustering analysis. In this way clusters of spectra were formed with similar spectral characteristics. Each group of spectra was assigned a color. Coloring all grid elements in a digital image of the grid, with the color of the cluster to which the measured spectrum belonged to, created a Raman map (figure 13b). For analysis of bladder wall tissue, the number of clusters may be chosen based on the number of layers, e.g. urothelium, connective tissue and muscle tissue. Choosing more clusters may reveal subgroups in one layer. This allows the detection of specific (unknown) biochemical components within their original bio-environment in a tissue sample that would have been missed in routine histology and immuno-histochemistry (figure 13c). Averaged spectra of each cluster are plotted in figure 13d. Although Raman spectroscopy has its roots in the late nineteen twenties, the combination of developments in monochromatic light sources, detection equipment, optical designs and computers with dedicated software to process the vast amount of spectral data in a structured manner, was needed to enable the use of Raman spectroscopy in biomedical research in the last fifteen years. Ongoing development, fuelled by research as presented in this thesis, allow this technique to be used in various clinical applications.

Scope of this thesis

The general scope of this thesis is to describe the relation between function and structure in normal bladders and bladders with a partial outlet obstruction. Two major study outlines are included that both relied on an animal model that simulates partial bladder outlet obstruction in young children. This model, for which Guinea pigs were used, is described in detail in section 'Urodynamic model' of this chapter. These two studies clarify the reason for and the possibility and benefit of using structural analysis for clinical monitoring of bladder function. Preliminary outcomes appear promising and monitoring bladder structure in a non-destructive and *in vivo* clinical application is subject for further research.

The first study outline was focused on the relation between bladder function and structure using urodynamic measurements and histochemical analysis of structure. In chapter 2 the histochemical analysis of bladder tissue from an animal model under various conditions of BOO is described. Here, the relation between bladder wall damage and the complete time-path of bladder functional changes was determined. A central element was the histochemical analysis of glycogen accumulation. Literature data suggests that glycogen accumulation is related to ischemia in muscle tissue [18, 46]. It can be detected both with simple histological staining techniques and Raman

spectroscopy. Actually the latter technique revealed that glycogen accumulation might be an indicator for previously existing ischemia. With detrusor tissue from either urodynamically normal animals and from animals with urethral obstruction, the correlation between the amount and location of glycogen accumulation in the detrusor and the stage of functional changes was studied. Subsequently, chapter 3 describes the changes in glycogen deposition after removal of the urethral obstruction. Chapters 4 and 5 describe how glycogen deposition is influenced by a known therapeutic agent, oxybutynin and an agent that is expected to affect ischemia, acetylsalicylic acid (aspirin). In chapter 6 the data from chapters 4 and 5 is re-evaluated to assess which urodynamic variables correlate best with ischemia.

The second study outline was focussed on characterizing changes in bladder wall structure with Raman spectroscopy. With *in vitro* Raman spectroscopic mapping of frozen sections of bladder tissue a detailed molecular analysis can be made. The principles of Raman spectroscopy and mapping are explained in detail in section 'Raman spectroscopy' of this chapter.

In chapter 7 the Raman mapping technique was applied to bladder tissue. It is shown that the different layers in the normal bladder wall are distinguished in exact accordance with the histology. In the following chapter the differences between Raman map measurements on unobstructed and obstructed bladder tissue sections have been analysed. This revealed collagen infiltration and glycogen accumulation. Chapter 9 describes a study to determine if Raman spectroscopy can discriminate between healthy and diseased tissues in human material. Therefore we applied this technique on frozen sections of biopsies from non-tumor and tumor bladder. Detailed analysis of the spectra from this data revealed biochemical differences between non-tumor and tumor tissue that were also described in literature, providing a proof of concept.

References

1. Smith's General Urology, E.A. Tanagho JW McAninch, 15th edition, Lange Medical Books/McGraw-Hill, New York, 2000.
2. Ghanem MA, Wolffenbuttel KP, De Vylder A, Nijman RJ. Long-term bladder dysfunction and renal function in boys with posterior urethral valves based on urodynamic findings. J Urol **171**:2409-2412., 2004.
3. Chromek M, Slamová Z, Bergman P, Kovács L, Podracká L, Ehrén I, Hökfelt T, Gudmundsson GH, Gallo RL, Agerberth B, Brauner A: The antimicrobial peptide cathelicidin protects the urinary tract against invasive bacterial infection. Nat Med **12**:636-641, 2006.
4. Garg SK, Abdurrahman MB, Momoh JT, Hargreaves HM, Narayana P, Lawrie JH. Congenital posterior urethral valves: problems of management in countries with limited facilities. Ann Trop Paediatr. **3**:201-205, 1983.
5. Wadie BS, Ibrahim EH, de la Rosette JJ, Gomha MA, Ghoneim MA. The relationship of the International Prostate Symptom Score and objective parameters for diagnosing bladder outlet obstruction. Part I: when statistics fail. J Urol **165**:32-34, 2001.

6. Hubert KC, Palmer JS. Current diagnosis and management of fetal genitourinary abnormalities. *Urol Clin North Am* **34**:89-101, 2007.
7. Neuhaus J, Dorschner W, Mondry J, Stolzenburg JU. Comparative anatomy of the male guinea-pig and human lower urinary tract: histomorphology and three-dimensional reconstruction. *Anat Histol Embryol* **30**:185-192, 2001.
8. Mostwin JL, Karim OM, Van Koevinge G, Seki N. Guinea pig as an animal model for the study of urinary bladder function in the normal and obstructed state. *Neurourol Urodyn* **13**:137-145, 1994.
9. Kok DJ, Wolffenbuttel KP, Minekus JP, et al. Changes in bladder contractility and compliance due to urethral obstruction: a longitudinal followup of guinea pigs. *J Urol* **164**:1021-1024, 2000.
10. Wolffenbuttel KP, Kok DJ, Minekus JP, et al. Urodynamic follow-up of experimental urethral obstruction in individual guinea pigs. *Neurourol Urodyn* **20**:699-713, 2001.
11. Kim KM, Kogan BA, Massad CA, Huang Y. Collagen and elastin in the obstructed fetal bladder. *J Urol* **146**:528-531, 1991.
12. Charlton RG, Morley AR, Chambers P, Gillespie JI. Focal changes in nerve, muscle and connective tissue in normal and unstable human bladder. *BJU Int* **84**:953-960, 1999.
13. Deveaud CM, Macarak EJ, Kucich U, Ewalt DH, Abrams WR, Howard PS. Molecular analysis of collagens in bladder fibrosis. *J Urol* **160**:1518-1527, 1998.
14. Kim JC, Yoon JY, Seo SI, Hwang TK, Park YH. Effects of partial bladder outlet obstruction and its relief on types I and III collagen and detrusor contractility in the rat. *Neurourol Urodyn* **19**:29-42, 2000.
15. Wang Z, Gopalakurup SK, Levin RM, Chacko S. Expression of smooth muscle myosin isoforms in urinary bladder smooth muscle during hypertrophy and regression. *Lab Invest* **73**:244-251, 1995.
16. Cher ML, Abernathy BB, McConnell JD, Zimmern PE, Lin VK. Smooth muscle myosin heavy-chain isoform expression in bladder-outlet obstruction. *World J Urol* **14**:295-300, 1996.
17. Austin LC, Chacko SK, DiSanto M, Cnning DA, Zderic SA. A male murine model of partial bladder outlet obstruction reveals changes in detrusor morphology, contractility and Myosin isoform expression. *J Urol* **172**:1524-1528, 2004.
18. Zhou Y, Ling EA. Neuronal nitric oxide synthase in the neural pathways of the urinary bladder. *J Anat* **194**:481-496, 1999.
19. Gabella G. Structure of the intramural nerves of the rat bladder. *J Neurocytol* **28**:615-637, 1999.
20. Maruyama S, Kurosawa S, Takagi Y, Oki T, Noguchi Y, Ukai M, Yuyama H, Ohtake A, Suzuki H, Sasamata M, Yamada S. Urodynamics and bladder muscarinic receptors in rats with cerebral infarction and bladder outlet obstruction. *Neurosci Lett* **414**:80-84, 2007.
21. Matsumoto S, Chichester P, Kogan BA, Levin RM. Structural and vascular response of normal and obstructed rabbit whole bladders to distension. *Urology* **62**:1129-1133, 2003.
22. Chichester P, Lieb J, Levin SS, Buttyan R, Horan P, Levin RM. Vascular response of the rabbit bladder to short term partial outlet obstruction. *Mol Cell Biochem* **208**:19-26, 2000.
23. Levin RM, Chichester P, Levin SS, Buttyan R. Role of angiogenesis in bladder response to partial outlet obstruction. *Scand J Urol Nephrol Suppl* **215**:37-47, 2004.
24. O'Connor LJ, Goldner CW, Lau ST, Hass MA, Levin RM. Effect of partial outflow obstruction on the distribution of free fatty acids and phospholipids in the rabbit bladder. *World J Urol* **17**:261-265, 1999.
25. Flynn BJ, Mian HS, Cera PJ, Kabler RL, Mowad JJ, Cavanaugh AH, Rothblum LI. Early molecular changes in bladder hypertrophy due to bladder outlet obstruction. *Urology* **59**:978-982, 2002.
26. Mirone V, Imbimbo C, Longo N, Fusco F. The detrusor muscle: an innocent victim of bladder outlet obstruction. *Eur Urol* **51**:57-66, 2007.

27. Greenland JE, Hvistendahl JJ, Andersen H, Jørgensen TM, McMurray G, Cortina-Borja M, Brading AF, Frokiaer J. The effect of bladder outlet obstruction on tissue oxygen tension and blood flow in the pig bladder. *BJU Int* **85**:1109-1114, 2000.
28. Pessina F, Solito R, Maestrini D, Gerli R, Sgaragli G. Effect of anoxia-glucopenia and re-perfusion on intrinsic nerves of mammalian detrusor smooth muscle: importance of glucose metabolism. *Neurourol Urodyn* **24**:389-396, 2005.
29. Chapple CR, Smith D. The patophysiological changes in the bladder obstructed by benign prostatic hyperplasia. *Br J Urol* **73**:117-123, 1994.
30. Freedman AL, Qureshi F, Shapiro E, Lepor H, Jacques SM, Evans MI, Smith CA, Gonzalez R, Johnson MP. Smooth muscle development in the obstructed fetal bladder. *Urology* **49**:104-107, 1997.
31. Levin RM, Haugaard N, O'Connor L, Buttyan R, Das A, Dixon JS, Gosling JA. Obstructive response of human bladder to BPH vs. rabbit bladder response to partial outlet obstruction: a direct comparison. *Neurourol Urodyn* **19**:609-629, 2000.
32. Chul Kim J, Il Seo S, Hyun Park Y, Kon Hwang TA. Changes in detrusor and urinary growth factors according to detrusor function after partial bladder outlet obstruction in the rat. *Urology* **57**:371-375, 2001.
33. Chertin B, Rolle U, Cascio S, Puri P. Alterations in cholinergic and neuropeptide innervation of urinary bladder following partial bladder outlet obstruction. *Pediatr Surg Int* **19**:427-431, 2003.
34. Burkhard FC, Katia Monastyrskaya K, Studer UE, Draeger A. Smooth muscle membrane organization in the normal and dysfunctional human urinary bladder: a structural analysis. *Neurourol Urodyn* **24**:128-135, 2005.
35. Hosgor M, Karaca I, Ulukus C, Ozer E, Ozkara E, Sam B, Ucan B, Kurtulus S, Karkiner A, Temir G. Structural changes of smooth muscle in congenital ureteropelvic junction obstruction. *J Pediatr Surg* **40**:1632-1636, 2005.
36. Hypolite JA, Chang S, Zheng Y, DiSanto ME, Zderic SA, Wein AJ, Chacko S. Partial bladder outlet obstruction induces urethral smooth muscle hypertrophy and decreased force generation. *J Urol* **175**:777-782, 2006.
37. Greenland JE, Brading AF. Urinary bladder blood flow changes during the micturation cycle in a conscious pig model. *J Urol* **156**:1858-1861, 1996.
38. Azadzoi KM, Pontari M, Vlachiotis J, Siroky MB. Canine bladder blood flow and oxygenation: changes induced by filling, contraction and outlet obstruction. *J Urol* **155**:1459-1465, 1996.
39. Azadzoi KM, Tarcan T, Kozłowski R, Krane RJ, Siroky MB. Overactivity and structural changes in the chronically ischemic bladder. *J Urol* **162**:1768-1778, 1996.
40. Greenland JE, Brading AF. The effect of bladder outflow obstruction on detrusor blood flow changes during the voiding cycle in a conscious pigs. *J Urol* **165**:245-248, 2001.
41. Brading A, Pessina F, Esposito L, Symes S. Effects of metabolic stress and ischaemia on the bladder, and the relationship with bladder overactivity. *Scand J Urol Nephrol Suppl* **215**:84-92, 2004.
42. Raman CV, Krishnan KS. A new type of secondary radiation. *Nature* **121**:501-502, 1928.
43. Smekal A. Zur Quantentheorie der Dispersion. *Naturwissenschaften* **11**:873-875, 1923.
44. Singh R, Riess F, Sir C. V. Raman and the story of the Nobel prize. *Curr sci* **75**:965-971, 1998.
45. Landsberg GS, Mandelshtam LI. *Naturwissenschaften* **16**:557, 1928.
46. Wein AJ, Gregory JG, Sansone TC, Rohner TJ, Schoenberg HW. Glycogen accumulation in neurogenic bladder muscle. A reappraisal. *Invest Urol* **10**:442-443, 1973.



Detrusor glycogen reflects the functional history of bladders with partial outlet obstruction

B.W.D. de Jong
K.P. Wolffenbuttel
M.E. Arentshorst
P. Lodder
D.J. Kok

BJU International
100:846-852, 2007

Chapter

2

Abstract

Objective: To assess the relationship between glycogen content in bladder detrusor tissue and historical bladder function in a guinea-pig model of partial bladder outlet obstruction (PBOO).

Materials and methods: In male immature guinea pigs PBOO was created with a silver ring around the proximal urethra; a control group had a sham operation for comparison. Longitudinal individual urodynamic data were obtained weekly, so that guinea pigs were killed at different levels of bladder dysfunction. Bladder sections were stained with periodic acid-Schiff (PAS) to assess overall morphology and glycogen granule density, scored from 0 (no glycogen) to 3. Glycogen scores were related to both the end-stage and historical extremes of bladder function values.

Results: Glycogen granules were seen only in the detrusor; as their number increased their location expanded from only close to the serosa (glycogen score 1), through the detrusor (score 2) up to the urothelium (glycogen score 3). A glycogen score of 0 correlated with normal values for all urodynamic variables. Compared with a glycogen score of 0 a score of 1 correlated with significant ($P < 0.05$) changes in end-stage compliance (decrease) and contractility (increase) and significantly higher historical values for contractility, pressure and number of unstable contractions (NUC). In the group with a glycogen score of 2 there were significant changes in both the end-stage values and historical extremes for compliance, pressure, contractility and NUC (all $P < 0.05$). In the group with a glycogen score of 3 all these changes were even more dramatic, except for the end-stage contractility, for which the increase was not significant. From glycogen score 0 to score 3 all changes increased in magnitude.

Conclusion: A high glycogen content reflects a history of abnormal urodynamic function. This finding exemplifies the added value of structural analysis to urodynamic studies. Further studies are needed to relate bladder structure to the potential for functional recovery.

Introduction

Functional bladder failure in infants has been well described as a major cause of ultimate kidney failure. Examples of this bladder failure are myelomeningocele (spina bifida), bladder exstrophy and partial bladder outlet obstruction (PBOO). PBOO, mainly caused by PUV, is diagnosed antenatally by ultrasonography or postnatally by cystography and direct visualization with cystoscopy. The treatment option is straightforward; in most cases endoscopic valve ablation followed by monitoring of bladder and kidney function is warranted.

However, the follow-up can be more difficult; after valve ablation bladder function will stabilize or even improve in many cases, but in some patients it deteriorates further. How to predict and monitor bladder function after valve ablation has been the subject of many studies [1–7], but they have not yet led to a clinical tool that predicts bladder outcome. The best option at present is to closely monitor bladder function after valve ablation and select cases of deterioration as they present [5]. Inherently this can lead to loss of valuable time. In addition, invasive urodynamic studies are difficult to conduct in young children.

The crux of this clinical problem might be the lack of insight into bladder function before de-obstruction. At best, urodynamic data from one sample time before valve ablation are available; what happened prenatally is unclear.

In an animal model of partial urethral obstruction the complete path of deterioration in bladder function can be followed in individual animals. We have shown that urodynamic data from one sample time do not clarify how far a bladder has proceeded along the path of functional deterioration [8,9]. Insight into the complete urodynamic history of the bladder is essential; unfortunately this cannot be obtained in children.

We hypothesized that changes in bladder tissue composition might reflect the pre-existing abnormalities in bladder function. The controlled conditions of our animal model for urethral obstruction provide us with bladder tissue for which the complete time path of changes in bladder function is known [8,9]. By harvesting bladder tissue from this model at different levels of bladder dysfunction, the relation between obstructive functional and structural changes can be established.

We focused on the level of glycogen deposition, in the form of granules within the detrusor smooth muscle cells. Glycogen accumulation in detrusor smooth muscle has been connected with hypertrophy for several decades [10]. More recently, glycogen accumulation is linked to adaptation of the detrusor to ischaemia induced by high bladder pressure [11–14]. It was proposed that when the bladder pressure exceeds capillary pressure, blood capillaries in the bladder wall become compressed and the affected muscle cells are forced to work in anaerobic conditions [13], and to use glycogen as energy source. Pessina *et al.* [15] reported a decrease in glycogen levels in isolated bladder detrusor smooth muscle strips of human, monkey and guinea pig

after a period of hypoxia. In the whole organ this *in vitro* effect of glycogen depletion paradoxically will be visible as the appearance of glycogen stores, as the bladder adapts to recurring periods of ischaemia induced high glycogen consumption. The more ischaemic periods that have occurred, the more glycogen granules will appear.

In the present study glycogen granules were visualized using periodic acid-Schiff (PAS) stain, scoring four levels of glycogen deposition, ranging from no glycogen granules within smooth muscle cells to dense glycogen accumulation, and correlated these findings with the urodynamic history of the bladders.

Materials and methods

Bladder tissue was obtained from a guinea-pig model of PUV; to allow for a urodynamic follow-up from the start of PBOO, and be able to surgically apply PBOO, the guinea pigs had to weigh ≈ 300 g (≈ 6 weeks old). The model was extensively described previously [8,9]. Briefly, bladder pressure was measured in each guinea pig through a suprapubic bladder catheter, and the urinary flow rate was measured using an ultrasound flow probe attached loosely around the penis. This was done weekly, starting just before imposing PBOO and ending just before the animal was killed. The guinea pigs were killed at different times to provide several levels of functional change in the bladders with PBOO. Table 1 gives an overview of the protocol, with the number of guinea pigs with PBOO and controls killed each week. From the weekly

Week	N obstructed	N sham-operated/controls
1	4	1
2	2	0
3	5	0
4	4	1
5	2	0
6	2	0
7	5	2
8	1	2
9	0	2
10	2	1
> 10	2	0

Table 1

The number of obstructed guinea pigs and sham-operated and control guinea pigs killed each week.

urodynamic data the number of unstable contractions (NUC), bladder pressure at maximum flow rate (pQ_{\max}), contractility (W_{\max}) and compliance ($\text{mL}/\text{cmH}_2\text{O}$) were calculated. Compliance was calculated as Δ infused volume/ Δ bladder pressure, and the contractility calculated according to Griffith *et al.* [16]. An unstable contraction was defined as one with a bladder pressure of > 10 cmH_2O (a third of the mean normal voiding pressure in these guinea pigs) unaccompanied by actual bladder emptying.

Bladder tissues were snap-frozen in liquid nitrogen-cooled isopentane and stored at -80°C until use. About half of each bladder tissue sample was later fixed in 10% buffered formalin (pH 7.4) and embedded in paraffin wax for sectioning. Cross-sections of $4\ \mu\text{m}$ covering all bladder wall layers were made for staining. In total we

used tissue from 39 guinea pigs, i.e. nine control/sham-operated and 30 obstructed, for variable periods.

The PAS stain is routinely used for visualizing sugar moieties, and provides an insight into the general structure, comparable to haematoxylin and eosin staining, combined with specific information on granular glycogen deposits. The number of glycogen granules staining in bladder sections was scored using light microscopy. Three researchers scored the bladder sections while unaware of origin, with scores of 0 (minimal staining) to 1 (little staining), 2 (strong staining) and 3 (maximum staining). The abundance of the staining correlated with the site of glycogen deposition; a score of 1 represented light glycogen granule staining only at the serosal side; a score of 2 represented more intense staining, where glycogen granules were found deeper into the muscle layer; a score of 3 represented strong staining of glycogen granules that were present throughout the muscle layer. With four scoring groups we could combine good differentiation of the amount of glycogen with group sizes that allow statistical analysis.

The glycogen scores were correlated with the urodynamic data in two ways. First, with the urodynamic variables measured immediately before harvesting the tissue, termed the 'end-stage' urodynamic variables. This reflects the clinical situation, where a biopsy is taken after a urodynamic study. Second, the glycogen scores were correlated with the extremes of all urodynamic variables measured in the weeks before death. Thus we used the highest value ever reached for contractility, bladder pressure and NUC, and the lowest compliance value. This was intended to provide information on whether tissue composition reflected the history of bladder function.

The distribution of most of the urodynamic variables was skewed because there were very low or high values from individual guinea pigs, and thus we used the median values with the 5%, 25%, 75% and 95% percentiles, rather than the mean (SD) for each urodynamic variable. The data are presented as box-whisker plots that visualize the distribution within data, showing the median as a bar with a box representing the 25% and 75% percentiles, and whiskers for the 5% and 95% percentiles. The Mann Whitney *U*-test was used to determine the significance of differences in urodynamic variables between the groups with a glycogen group of 0 and the groups with other glycogen scores.

Group	Glycogen score			
	0	1	2	3
Control/sham	6	2	1	0
Obstructed	2	6	17	5
Total	8	8	18	5

Table 2

Glycogen scoring on control/sham-operated and obstructed bladder detrusor tissue sections.

Results

For glycogen scoring, the inter-observer differences for one tissue sample were < 1 score value; the results of the three observers were averaged to obtain the mean score for each tissue. Table 2 shows the distribution of the 39 bladder tissues (nine control/sham-operated, 30 obstruction) over the four glycogen score groups. The site of glycogen deposition expanded as there were more stained granules. Figure 1a

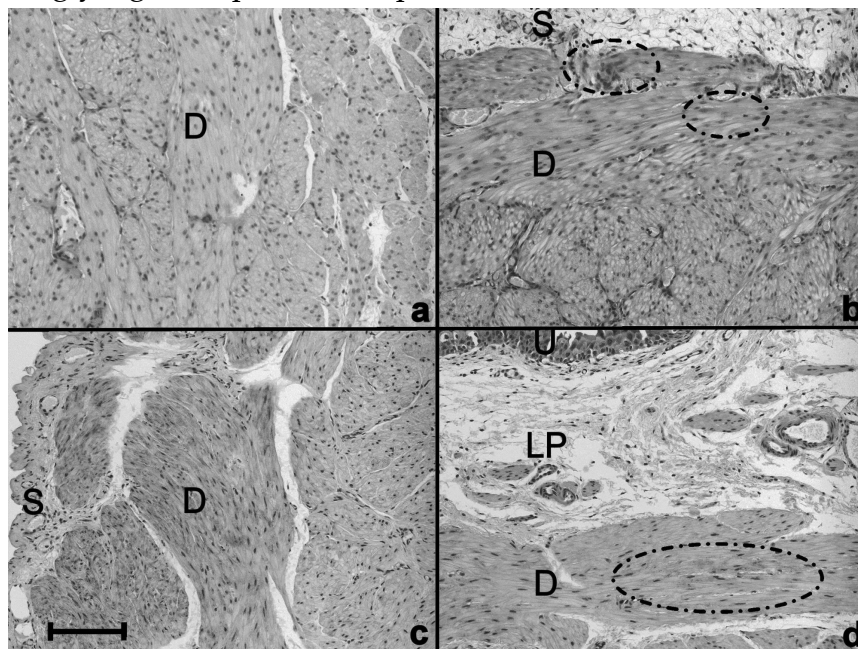


Figure 1

Examples of PAS stains with scores 0 (a), 1 (b), 2 (c) and 3 (d). D, detrusor layer; S, serosa; LP, lamina propria; and U, urothelium. Dotted circles show the small groups of glycogen granules. Bar = 200 μ m. Color image: see appendix

shows a tissue with glycogen score 0, i.e. no glycogen granules visible. For glycogen score 1 there were a few glycogen granules only close to the serosa in the detrusor layer, accentuated by dotted circles in Fig. 1b. For glycogen score 2 the amount of staining was clearly greater (Fig. 1c) and granules appear deeper into the muscle layer towards the urothelium. Glycogen score 3 had the most stained granules, which were visible throughout the whole detrusor layer. Figure 1d shows glycogen granules in muscle cells directly near the lamina propria, accentuated by a dotted circle. Overall, with increasing accumulation the site of glycogen deposition increased from only close to the serosa up to the lamina propria. Glycogen granules always appeared within the cytoplasm of muscle cells.

Figure 2a shows the positive correlation between the glycogen score and the duration of PBOO; a glycogen score of 0 was found mostly in sham-operated guinea pigs. Two guinea pigs with 2 weeks of obstruction also scored zero, but these data were outside the 95% range and therefore not plotted. The glycogen scores 1, 2 and 3 represent groups of guinea pigs with progressive significant increases in the duration of PBOO. While this trend is clear for the groups as a whole, the wide distribution in the data indicates that the individual response is variable. In the group with a glycogen score of 2 the 5–95% percentiles are at 0 and 10 weeks.

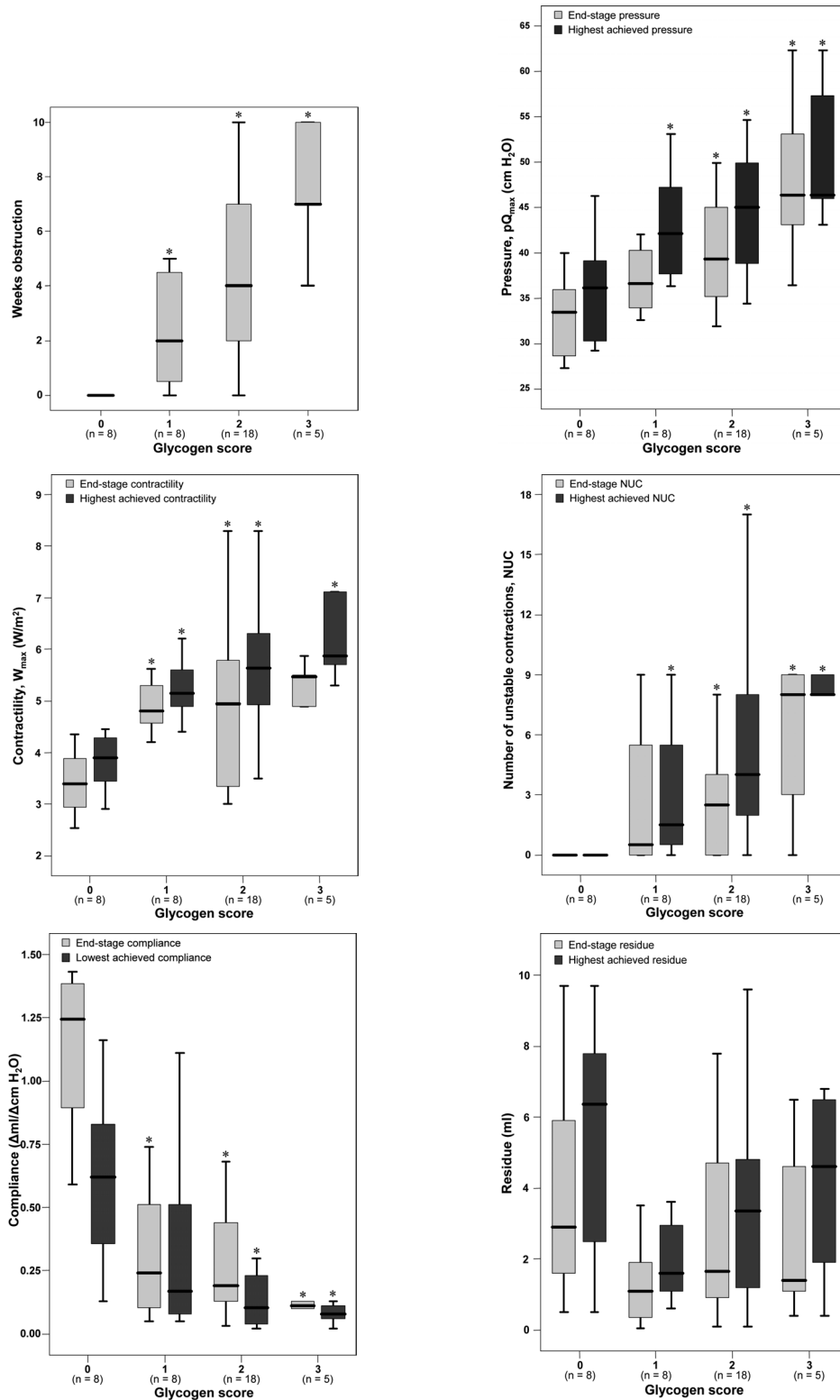


Figure 2

Box-whisker plots of the correlation between glycogen scores and: a, the number of weeks of obstruction (* $P < 0.05$ vs glycogen score 0); b, bladder pressures; c, bladder contractility; d, NUC; e, bladder compliance; and f, residual volumes. In plots b–f, the light grey bars represent the end-stage value and the dark grey bars the highest achieved values, with * $P < 0.05$ vs glycogen score 0 for end-stage and highest achieved values, respectively.

Figure 2b shows the correlation between the glycogen score and both the end-stage bladder pressure and the highest bladder pressure during the course of PBOO. The median values of both the end-stage bladder pressure and the highest bladder pressure were significantly higher in the groups with a glycogen score of 2 and 3 than in that with glycogen score 0. The median pressure in the glycogen score 1 group was increased, but not significantly different, from that in the glycogen score 0 group.

Compared with the glycogen score 0 group the median of the highest achieved contractility was significantly greater all other three groups (Fig. 2c). The same was true for the median of the end-stage contractility in the glycogen score 1 and 2 groups. The increase in the end-stage contractility in the glycogen score 3 group was not significant. This group of five guinea pigs contains one outlier with an end-stage contractility of 2.50, which is even below the minimum value of end-stage contractility at glycogen score 0 (2.53). (As this outlier is outside the 5% percentile it is not plotted but was included in the dataset for statistics). We previously reported that during obstruction the bladder contractility reaches a plateau value at which it remains stable for some time and from which it finally starts to decline again. The outlier here represents a guinea pig that has passed the peak contractility and reached a state of reduced contractility. Possibly this bladder is entering a state of decompensation after a history of a high contractility that is still reflected in its high glycogen score.

The medians of both end-stage NUC and highest achieved NUC tended to increase with increasing glycogen score (Fig. 2d). At a glycogen score of 2 and 3 the increase compared with the glycogen score 0 group was significant for both the end-stage and highest achieved NUC. In the glycogen score 0 groups some guinea pigs had unstable contractions at some point, but the median values for both end-stage and highest achieved NUC were zero. Both end-stage and highest achieved NUC increased with increasing glycogen score.

Both end-stage compliance and lowest measured compliance decreased progressively with increasing glycogen score (Fig. 2e). Compared to the glycogen score 0 group the decrease was significant for both variables in all three glycogen groups, except for the lowest achieved compliance in the glycogen score 1 group. The latter decrease was not significant due to a large upward spread in the glycogen 1 group; this is intrinsic to compliance. In a normal guinea pig bladder, with compliance values of ≈ 1 , the increase in bladder pressure during filling is 0.1–0.3 cmH₂O. A small error in bladder pressure measurement will greatly affect the calculated compliance value. In a bladder with decreased compliance the increase in bladder pressure during filling is usually > 1 and sometimes approaches 20 cm H₂O. Errors of similar magnitude then have little effect on the calculated compliance. This explains the wide distribution in the data of the glycogen 0 group vs. the small distribution in values of the glycogen 3 group. The bladder residual volumes did not differ significantly among the four glycogen score groups (Fig. 2f).

Figure 3 shows the end-stage and maximum achieved urodynamic values for two guinea pigs where the glycogen score was 1 and 3, respectively. On the basis of the end-stage urodynamic values both guinea pigs cannot be distinguished, but their historical values differ greatly.

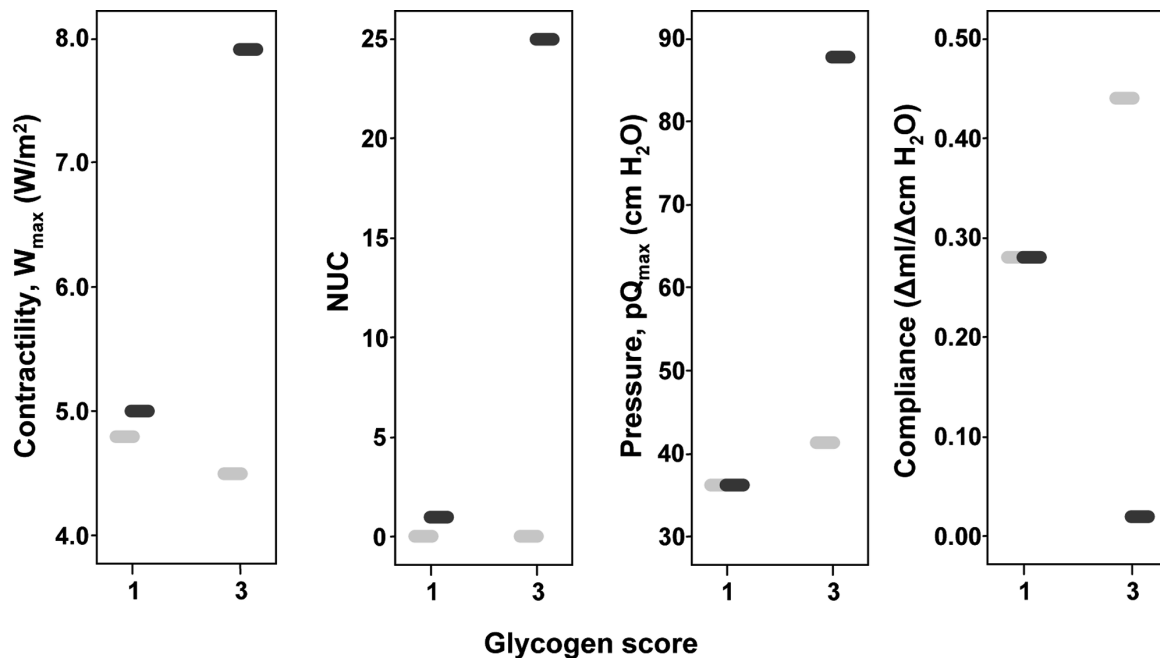


Figure 3

Examples of bladder tissue glycogen scores 1 and 3 with corresponding urodynamic values for end-stage (light grey) and maximum achieved (dark grey) values.

Discussion

In patients with neurogenic and structural BOO the urologist is faced with the task of preventing any loss of bladder function. In patients with functional BOO the original cause, PUV, can be treated successfully but the patients start with an already abnormally functioning bladder. However, a neurogenic bladder usually starts with normal function but is at risk of losing function due to bladder overactivity and/or detrusor-sphincter dyssynergia. To conserve bladder function, the treatment and follow-up for both patient groups are usually based on (combinations of) anticholinergics, antibiotics, clean intermittent catheterization and periodic urodynamic assessment of bladder function. This approach is effective but not for all patients. A major problem is how to identify those patients at risk of losing bladder function. To solve this problem several questions must be addressed. By what mechanism and time course does a bladder change from normal function to dysfunction? How can the stage of deterioration of a specific bladder be determined and placed on this time course of functional loss? Can this information be linked to the potential to conserve or even regain function?

The answers must come from an analysis of bladder function and structure, but the number of biopsies and urodynamic studies needed limit this approach. Furthermore, part of the deterioration in bladder function occurs beyond the reach of diagnostic tools, in the fetus. For these reasons we previously devised an animal model to study how bladder function develops after placing a urethral obstruction. The advantage of this model is that urodynamic investigations are possible weekly and bladder tissue is available for analysis of its structure. This model allowed us to describe the time course by which a bladder deteriorates from normal function to hypercontractility and noncompliance or even to acontractility [8,9]. An interesting aspect of these results was that we could describe the condition of the individual bladders, knowing their complete urodynamic history. However, we could not determine how far a bladder had deteriorated using only the data from one urodynamic study and being unaware of the functional history of that bladder. This reflects the clinical situation, where the urologist must rely on a urodynamic study at one sample time to describe the functional situation of the whole period before that analysis. Previous deviations from this registration will be missed.

However, the bladder tissue will reflect adaptation to those previous situations. Our working hypothesis is thus that the structure of a bladder reflects adaptation to previous anomalies in its function. In particular we focused on the accumulation of glycogen granules, which is correlated with adaptation to ischaemic conditions. In other tissues glycogen stores have also been connected with ischaemia, e.g. in chronic high-altitude hypoxia in fetal hearts [17]. In the bladder, ischaemia might also underlie the nerve damage [15,18,19], the angiogenesis [20,21] and the increase in the myosin subtypes SM1/SM2 ratio in muscle cells, that were described for the obstructed bladder [22–24].

In the present study we showed that the extent and the pattern of glycogen deposition in a bladder is related to its urodynamic function at the time when the tissue was taken, but more so to the historical developments in function. The glycogen score increased both with increasing severity of historical bladder dysfunction and increased duration of obstruction. In experimental models of BOO the individual animals differ in the extent and rate of their response to obstruction [20]. The glycogen score is less affected by these individual variations and appears to reflect the combined result of the severity and duration of the obstruction. In the clinical situation the glycogen score might thus help in deciding how far a bladder has deteriorated and might provide an insight into the history of that bladder. The glycogen score might help to differentiate a bladder that has passed its peak in compensation from one that is still in its compensatory phase. Both might yield comparable values for bladder pressure, compliance and contractility, but different glycogen scores. A high glycogen score would then indicate a bladder that has passed its peak in adaptation. A clear example of this is shown in Fig. 3; two guinea pigs cannot be distinguished by their end-stage urodynamic values, but differed in their

glycogen score that reflects their very different urodynamic histories. Whether a high glycogen score also means that a bladder has less potential for functional recovery is a question for further research.

While in the clinic a residual volume is associated with abnormal bladder function, there were no significant changes in residual function in the present model. The main reason is that unobstructed guinea pigs already have a large residual volume. Whether this is an experimental feature, e.g. related to anaesthesia, or a normal feature of the guinea pig, is not known.

The present data also shed light on the mechanism by which an obstructed bladder changes in function and structure. We found that a high glycogen content was related more to a history of high contractility than to the end value of the contractility. Although clinicians do not routinely involve bladder contractility when they assess bladder function, this variable was useful for elucidating the mechanism by which a bladder loses function. The decreased relation between glycogen content and end-stage contractility was apparent in individual guinea pigs that had passed the stage with high contractility and already had deteriorating bladder contractility [9]. As long as there remains muscle tissue that must work under ischaemic conditions these stores will remain. Possibly the glycogen stores might disappear in bladders that become completely acontractile.

The occurrence of ischaemia during obstruction might also explain the apparent discrepancy between our finding that the contractility of the bladder as a whole increases in response to obstruction, while Levin *et al.* [25] found that bladder muscle strips *in vitro* lose contractility under ischaemic conditions. Possibly the individual muscle cells work less efficiently under the ischaemic conditions and the bladder compensates for this intrinsic loss by increasing the total muscle mass. Apparently this increase in muscle mass is limited and therefore at some stage a maximum bladder contractility is reached. This might be the point after which continuing ischaemic pressure can no longer be compensated by the bladder, and the bladder will start to lose its ability to produce the pressure needed to empty itself against the existing urethral resistance. If this proposed mechanism is valid, the relief of ischaemia in a compensated bladder should result in an immediate increase in its contractility, as the increased muscle mass can work under the more efficient aerobic conditions.

However, at some point the changes might become less reversible, e.g. when the change in myosin subtypes has proceeded too far, or when adaptation of the collagen matrix to the new situation of increased muscle mass and high pressures has proceeded too far. At that point the potential of the bladder to regenerate its function might be reduced. Further research must determine whether the occurrence of glycogen deposits in the detrusor near the lamina propria is an indicator of such a point of no return. Presently we are therefore studying the effect of de-obstruction at different levels of bladder function loss in the guinea pig model.

In conclusion, structural analysis such as reported here using PAS stain can give information on pre-existing bladder function. In the clinic this could be valuable, as urodynamic data alone are insufficient to completely characterize the degree of bladder damage in an individual patient. Combined with the current development of non-destructive, fibre-optic based Raman spectroscopy for *in vivo* tissue analysis, that obviate the need for biopsies, such data would greatly assist the application of structural analysis in the clinic.

Acknowledgements

We thank the 'Stichting Urologisch Wetenschappelijk Onderzoek' and the Dutch kidney foundation (NSN) for their financial support to this work.

References

1. Lopez Pereira P, Martinez Urrutia MJ, Espinosa L, Lobato R, Navarro M, Jaureguizar E. Bladder dysfunction as a prognostic factor in patients with posterior urethral valves. *BJU Int* **90**: 308–311, 2002.
2. Lopez Pereira P, Espinosa L, Martinez Urrutia MJ, Lobato R, Navarro M, Jaureguizar E. Posterior urethral valves: prognostic factors. *BJU Int* **91**: 687–690, 2003.
3. Holmdahl G, Sillen U, Hellstrom AL, Sixt R, Solsnes E. Does treatment with clean intermittent catheterization in boys with posterior urethral valves affect bladder and renal function? *J Urol* **170**: 1681–1685, 2003.
4. Holmdahl G, Sillen U. Boys with posterior urethral valves. outcome concerning renal function, bladder function and paternity at ages 31–44 years. *J Urol* **174**: 1031–1034, 2005.
5. Schober JM, Dulabon LM, Woodhouse CR. Outcome of valve ablation in late-presenting posterior urethral valves. *BJU Int* **94**: 616–619, 2004.
6. Becker A, Baum M. Obstructive uropathy. *Early Hum Dev* **82**: 15–22, 2006.
7. Yohannes P, Hanna M. Current trends in the management of posterior urethral valves in the pediatric population. *Urology* **60**: 947–953, 2002.
8. Wolffenbuttel KP, Kok DJ, Minekus JP, van Koeveringe GA, van Mastrigt R, Nijman JM. Urodynamic follow-up of experimental urethral obstruction in individual guinea pigs. *Neurourol Urodyn* **20**: 699–713, 2001.
9. Kok DJ, Wolffenbuttel KP, Minekus JP, van Mastrigt R, Nijman JM. Changes in bladder contractility and compliance due to urethral obstruction: a longitudinal followup of guinea pigs. *J Urol* **164**: 1021–1024, 2000.
10. Wein AJ, Gregory JG, Sansone TC, Rohner TJ, Schoenberg HW. Glycogen accumulation in neurogenic bladder muscle. A reappraisal. *Invest Urol* **10**: 442–443, 1973.
11. Azadzoi KM, Tarcan T, Kozlowski R, Krane RJ, Siroky MB. Overactivity and structural changes in the chronically ischemic bladder. *J Urol* **162**: 1768–1778, 1999.
12. Brading A, Pessina F, Esposito L, Symes S. Effects of metabolic stress and ischaemia on the bladder, and the relationship with bladder overactivity. *Scand J Urol Nephrol Suppl* **215**: 84–92, 2004.
13. Greenland JE, Hvistendahl JJ, Andersen H, Jørgensen TM, McMurray G, Cortina-Borja M, Brading AF, Frøkiaer J. The effect of bladder outlet obstruction on tissue oxygen tension and blood flow in the pig bladder. *BJU Int* **85**: 1109–1114, 2000.

14. Gosling JA, Kung LS, Dixon JS, Horan P, Whitbeck C, Levin RM. Correlation between the structure and function of the rabbit urinary bladder following partial outlet obstruction. *J Urol* **163**: 1349–1356, 2000.
15. Pessina F, Solito R, Maestrini D, Gerli R, Sgaragli G. Effect of anoxia-glucopenia and re-perfusion on intrinsic nerves of mammalian detrusor smooth muscle: importance of glucose metabolism. *Neurourol Urodyn* **24**: 389–396, 2005.
16. Griffiths DJ, Constantinou CE, van Mastrigt R. Urinary bladder function and its control in healthy females. *Am J Physiol* **251**: R225–R230, 1986.
17. Thompson LP. Effects of chronic hypoxia on fetal coronary responses. *High Alt Med Biol* **4**: 215–224, 2003.
18. Hu J, Chin CM, Png JC, Ng YK, Ling EA. The effect of chronic bladder outlet obstruction on neuronal nitric oxide synthase expression in the intramural ganglia of the guinea pig bladder. *J Urol* **172**: 1160–1165, 2004.
19. Chertin B, Rolle U, Cascio S, Puri P. Alterations in cholinergic and neuropeptide innervation of urinary bladder following partial bladder outlet obstruction. *Pediatr Surg Int* **19**: 427–431, 2003.
20. Levin R, Chichester P, Levin S, Buttyan R. Role of angiogenesis in bladder response to partial outlet obstruction. *Scand J Urol Nephrol Suppl* **215**: 37–47, 2004.
21. Ghafar MA, Anastasiadis AG, Olsson LE, Chichester P, Kaplan SA, Buttyan R, Levin RM. Hypoxia and an angiogenic response in the partially obstructed rat bladder. *Laboratory Invest* **82**: 903–909, 2002.
22. Burkhard FC, Lemack GE, Zimmern PE, Lin VK, McConnell JD. Contractile protein expression in bladder smooth muscle is a marker of phenotypic modulation after outlet obstruction in the rabbit model. *J Urol* **165**: 963–967, 2001.
23. Austin JC, Chacko SK, DiSanto M, Canning DA, Zderic SA. A male murine model of partial bladder outlet obstruction reveals changes in detrusor morphology, contractility and Myosin isoform expression. *J Urol* **172**: 1524–1548, 2004.
24. Wilson TS, Aziz KA, Vazques D, Wuermser LA, Lin VK, Lemack GE. Changes in detrusor smooth muscle myosin heavy chain mRNA expression following spinal cord injury in the mouse. *Neurourol Urodyn* **24**: 89–95, 2005.
25. Levin RM, Reed TP, Whitbeck C, Chichester P, Damaser M. Effect of strip length on the contractile dysfunction of bladder smooth muscle after partial outlet obstruction. *Urology* **66**: 659–664, 2005.

The detrusor glycogen content of a de-obstructed bladder reflects the functional history of that bladder during PBOO

B.W.D. de Jong
K.P. Wolffenbuttel
J.R. Scheepe
D.J. Kok

Chapter

3

Neurourology &
Urodynamics
Accepted for publication

Abstract

Aims: To determine if detrusor glycogen content in a bladder after removal of a urethral obstruction reflects the situation of bladder dysfunction as it existed during the period of obstruction.

Methods: The glycogen content of the detrusor was scored using a Periodic Acid Schiff's (PAS) staining. It was related to the functional history of the bladder. Bladder tissue was obtained from a guinea-pig model for posterior urethral valves where animals had been obstructed for up to 10 weeks, de-obstructed and allowed to recover for 2-8 weeks. Bladder urodynamic function had been documented with multiple measurements for the complete period of obstruction and de-obstruction.

Results: The degree of glycogen deposition in a bladder after de-obstruction correlated directly with bladder function during obstruction. The strongest glycogen deposition was found in bladders having experienced the highest pressures, most instabilities, lowest compliance and highest contractility. In contrast, the bladder glycogen content was not related to the function of the bladder at the day the tissue was obtained, except for a relation between high glycogen content and continuing low compliance.

Conclusions: The glycogen content of a bladder reflects the history of bladder dysfunction, also when measured during a recovery period. This window on the functional history of a bladder may be of clinical value for picking out potential bad-responders to therapy in patients with incomplete data on bladder function during a previous period of bladder obstruction.

Introduction

Congenital urethral valves and a dysfunctional sphincter after spina bifida are the two major causes for a partial urethral obstruction in children. These are accompanied by a number of complications such as increase in contractility and loss of compliance. A deficiency in oxygen rich blood supply, also known as ischemia can cause damage to the neurological system and result in overactive bladder. When the cause of the obstruction is removed in time, the bladder can recover and no further consequences occur. However, when the development of bladder wall damage during obstruction progressed for a long time, a recovery of normal bladder function is no longer possible. For this reason, children with a partial bladder outlet obstruction (PBOO) are still at risk for reflux related kidney damage. Guarding the bladder function is a pivotal element of their treatment [1]. This treatment may furthermore include clean intermittent catheterization, intervention with anticholinergics or training of voiding. The success of this treatment (surgically and/or pharmacologically) depends on early recognition of the obstruction, diagnosis of the severity of the bladder dysfunction and accurate follow-up of bladder function. This success is currently large but not complete. Continuing loss of bladder and renal function is still encountered [2, 3]. The presence of PBOO problems is usually recognized pre-natal by echography or soon after birth. The severity of the obstructive changes in bladder function can be documented with urodynamic investigations. Unfortunately, during the pre-natal period as well as in very young and non-toilet trained children standard (video) urodynamic data is impossible or difficult to obtain. This frustrates the initiation and follow-up of treatment both in patients born with an anatomical obstruction that can be removed, like urethral valves, and in patients with inborn neurogenic bladder dysfunction in whom the obstruction remains present.

The accuracy of diagnosis may thus be improved when early assessment of the severity of bladder function deterioration becomes possible and when it is established what such changes mean for

the potential for recovery of bladder function. In concept, a bladder that has been severely dysfunctional for a prolonged time and is reaching a decompensated phase may have less potential for recovery of function than a bladder that has just entered dysfunction. This is subscribed by data from pre-natal de-obstruction performed in fetal sheep [4, 5]. In clinical practice urodynamic investigations are insufficient to predict the ability of the bladder to rehabilitate after de-obstruction [6]. Previously we have simulated this problem in an animal model where the complete urodynamic function of a bladder was followed both during BOO and during a period after removal of the obstruction. The severity of bladder damage can be exactly described on basis of the complete data set from both periods [7]. However, when blinded to the developments that occurred during obstruction and relying only on one urodynamic

measurement, it is impossible to distinguish a bladder that just entered the path of functional loss from a bladder that is close to decompensation.

One way of revealing the history of bladder dysfunction may be analysis of the bladder structure. The tissue of a bladder will have adapted to its previous dysfunction. For instance, it is well known that high bladder pressure induces adaptive changes in the bladder structure [8] that in the long term are visible as muscle enlargement [9,10] and collagen deposition. Other studies have shown that ischemia in the bladder wall may enhance bladder dysfunction [11, 12]. Glycogen deposition may be a marker for this. During ischemia glycogen is used as an alternative energy supplier [13]. Upon chronic ischemic periods the bladder may adapt to this by increasing the amount of glycogen stored in muscle cells. We previously examined the intensity of glycogen deposition in the tissue from guinea pigs that had surgically induced PBOO for various periods of time [14]. We found that an increase in glycogen deposits correlated with an increase in bladder abnormality: decreasing compliance and increasing bladder contractility, pressure at maximum flow and the number of unstable contractions. This was true for the situation at the time of tissue collection. Interestingly, an even better correlation of the glycogen score was found with the degree of bladder dysfunction previous to the time of tissue collection. When comparing a bladder that had just started to deteriorate to a bladder that was near decompensation, both could not be definitely distinguished from each other on basis of their end-point function. They did, however, differ greatly in PAS staining intensity. This raised the hope that analysis of the bladder structure and more specifically the glycogen content can be used in the prognosis of functional recovery after removal of an obstruction.

Here we studied how detrusor glycogen content changes after removal of a urethral obstruction: it may either reflect historic urodynamic function before de-obstruction or it may reflect bladder function measured after de-obstruction. In addition we established how the changes in bladder function after de-obstruction relate to the degree of glycogen deposition at the time of de-obstruction.

Materials and Methods

Tissue collection

Bladder tissue was obtained from our PBOO animal model using guinea pigs. The model was extensively described in previous articles [15, 16]. In short, with surgery a partial outlet obstruction was created by placing a silver ring around the urethra. The ring causes fibrosis on the outer side of the urethra. This fibrosis, together with the ring, restricts the normal expansion of the urethra as urine is pushed through by bladder contraction, hence a partial obstruction. Bladder pressure was measured through a suprapubic bladder catheter and urine flow rate was measured by means of

an ultrasound flow probe attached loosely around the penis. From the measured pressure/flow data the number of unstable contractions (NUC), bladder pressure at maximum flow rate (pQ_{\max}), contractility (W_{\max}) and compliance (ml H₂O/ cm H₂O) were calculated. Compliance was calculated as Δ infused volume/ Δ bladder pressure. Contractility was calculated according to Griffith et al. [17]. An unstable contraction was defined as a contraction with a bladder pressure of >10 cm H₂O (one-third of the average normal voiding pressure in our animals) unaccompanied by actual bladder emptying.

To achieve different levels of functional changes upon PBOO, we applied different time-periods of obstruction [7]. This previous study showed that although the level of functional changes is related to the length of the obstructive period individual variation in the response to PBOO does occur. Since each animal was urodynamically monitored each week, the rate of functional changes rather than the duration of obstruction was used as measure to decide the time of sacrifice. Therefore we have also chosen to correlate the urodynamic changes as a variable to structural changes reflected by the glycogen scores. This monitoring also prevented appearance of uremic conditions after complete obstruction since this would have been detected in time.

At different levels of functional changes the silver ring was surgically removed. This allowed the urethra to extend again. Bladder functional monitoring with urodynamic measurements continued. At a maximum of 11 weeks after de-obstruction

Bladder tissues were snap-frozen and stored at -80°C until use. Approximately half of each bladder tissue was later fixated in 10% buffered formalin (pH 7.4) and embedded in paraffin for sectioning. Cross-sections of 4 μm covering all bladder wall layers were made for staining with periodate acid Schiff's protocol (PAS). Tissues from 10 sham / control animals and 28 obstructed & de-obstructed animals were used, in total 38.

Histochemical stains

The PAS stain is a routine procedure to visualize sugar moieties. It gives insight into the general structure, comparable to a Haematoxylin - Eosin stain, combined to specific insight into granular glycogen deposits. The number of stained granules was counted and scored. Three researchers scored the bladder sections in a blinded fashion. The obtained glycogen score ranged from 0, no staining of glycogen granules to 3, the most intense staining. Previously we found that an increase in glycogen score coincided with a change in the location of deposition, from only the serosal side at a score of 1 to increasingly throughout the muscle at score 2 and intense staining up to the urothelium at the score of 3 [14]. In this study the scoring was therefore based on both the intensity and the distribution of glycogen granules. Thus we obtained four "glycogen score" groups that were then analyzed for differences in bladder function.

Graphs and statistics

Our hypothesis was that the glycogen scores reflect functional changes upon PBOO even after a time of de-obstruction. Therefore, urodynamic variables were plotted at three different periods during the experiment and compared to the glycogen scores. The highest achieved values for all urodynamic variables are measured in the weeks of obstruction to indicate how extreme the changes were for each variable. This was intended to provide information on whether tissue composition reflected the history of bladder function. Next to that the urodynamic variables measured at the time of de-obstruction and immediately before harvesting the tissue, termed the 'end-stage' urodynamic variables, are plotted. With this approach a clear insight in the glycogen scores being representative for bladder functional changes during obstruction could be gained.

The distribution of most of the urodynamic variables was skewed due to some very low or high values from individual animals. The data are therefore best plotted in box-whisker plots that visualize the distribution within data and instead of averages and standard deviations show median values together with the 5%, 25%, 75% and 95% percentiles. In the box whisker plots a bar represents the median and is surrounded by respectively a box of which the bottom denotes the 25% and the top the 75% percentiles and whiskers at the 5% (bottom) and 95% (top) percentiles. Note that although outliers are not shown in the box whisker plot when they are outside the 5th or 95th percentile they do contribute in the statistical analysis.

We tested if the four glycogen score groups (0, 1, 2 and 3) differed in:

- The urodynamic variables at end-stage (also being the day of tissue collection).
- The urodynamic variables at de-obstruction.
- The highest achieved values during the obstructive period.
- The recovery of urodynamic variables after de-obstruction.

The Mann Whitney U-test was used to determine the significance ($p < 0.05$) of differences in urodynamic values between the group with glycogen score 0 and the other glycogen score groups. The Wilcoxon Signed Ranks test was used to determine the significance ($p < 0.05$) of differences between urodynamic values measured at de-obstruction and end-stage urodynamics within each glycogen score group. All data analysis was performed in SPSS, release 12.0.1, Chicago, Illinois, US.

Results

Examples of a glycogen score 0 and 3 with inserts of a close-up of a glycogen granule staining are shown in figure 1. Each granule represents a glycogen deposit. The variance of scoring of glycogen by three co-workers was on average 0.38 (standard deviation). The difference between scoring of the three co-workers of one section was never larger than one score.

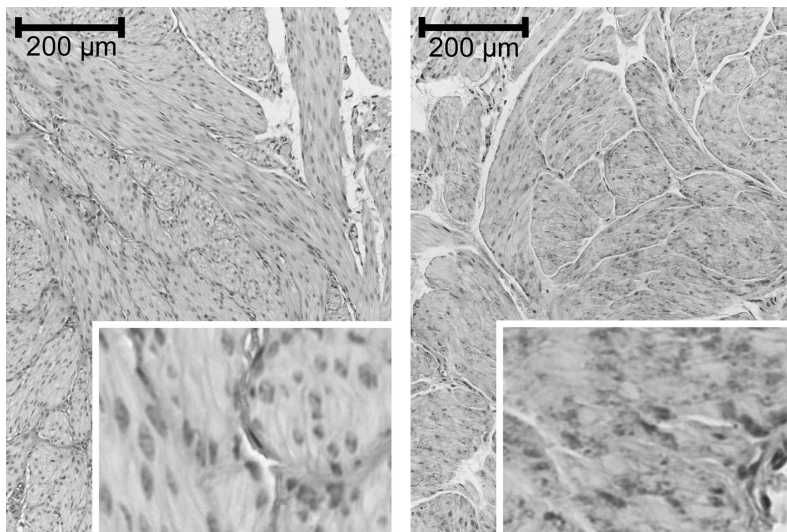


Figure 1:
Example of PAS stains of bladder detrusor layer with score 0 (left) and 3 (right). Bar = 200 µm. Inserts are 4x enlargements.
Color image: see appendix.

The effect of individual variation in the response upon placement of PBOO is visible in our present data. As table 1 shows, the mean glycogen score increases with increasing duration of obstruction but the ranges of the obstructive periods for the several glycogen score groups show a large overlap.

Glycogen score	0	1	2	3
Sham / control animals	8	2	0	0
Treated animals	2	10	11	5
Weeks obstruction, range (mean)	2, 4*	0 – 10 (6)	3 – 10 (7)	8 – 17 (11)
Weeks de-obstruction, range (mean)	3, 9*	0 – 8 (4)	4 – 11 (7)	3 – 8 (6)
total	10	12	11	5

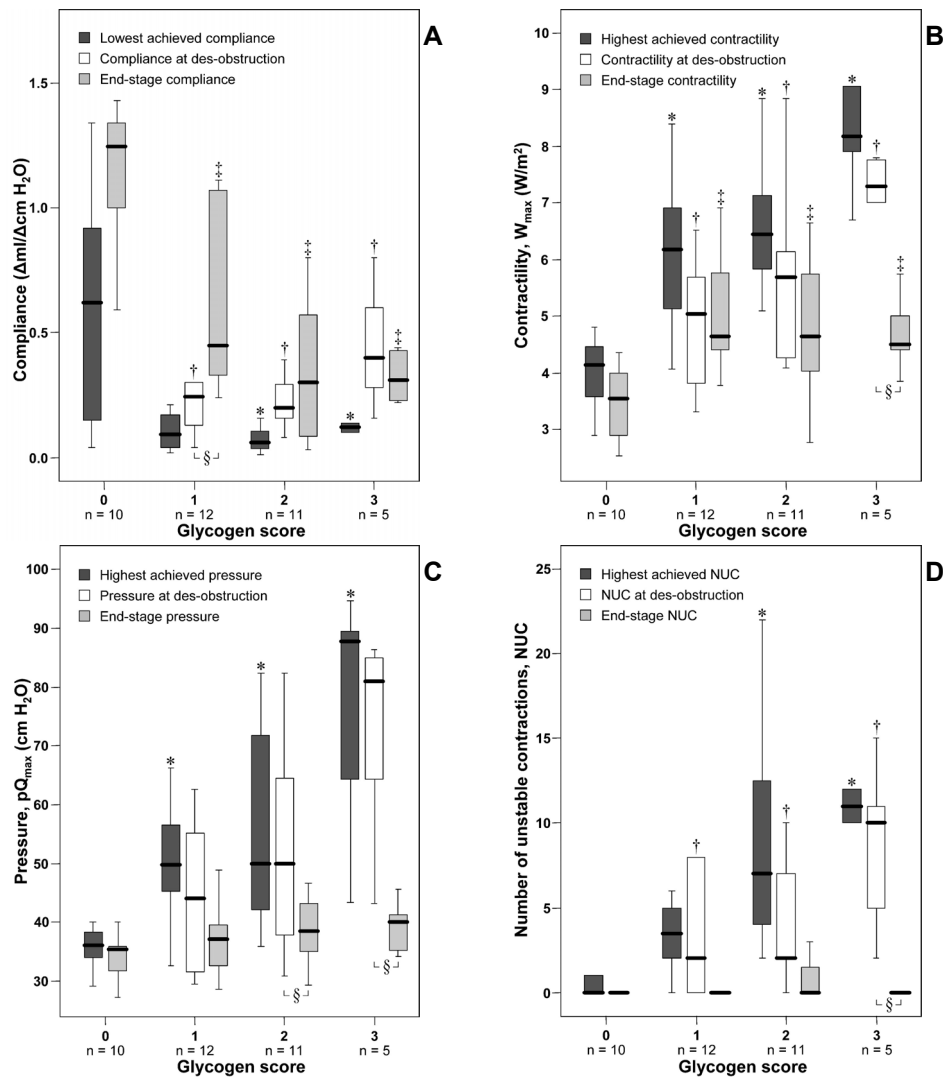
Table 1

* Values for the two individual animals.

The sham-operated animals did not undergo de-obstruction. Thus their data was removed from the calculations below when values for the day of de-obstruction in the different groups were compared. Ideally, all urodynamic variables at de-obstruction and at end-stage for glycogen scores 1, 2 and 3 should be compared to the urodynamic variables at de-obstruction and at end-stage for glycogen score 0. However, since 8 out of the 10 animals in the glycogen score group 0 were sham-operated, no good statistical comparison for urodynamic variables at de-obstruction between score 0 and the scores at 1, 2 and 3 could be made. Therefore, urodynamic variables at de-obstruction and at end-stage for glycogen scores 1, 2 and 3 were only compared to the end-stage urodynamic variables at score 0.

Glycogen scores vs. urodynamic variables at end-stage.

Comparison of the end-stage urodynamics from the glycogen score 0 group to the end-stage urodynamics of glycogen score 1, 2 and 3 groups tests to what extent normalization of bladder function after de-obstruction is accompanied by structural changes.

**Figure 2**

A: Box-whisker plots of correlation between glycogen scores and compliance. Dark grey bars represent the lowest achieved compliance in history, white bars the compliance at the time of des-obstruction and light grey bars the end-stage compliance. * Denote $p < 0.05$ to lowest achieved compliance at glycogen score 0, † and ‡ denote $p < 0.05$ to end-stage compliance at glycogen score 0 for compliance at des-obstruction and end-stage compliance respectively, § denote $p < 0.05$ between compliance at the time of des-obstruction and end-stage compliance.

B: Box-whisker plots of correlation between glycogen scores and contractility. Dark grey bars represent the highest achieved contractility in history, white bars the contractility at the time of des-obstruction and light grey bars the end-stage contractility. * Denote $p < 0.05$ to highest achieved contractility at glycogen score 0, † and ‡ denote $p < 0.05$ to end-stage contractility at glycogen score 0 for contractility at des-obstruction and end-stage contractility respectively, § denote $p < 0.05$ between contractility at the time of des-obstruction and end-stage contractility.

C: Box-whisker plots of correlation between glycogen scores and pressure. Dark grey bars represent the highest achieved pressure in history, white bars the pressure at the time of des-obstruction and light grey bars the end-stage pressure. * Denote $p < 0.05$ to highest achieved pressure at glycogen score 0, † and ‡ denote $p < 0.05$ to end-stage pressure at glycogen score 0 for pressure at des-obstruction and end-stage pressure respectively, § denote $p < 0.05$ between pressure at the time of des-obstruction and end-stage pressure.

D: Box-whisker plots of correlation between glycogen scores and NUC. Dark grey bars represent the highest achieved NUC in history, white bars the NUC at the time of des-obstruction and light grey bars the end-stage NUC. * Denote $p < 0.05$ to highest achieved NUC at PAS score 0, † and ‡ denote $p < 0.05$ to end-stage NUC at glycogen score 0 for NUC at des-obstruction and end-stage NUC respectively, § denote $p < 0.05$ between NUC at the time of des-obstruction and end-stage NUC.

The end-stage compliance at glycogen scores 1, 2 and 3 (figure 2a) was significantly lower than the end-stage compliance at glycogen score 0 ($p < 0.05$).

The end-stage values for contractility (figure 2b) were significantly higher for the glycogen score 1, 2 and 3 groups as compared to the value for the glycogen score 0 group ($p < 0.05$). Between these three groups they did not differ significantly.

At end-stage the pressure was similar in all four glycogen score groups and within the normal ranges of bladder pressure during voiding (figure 2c).

End-stage values for NUC were similar at all glycogen scores (figure 2d).

Glycogen scores vs. urodynamic variables at de-obstruction.

Comparison of the end-stage urodynamics from the glycogen score 0 group to the urodynamics at de-obstruction from the glycogen score 1, 2 and 3 groups tests the opposite of the previous comparison; does the bladder structure correlate to bladder function before de-obstruction.

The glycogen score group 3 had the highest value for NUC at the time of de-obstruction. Compared to the end-stage value of NUC in the score 0 group NUC was significantly higher in all three groups ($p < 0.05$).

The compliance at the time of de-obstruction was significantly lower at glycogen scores 1, 2 and 3 as compared to the glycogen score 0 group at end-stage ($p < 0.05$). The compliance at de-obstruction is higher in the glycogen score 3 group as compared to groups 1 and 2 but this difference is statistically insignificant.

The contractility at the time of de-obstruction was significantly higher for the glycogen score 1, 2 and 3 groups as compared to the end-stage value of the glycogen score 0 group ($p < 0.05$).

The pressure at the day of de-obstruction was higher in the score 1, 2 and 3 groups as compared to the end-stage values for the score 0 group. However, this trend did not reach significance ($p = 0.23$, $p = 0.057$, $p = 0.098$ for groups 1, 2 and 3 respectively).

The relation between the glycogen score of a bladder, measured at end-point and the function of that bladder at de-obstruction shows to what extent the ability of a bladder structure to normalize depends on the functional condition at the time of de-obstruction. For this we used a Wilcoxon signed Ranks test. As is shown in figure 2d, in the glycogen score 3 group the end-stage the value for NUC was significantly lower than the values at de-obstruction. In the glycogen score 1 group the compliance at end-stage was significantly higher than the compliance at de-obstruction ($p < 0.05$) and approaches normal values. At glycogen score 3 the end-stage contractility is significantly lower as compared to the day of de-obstruction ($p < 0.05$). In the score groups 2 and 3 end-stage pressure had decreased significantly as compared to the pressure at the day of de-obstruction.

Glycogen scores vs. the maximum values for the urodynamic variables.

All maximum achieved urodynamics were reached before or at the moment of de-obstruction and therefore resemble the history of a bladder during PBOO. In this comparison we therefore included the data from all animals. The comparison will show if the glycogen score, measured at end-point is related to the historic extremes in bladder function.

Compared to the score 0 group, the highest achieved value for NUC was significantly higher in the score 2 and 3 groups ($p < 0.05$).

The lowest achieved compliance was significantly lower in groups 2 and 3 as compared to the score 0 group, $p < 0.05$. In score group 1 the decrease did not reach statistical significance ($p = 0.06$).

The highest achieved values for the contractility was significantly higher in the score groups 1,2 and 3 as compared to score group 0 ($p < 0.05$).

The highest achieved pressures at glycogen scores 1, 2 and 3 was significantly higher as compared to the highest achieved pressure from the score 0 group ($p < 0.05$).

Discussion

In this study we determined which changes occur in bladder glycogen content after removal of a urethral obstruction and assessed how these changes relate to the historic urodynamic function of the bladder and to its recovery of function after de-obstruction. For this, we related the bladder function during obstruction, at the time of de-obstruction, during de-obstruction and at end-stage after a period of de-obstruction to the degree of glycogen deposition. The maximum achieved values in altered bladder function were used as a measure of the severity of the PBOO induced changes in the history of the bladder. In our previous work we extensively described the accumulation of glycogen as an adequate measure for changes in bladder structure upon PBOO [14]. During obstruction the bladder muscle reduces its own oxygen supply by producing pressures that compress the small blood vessels [18-20]. This prompts parts of the bladder muscle to function anaerobic. The build-up of glycogen stores is witness to this. Based on the combination of the intensity and the location of the glycogen staining four glycogen score groups could be distinguished, from 0 (absent) to 3 (strongest). Most bladder tissues from sham-operated and control animals scored as 0, only two samples as 1. A glycogen score of 1 may denote the beginning of ischemic conditions. On average, this group had endured the shortest period of PBOO. However, in some animals glycogen deposition occurred only after a prolonged period of PBOO. This underscore the relevance of obtaining a marker that reflects the severity of the obstructive changes better than the duration of obstruction alone. The finding that the first small deposition occurred close to the serosal side of the detrusor layer may have an anatomical reason. These areas are farthest away from

the blood supply out of the lamina propria and therefore will be the first to experience disturbances of the supply. A glycogen score of 2 may represent progressive ischemic conditions. The glycogen deposits cover larger areas within the detrusor layer but these are mostly still close the serosa. Also, there is local variation with muscle bundles containing large deposits of glycogen next to bundles without such deposits. A glycogen score of 3 showed glycogen accumulation throughout the whole detrusor layer. Some areas were less dense with glycogen than others but all tissues showed large amounts of glycogen close to the lamina propria and urothelium. In our set-up strong glycogen deposition was still found some time after removal of the obstruction. The period of monitoring after de-obstruction varied from two to eleven weeks. Whether the glycogen deposition will reduce after longer periods of recovery cannot be concluded. There appears to be a slow trend for reduction as the glycogen scores in animals who were allowed a recovery period after obstruction tended to be lower than the glycogen scores that we previously reported [14] for animals who had the same duration of obstruction but without a recovery period. A few animals that expressed mild urodynamic changes after a short period of PBOO regained normal bladder function rapidly and needed no further monitoring. But most animals with more severe historic changes in bladder function were monitored longer as bladder function did not regain normal function, at least during the time of follow-up after de-obstruction. Despite this variation in follow-up time a clear correlation between glycogen scoring and all maximum achieved urodynamics during PBOO was found. This correlation was also found in our study of glycogen score after PBOO alone [14]. We also tested for each glycogen score group (except glycogen 0) if end-stage urodynamic variables were significantly changed from these variables at the time of de-obstruction. In the glycogen score 1 group only the compliance showed a significant difference between the end-stage value and the value at the time of de-obstruction ($p < 0.05$), becoming normal again. The other urodynamic values show a trend for improvement but the changes are not significant and occur within the normal ranges. In the glycogen score 2 and 3 groups the end-stage compliance values are almost similar to the compliance values at the time of de-obstruction. In the glycogen score 3 group there even is an, insignificant, trend for further decline. From these findings we want to conclude that little glycogen deposition prognoses a good recovery of bladder compliance.

After de-obstruction instability largely disappears from most animals. The instability at end-point thus yields no information on the burden of instability that an individual bladder experienced during its obstructive period. The glycogen score, however, does reveal the history of instability, being highest in animals with the most severe history of NUC.

High pressures at the time of de-obstruction as well as the highest achieved pressure at all glycogen scores more than doubled at glycogen score 3 compared to normal

values. But at end-stage bladder pressure at all glycogen scores was statistically similar, because the outflow resistance has been minimized.

After de-obstruction the contractility decreases in all animals, significant only in the glycogen score 3 group. However, at end-stage it remains elevated compared to the sham operated animals and furthermore reaches similar values in all animals. Here also the glycogen score is the only indicator of the situation before de-obstruction. The glycogen score 3 group had the history of the highest contractility values.

In our envision the glycogen scoring may ultimately become a clinical tool in assessing the level of functional changes before the first urodynamic measurement and may also provide insight in functional development between two measurements for follow-up. Combined with urodynamic measurement a clear insight in history and actual condition of bladder function is obtained.

Basic research on the molecular level such as gene expressions of TGF-beta and many other biochemical compounds that have a role in one of the regulatory pathways are nowadays a major topic in bladder outlet obstruction research. This is one of the many subjects in future investigation for basic knowledge and for designs of new targets of (pharmalogical) treatment. Our direct focus for further investigation is aimed at developing the glycogen scoring as a clinical tool by non-destructive fiber optic techniques such as Raman spectroscopy.

Conclusion

The glycogen content in a bladder during obstruction correlated directly with high pressures during voiding, instabilities, lowered compliance and a high contractility. In contrast, the bladder glycogen content was not related to the function of the bladder after de obstruction, except for a relation between high glycogen content and continuing low compliance. In conclusion, the glycogen content of a bladder is a clear marker of the severity of functional changes that bladder has undergone in its history and this is true also after a period of recovery.

These findings may have direct impact on clinical monitoring of bladder function. Patients who were subjected to urodynamic measurements after valve ablation or bladder treatment for e.g. spina bifida may exhibit improved bladder function but have nevertheless developed a decompensated bladder later on. Analyzing the amount of glycogen deposits by glycogen scoring may give insight in the severity of bladder damage and thereby contribute in making an accurate prognosis of bladder function. However, for *in vivo* diagnostic applications the structural analysis should be non-destructive, thus without the need for biopsies. Earlier we have shown the use of Raman spectroscopy to detect both collagen infiltration and glycogen accumulation in bladder tissues with partial outlet obstruction *in vitro* [21]. Recent developments in the fiber-optic Raman spectroscopic technology would make this *in vivo* non-destructive structural analysis possible [22].

Acknowledgements

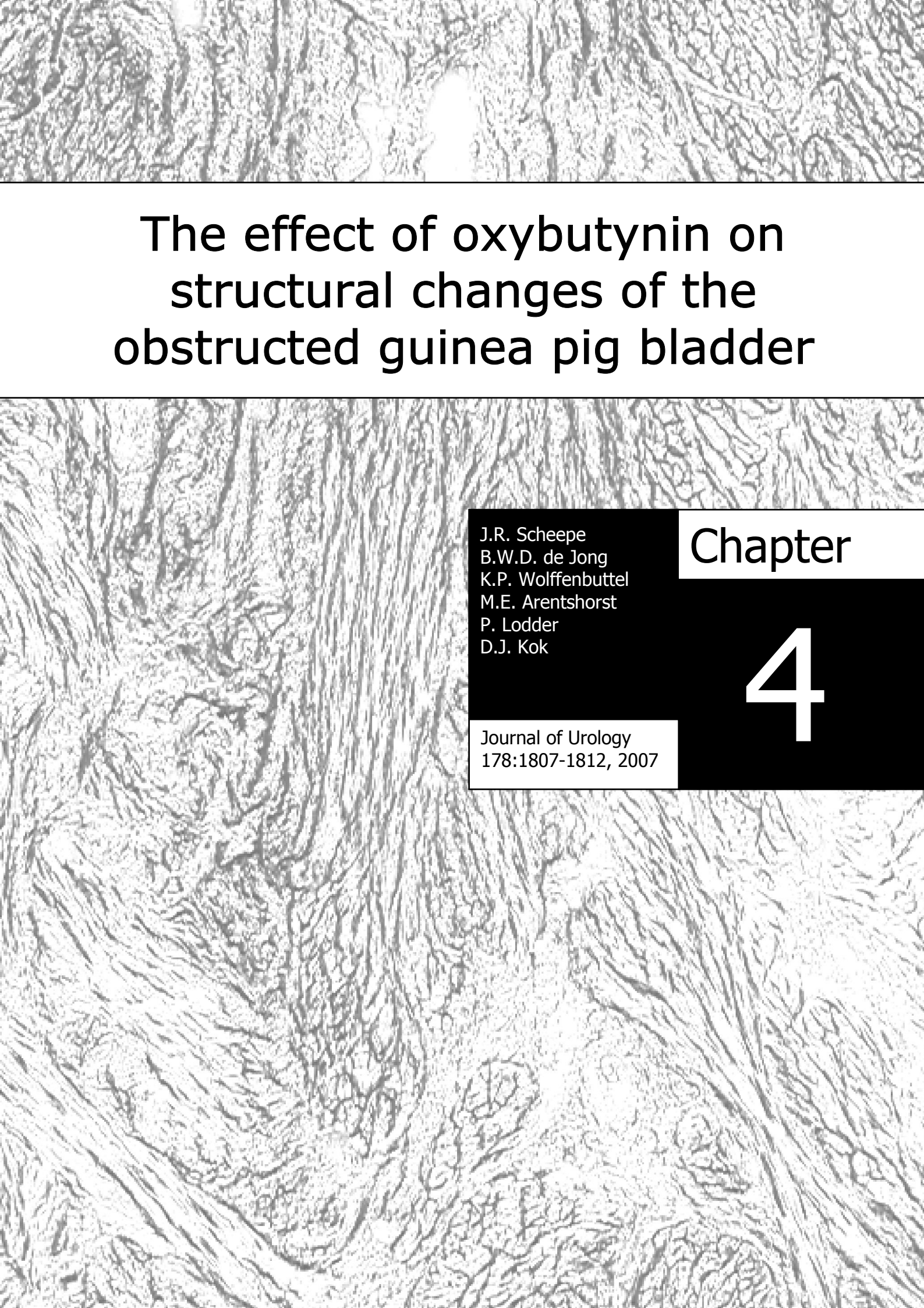
This study was supported by the Dutch Kidney Foundation, grant C03.2070.

The authors like to thank the co-workers at the department of Urology, sector FUIRORE, for their help during the experiments.

References

1. Yohannes P, Hanna M. Current trends in the management of posterior urethral valves in the pediatric population. *Urology* **60**:947-953, 2002.
2. Mishra SC. Can urodynamic studies be dispensed with in the initial urologic management of children with meningomyelocele? A study of 30 cases and review of the literature. *J Pediatric Urol* **3**:195-199, 2007.
3. Wen JG, Li Y, Wang QW. Urodynamic investigation of valve bladder syndrome in children. *J Pediatric Urol* **3**:118-121, 2007.
4. Farrugia MK, Long DA, Godley ML, Peebles DM, Fry CH, Cuckow PM, Woolf AS. Experimental short-term fetal bladder outflow obstruction: I. Morphology and cell biology associated with urinary flow impairment. *J Pediatric Urol* **2**:243-253, 2006.
5. Farrugia MK, Godley ML, Woolf AS, Peebles DM, Cuckow PM, Fry CH. Experimental short-term partial fetal bladder outflow obstruction: II. Compliance and contractility a urinary flow impairment. *J Pediatric Urol* **2**:254-260, 2006.
6. Ghanem MA, Wolffenbuttel KP, De Vylder, Nijman RJ. Long-term bladder dysfunction and renal function in boys with posterior urethral valves based on urodynamic findings. *J Urol* **171**:2409-2412, 2004.
7. Wolffenbuttel KP, de Jong BWD, Scheepe JR, Kok DJ. Potential for recovery in bladder function after removing a urethral obstruction. *Neurol Urodyn*, accepted for publication.
8. Lee SD, Akbal C, Jung C. Intravesical pressure induces hyperplasia and hypertrophy of human bladder smooth muscle cells mediated by muscarinic receptors. *J Pediatric Urol* **2**:271-276 2006.
9. Deveaud CM, Macarak EJ, Kucich U, Ewalt DH, Abrams WR, Howard PS. Molecular analysis of collagens in bladder fibrosis. *J Urol* **160**:1518-1527, 1998.
10. Lee SD, Akbal C, Miseeri R. Collagen prolyl 4-hydroxylase is up-regulated in an acute bladder outlet obstruction. *J Pediatric Urol* **2**: 225-232, 2006.
11. Saito M, Yokoi K, Ohmura M, et al. Effect of ischemia and partial outflow obstruction on rat bladder function. *Urol Res* **25**:207-211, 1997.
12. Azadzoi KM, Tarcan T, Kozlowski R, Krane RJ, Siroky MB. Overactivity and structural changes in the chronically ischemic bladder. *J Urol* **162**: 1768-1778, 1999.
13. Pessina F, Solito R, Maestrini D, Gerli R, Sgaragli G. Effect of anoxia-glucopenia and re-superfusion on intrinsic nerves of mammalian detrusor smooth muscle: importance of glucose metabolism. *Neurourol Urodyn* **24**: 389-396, 2005.
14. De Jong BWD, Wolffenbuttel KP, Arentshorst ME, Lodder P, Kok DJ. Detrusor glycogen reflects the functional history of bladders with partial outlet obstruction. *BJU Int* **100**:846-52, 2007.
15. Kok DJ, Wolffenbuttel KP, Minekus JP, van Mastrigt R, Nijman JM. Changes in bladder contractility and compliance due to urethral obstruction: a longitudinal followup of guinea pigs. *J Urol* **164**: 1021-1024, 2000.
16. Wolffenbuttel KP, Kok DJ, Minekus JP, van Koeveeringe GA, van Mastrigt R, Nijman JM. Urodynamic follow-up of experimental urethral obstruction in individual guinea pigs. *Neurourol Urodyn* **20**: 699-713, 2001.

17. Griffiths DJ, Constantinou CE, van Mastrigt R. Urinary bladder function and its control in healthy females. *Am J Physiol* **251**:R225–R230, 1986.
18. Azadzoï KM, Pontari M, Vlachiotis J, Siroky MB. Canine bladder blood flow and oxygenation: changes induced by filling, contraction and outlet obstruction. *J Urol* **155**:1459-1465, 1996.
19. Greenland JE, Hvistendahl JJ, Andersen H, Jørgensen TM, McMurray G, Cortina-Borja M, Brading AF, Frøkiaer J. The effect of bladder outlet obstruction on tissue oxygen tension and blood flow in the pig bladder. *BJU Int* **85**: 1109–1114, 2000.
20. Greenland JE, Brading AF The effect of bladder outflow obstruction on detrusor blood flow changes during the voiding cycle in conscious pigs. *J Urol* **165**:245-248, 2001.
21. De Jong BWD, Bakker Schut TC, Coppens J, Wolffenbuttel KP, Kok DJ, Puppels GJ. Raman spectroscopic detection of changes in molecular composition of bladder muscle tissue caused by outlet obstruction. *Vibrational Spectroscopy* **32**:57-65, 2003.
22. Santos LF, Wolthuis R, Koljenović S, Almeida RM, Puppels GJ. Fiber-optic probes for in vivo Raman spectroscopy in the high-wavenumber region. *Anal Chem* **77**:6747-6752, 2005.

A grayscale microscopic image of bladder tissue, showing a complex network of fibers and cellular structures. The image is used as a background for the chapter title and authors.

The effect of oxybutynin on structural changes of the obstructed guinea pig bladder

J.R. Scheepe
B.W.D. de Jong
K.P. Wolffenbuttel
M.E. Arentshorst
P. Lodder
D.J. Kok

Chapter

4

Journal of Urology
178:1807-1812, 2007

Abstract

Purpose: Oxybutynin is used clinically to lower intravesical pressure (P) and detrusor overactivity (DO). In vitro it inhibits stretch-induced bladder smooth muscle cell proliferation. We tested if Oxybutynin also prevents hypertrophic bladder changes in vivo in a model of partial bladder obstruction.

Materials and Methods: Subvesical obstruction was induced in immature guinea pigs by a silver ring around the urethra. 8 animals received Oxybutynin, 0.4 mg/b.w./day in 2 doses. Control groups were: obstructed without oxybutynin treatment or sham operated. Urodynamic pressure flow studies were performed at 1-week intervals for 10 weeks in all animals under anesthesia with ketamine/xylazine. After 10 weeks the animals were sacrificed and the bladder was removed for structural analysis with a PAS-stain in which also the number of glycogen granules was scored as a measure for previous ischemia.

Results: Compared to the sham group, obstructed animals have a significantly higher P and DO, a lower compliance and increased contractility. Obstructed animals that receive oxybutynin retain a normal P, DO and compliance. Their bladder contractility increases like in obstructed animals. The Oxybutynin group showed less collagen infiltration in the detrusor and fewer glycogen granules compared to the obstructed animals.

Conclusions: Our results demonstrate that Oxybutynin has a protective effect on bladder function and structure. Prevention of hypertrophic and ischemic bladder changes is an argument for an early start of Oxybutynin treatment in children with inborn neurogenic bladder dysfunction like spina bifida or in patients with urethral valves.

Introduction

Anticholinergics in combination with clean intermittent catheterisation (CIC) are the mainstays in the current treatment of neurogenic bladder dysfunction [1,2], a disease often characterized by detrusor overactivity (DO) and functional bladder outlet obstruction (BOO) (detrusor-sphincter-dyssynergia). Antimuscarinic drugs like Tolterodin or Oxybutynin suppress DO and partly lower intravesical pressure. This, in combination with CIC usually results in a low-pressure system preserving renal function. Also in non-neurogenic BOO (e.g. posterior urethral valves) a combination of detrusor hypertrophy, DO, a low compliance bladder and high intravesical pressure is encountered. With current treatment progression of smooth muscle cell hypertrophy and bladder wall fibrosis is still common. To prevent the last treatment option, invasive surgery including bladder augmentation or any form of urinary diversion, and its associated complications a better understanding of the road to the end stage bladder and of the way that compounds like Oxybutynin interfere is needed.

From literature [3-6] the following is known: An obstructed bladder increases its muscle volume to produce the higher pressure needed to overcome the obstruction. This muscle hypertrophy is accompanied by collagen deposition and may end in a thick-walled high pressure bladder. After this stage the bladder may reverse in strength and mass. At some point intrinsic bladder wall processes start to drive hypertrophy. The start may be reduction of bladder blood flow by the high bladder pressure, inducing local hypoxia [7, 8] and activating anaerobic detrusor function [9,10]. Chronic hypoxia induces hyper-excitation of the afferent nerves that are involved in DO [11], fibrosis, collagen deposition, and glycogen storage [11-16].

In vitro relaxation of bladder smooth muscle by the anticholinergic agent Oxybutynin [15] or the smooth muscle cell relaxant nitric oxide inhibits stretch-induced bladder smooth muscle cell proliferation [15, 17].

This effect of Oxybutynin has not been studied in vivo yet. Here we evaluated the effect of Oxybutynin on bladder structure, with emphasis on signs of hypoxia, in a Guinea pig model of partial bladder obstruction and related this effect to longitudinally followed bladder function.

Materials and Methods

The Guinea pig model for gradual urethral obstruction as described by Wolffenbuttel et al [6,7] was used. Immature male albino Guinea pigs, Hartley strain, weighing approximately 250 g were used.

Study design

Data is obtained from each animal every week. Analysis of the response to obstruction and treatment is based on individual longitudinal data. In the reference groups (sham operated and obstructed) this availability of longitudinal data in individual animals allowed us to sacrifice animals and obtain tissue at variable end-points. Consequently, the number of animals in these groups decreases during the experiment. The size of the Oxybutynin group did not allow this division over time-end points. Thus these were all followed for 10 weeks and sacrificed at the same end point.

The sham group consisted of 9 animals that were sham-operated and two animals that were not operated. Seven animals underwent weekly urodynamic studies for up to nine weeks. Four animals were measured with a lower frequency. The animals were sacrificed at different time points. From week 0 (pre-obstruction) to week 9 the number of animals included in the analysis thus was: 11, 10, 10, 8, 3, 3, 6, 7, 4, 2. Each obstructed/ Oxybutynin treated animal also has as individual reference the initial measurement before placing the obstruction.

Obstructed group

93 Animals received an obstruction after their first urodynamic evaluation at day 0 and were measured weekly or bi-weekly thereafter. From week 0 to week 10 the number of analysed obstructed animals was: 93, 66, 76, 61, 55, 47, 46, 26, 14, 14, 11. In the staining procedures the tissue from the group of 11 animals that completed 10 weeks of obstruction was compared to tissue from sham-operated animals and Oxybutynin treated animals (that also had 10 weeks of obstruction).

Oxybutynin group

Eight animals were obstructed and received Oxybutynin from that moment on for a period of 10 weeks. Two animals were taken out of the experiment the first week (discomfort due to operation wound) respectively the 5th week (failure to thrive). Only the remaining 6 animals were used for the analysis. (Up to the point that the 2 animals were removed from the study their urodynamic parameters did not differ from the rest of the group but all their data was excluded). The applied dosage of Oxybutynin was 0.4 mg/kg/ day divided over 2 doses.

Urodynamic Procedure [6,7]

The animals were anesthetized using ketamine (43 mg/kg i.m.) and xylazine (0.9 mg/kg i.m.). Through a 24-gauge suprapubic catheter bladder pressure was measured and the bladder was filled continuously with sterile saline at a rate of 0.23 mL per minute. Flow rate was measured with an ultrasound transducer (T106 small animal Flow meter, Transonic Systems, Ithaca, NY) around the penis. The volume voided was collected in tubes and used to calibrate the flow-rate signal of each voiding. After the last voiding the residual fluid was measured.

Operative Procedure

Under ketamine/xylazine anesthesia the peritoneal cavity was accessed via a lower vertical midline abdominal incision. A silver jeweler's jump ring, internal diameter 2.2 mm, was placed around the bladder neck above the prostate.

End-Point Procedure

After the final urodynamic study the animal was sacrificed and the bladder was removed immediately. Part was snap-frozen and stored at -80°C , part was fixated in 10% buffered formalin (pH 7.4) and embedded in paraffin.

Calculations

Detrusor overactivity (DO) was assessed visually as the number of detrusor contractions of 10 cm H₂O (one third of the mean voiding pressure at week 0) without urine-flow during the filling phase. The maximum flow rate [Q_{\max}], the associated bladder pressure [$p_{\det}Q_{\max}$], bladder compliance [ml/ cm H₂O] and bladder contractility [W_{\max}] were calculated from the pressure flow plot (figure 1) as described previously [5,6].

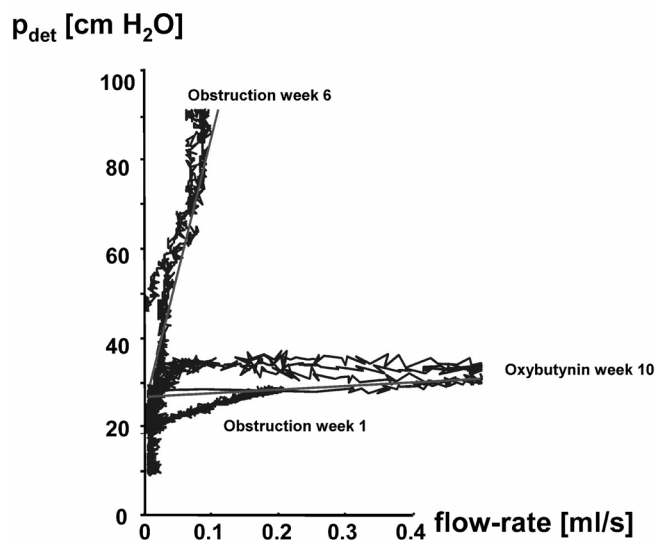


Figure 1

A pressure flow plot showing the relation between the bladder pressure, P_{\det} and the flow-rate, Q . Each curve represents one voiding. After ten weeks of obstruction the curve for the Oxybutynin treated animal is still close to the curve for the untreated animal after 1 week of obstruction.

PAS-stain and PAS-score

Cross-sections of 4 μm covering all bladder wall layers were stained with the periodate acid Schiff's protocol (PAS). This procedure stains sugar moieties to visualize the general structure, figure 2. At what we defined as score 0 linear structures like cell membranes are visible. In the higher scores granular staining appears inside the muscle cells. We counted the number of these granules and the increasing number was defined as score 1, 2 or 3. We observed that concomitant with the increase in number of granules their location changed. At score 1 the granules

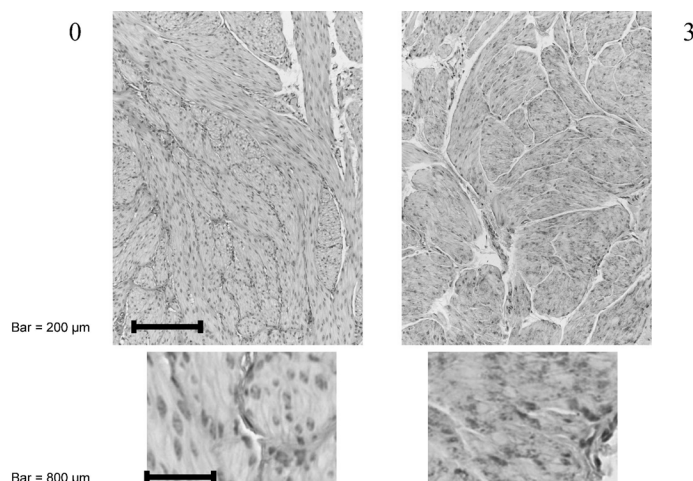


Figure 2

Examples of the lowest PAS score 0, left, and the highest PAS score 3, right. At the PAS score of 0 a distinct line pattern of amongst others membranous staining is visible. At higher scores additional staining occurs in the form of granules, here shown for score 3. At higher magnification, bottom, these granules appear to be located inside the muscle cells.

Color image: see appendix.

were located near the adventitium. At score two they were also found in the middle of the muscle layer and at score 3 they were throughout the muscle up to the urothelium. With biochemical analysis a high count of PAS stained granules in tissue was correlated with a high glycogen content [16]. With Raman spectroscopy we have shown that these granules contain high amounts of glycogen [12].

Elastic von Gieson stain (EVG)

In the EVG procedure collagen stains red, elastin black and the rest of the tissue yellow. Three investigators have visually assessed the percentage of red within the muscle layer and scored this from 1 to 3.

Statistics

All values are expressed as the mean \pm SEM. Statistical significance was determined by two-sided unpaired Student's t-tests with $p < 0.05$ considered statistically significant. Note that because of our specific study protocol the numbers of animals in the comparison changes from week to week (as explained above).

The protocol was approved by the institutional animal care and use committee of the Erasmus University and was in line with guidelines by the EU.

Results

Pressure-flow plots

Figure 1 shows the pressure-flow plots for an obstructed animal and an obstructed/Oxybutynin treated animal. In the obstructed animal bladder pressure increases with duration of the obstruction and urine flow-rate decreases. In the Oxybutynin treated obstructed animal the pressure was only slightly increased after ten weeks and the urine flow-rate was increased greatly.

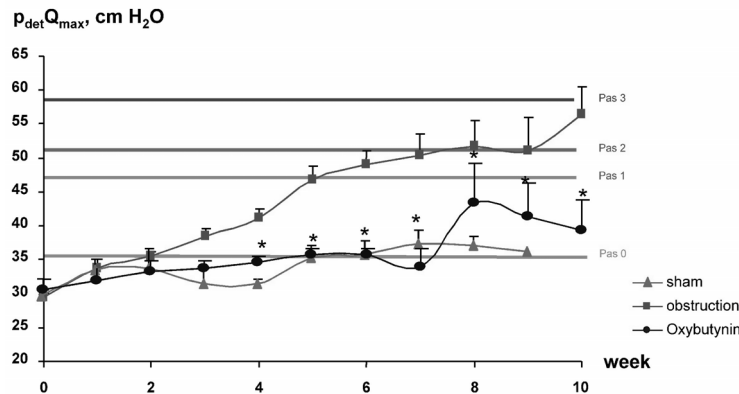


Figure 3

Effect of Oxybutynin on $p_{det}Q_{max}$ during 10 weeks of obstruction. Solid lines represent average $p_{det}Q_{max}$ for animals with PAS score of 0 to 3 respectively. Values on which these lines are based were taken from de Jong et al. [14]. Asterisk indicates significant difference vs obstruction ($p < 0,05$).

Bladder pressure ($p_{det}Q_{max}$)

Compared to the sham group, the $p_{det}Q_{max}$ increases significantly ($p < 0,05$) in the obstructed group, figure 3. In the obstructed animals that received Oxybutynin the $p_{det}Q_{max}$ did not differ from the sham group and was significantly ($p < 0,05$) lower than in the obstruction group.

In a previous publication [14] we have divided the group of obstructed animals according to the PAS score (0,1,2 or 3) of their bladder tissue at end point. The average end point bladder pressure for these PAS score groups is represented in figure 3 as solid lines. For the group with a PAS score of 1 the average end point bladder pressure was 47 cm H₂O. The average bladder pressure in the Oxybutynin group remained below this level all 10 weeks.

In Figure 4 the individual longitudinal data are shown. In 4 out of 6 Oxybutynin treated animals the $p_{det}Q_{max}$ remains close to normal the whole period. Their bladder tissue had a PAS score of 1. In 1 animal there is a transient increase in $p_{det}Q_{max}$ at week 8 up to the level of the obstructed group. In this animal the PAS score was 2. In 1 animal the $p_{det}Q_{max}$ is continuously elevated during the last 3 weeks. In this animal the PAS score was 3.

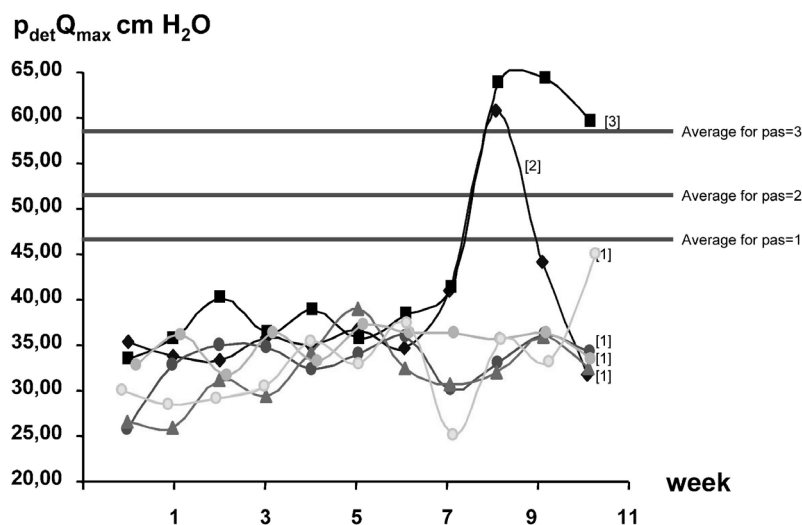


Figure 4

Values of $p_{det}Q_{max}$ in individual oxybutynin treated animals. Each symbol represents individual animal. Solid lines represent average $p_{det}Q_{max}$ for groups with PAS score of 1 to 3 respectively [14].

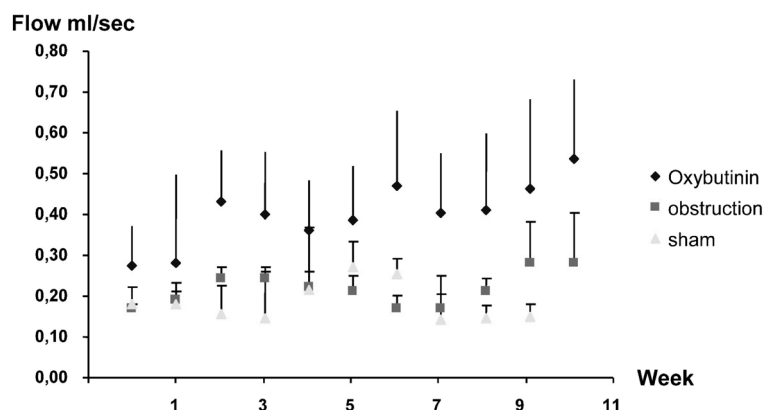


Figure 5
Effect of Oxybutynin on the flow rate during 10 weeks of obstruction.

Urine flow rate

The urine flow-rate was higher in the Oxybutynin group than in the obstructed and sham-operated animals throughout the test period, Figure 5. Compared to the sham group the difference reached significance from week 1 onwards. Compared to the obstructed group, the difference was significant at weeks 2, 3, 5, 6 and 7.

Contractility

Compared to the sham group, bladder contractility increased significantly ($p < 0.05$) in both the obstructed animals and the animals that received Oxybutynin, Figure 6. The latter two did not differ from each other.

Compliance

Bladder compliance in sham-operated animals fluctuates around 1 during the whole study period, Figure 7. In the obstructed animals compliance decreases significantly ($p < 0.05$) compared to the sham group. In the Oxybutynin treated animals compliance remains normal and is significantly higher ($p < 0.05$) compared to the obstruction group.

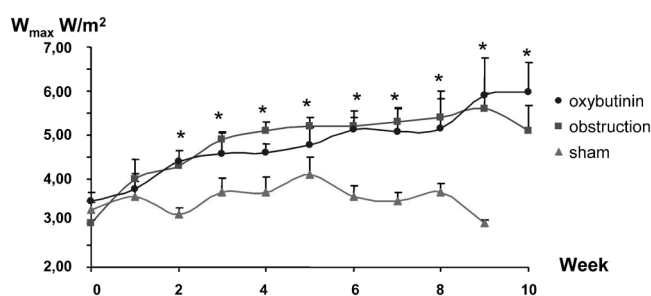


Figure 6
Effect of Oxybutynin on contractility during 10 weeks of obstruction. W_{max} : bladder contractility. Asterisk indicates significant difference treatment vs sham ($p < 0.05$).

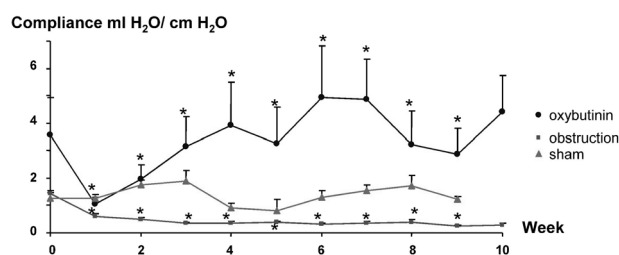


Figure 7
Effect of Oxybutynin on compliance during 10 weeks of obstruction. W_{max} : bladder contractility. Asterisk indicates significant difference treatment vs sham ($p < 0.05$).

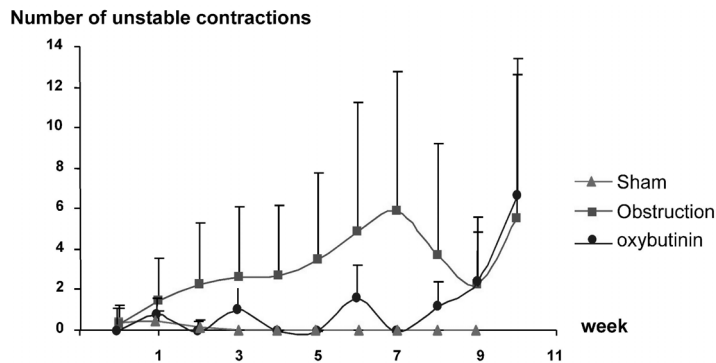


Figure 8
Effect of Oxybutynin on DO during 10 weeks of obstruction.

Detrusor overactivity

In sham-operated animals DO is rare. Obstruction induces DO. This starts the first week after obstruction and increases in severity the following weeks. In obstructed animals receiving Oxybutynin some DO occurs, but significantly less than in the obstructed group. The final weeks DO increases in the Oxybutynin group. This increase is caused entirely by the two animals in which suppression of high bladder pressure fails during those weeks.

EVG

The EVG score for the Oxybutynin treated animals $1,7 \pm 0,2$ was significantly ($p < 0,05$) lower than the score for the animals obstructed 10 weeks $2,4 \pm 0,2$ and significantly higher ($p < 0,05$) than the score for the sham operated animals, $1,1 \pm 0,1$. The Oxybutynin treated animals thus show less collagen infiltration into the bladder muscle.

Discussion

Oxybutynin is a drug with non-specific antimuscarinic properties used in clinic to suppress bladder overactivity in patients with obstructive bladder disease. In our model Oxybutynin prevents obstruction induced increases in bladder pressure and instability and preserves bladder compliance but does not prevent the increase in bladder contractility. Unexpectedly the flow-rate is increased by oxybutynin. The latter may point to some unknown effect on sphincter or urethral relaxation and warrants further investigation.

It was not known what effect long-term Oxybutynin treatment in vivo has on bladder structure. Smooth muscle cells of the bladder respond to mechanical stretch by changes in cell proliferation and protein synthesis [18,19]. It is well documented that several smooth muscle relaxants including Oxybutynin can suppress detrusor muscle cell proliferation in vitro [15]. We show that Oxybutynin also decreases collagen infiltration into the bladder muscle in vivo. Less hypertrophy and less matrix deposition may explain part of the maintenance of a good compliance under Oxybutynin. Improved muscle relaxation during the filling phase could be a second mechanism. We also find that under Oxybutynin treatment less glycogen

accumulation occurs in the muscle cells. This may be a sign that the Oxybutynin treatment has reduced the occurrence of hypoxia in the bladder wall and may be related to the reduction in detrusor overactivity. Several investigators have suggested that a reduced bladder wall blood flow leading to hypoxia links high intravesical pressure to detrusor overactivity [11, 16, 20]. The afferent nerves in the bladder wall that regulate the detrusor overactivity may be damaged by oxidative stress during reperfusion [11]. Muscle cells may reduce the oxidative stress by turning to anaerobic metabolism of glycogen. Bladder muscle cells that more often encounter high bladder pressure for prolonged times have more glycogen stores [16]. In vitro strips of muscle cells that do originally do not express overactivity become overactive when they are first depleted of glycogen. It has previously been shown [12, 16] that granules are stained with a PAS procedure are intracellular glycogen stores. Here we show that during obstruction the guinea pig detrusor cells build up these PAS stained glycogen granules. The obstructed animals that maintain a low bladder pressure, a good compliance and no detrusor overactivity during treatment with Oxybutynin do not show this build-up. In two animals where the suppression of high bladder pressure and overactivity transiently fails glycogen stores the build-up does occur. In the review of Brading [11] it is mentioned that the bladder blood flow completely ceases when bladder pressure exceeds 30 mmHg (=41 cm H₂O). The four animals in our study that have no glycogen build-up all remain below this 41 cm H₂O bladder pressure during the whole period. The two animals that do show glycogen build-up surpass this value. Why the suppression by Oxybutynin fails in these animals is unclear. It may be due to inadequate intake of the drug during several days or to some unknown oxybutynin resistancy. Since the effect is transient in one animal we favour the first explanation. The finding does however highlight the fact that although the bladder in these animals may seem normal at the surface, low pressure, no overactivity, good compliance it can revert to a situation where it damages itself very quickly, probably because of its increased contractility.

During obstruction the bladder contractility increases because more effort is needed to empty the bladder against the obstruction. Obstructed animals that are treated with Oxybutynin show the same increase in contractility, they have to overcome the same obstruction. The increased flow in the Oxybutynin group suggests that there is some overcompensation.

Such an effect could underlie the experience in patients under long-term treatment with Oxybutynin where unexplained sudden deterioration of bladder function can occur. Possibly in these patients the Oxybutynin treatment for some reason, temporarily, fails and the increased contractility of that bladder allows it to produce high pressures that switch on the cycle of reduced blood flow, hypoxia, nerve damage and overactivity. A question for future study is whether treatment with compounds that aim to improve blood microcirculation, as single compound or in combination

with Oxybutynin will keep the bladder wall in better shape and further reduce the chance for ischemia.

Our results demonstrate that Oxybutynin might have a protective effect on bladder function. Prevention of hypertrophic bladder changes related to ischemia is an argument for an early start of Oxybutynin treatment in children with inborn neurogenic bladder dysfunction like spina bifida or in patients with urethral valves.

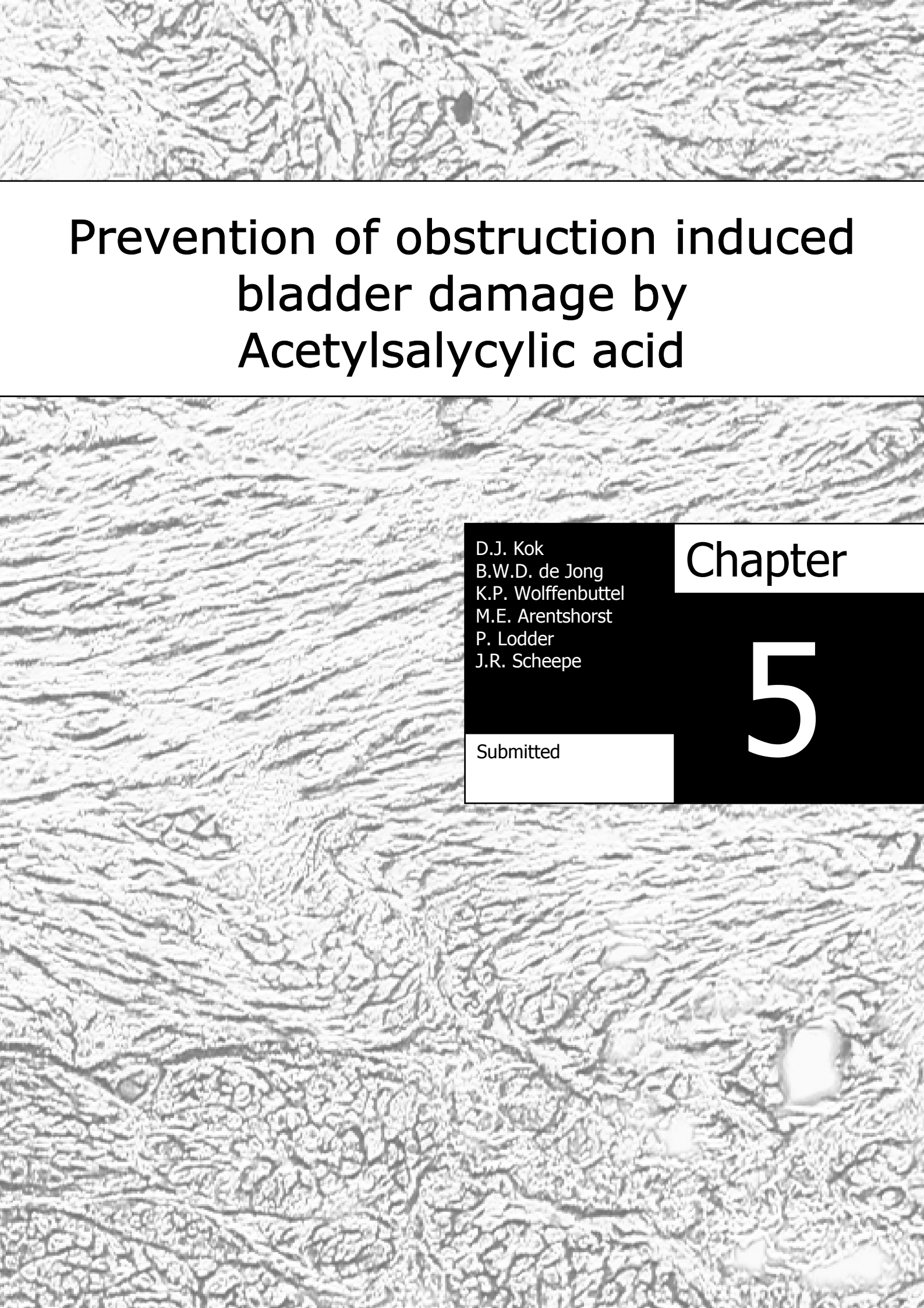
Acknowledgements

This study was supported by the Dutch Kidney Foundation.

References

- 1 Kasabian NG, Bauer SB, Dyro FM, Colodny AH, Mandell J, Retik AB. The prophylactic value of clean intermittent catheterization and anticholinergic medication in newborns and infants with myelodysplasia at risk of developing urinary tract deterioration. *Am J Dis Child* **146**:840-843, 1992.
- 2 Dik P, Klijn AJ, van Gool JD, de Jong-de Vos van Steenwijk CC, de Jong TP. Early start to therapy preserves kidney function in spina bifida patients. *Eur Urol* **49**:908-913, 2006.
- 3 Steers WD, De Groat WC. Effect of bladder outlet obstruction on micturition reflex pathways in the rat. *J Urol* **140**:864-871, 1988.
- 4 Levin RM, Haugaard N, O'Connor L, Buttyan R, Das A, Dixon JS, Gosling JA. Obstructive response of human bladder to BPH vs. rabbit bladder response to partial outlet obstruction: a direct comparison. *Neurourol Urodyn* **19**:609-629, 2000.
- 5 Wolffenbuttel KP, Kok DJ, Minekus JP, van Koevinge GA, van Mastrigt R, Nijman JM. Longitudinal urodynamic follow-up of experimental urethral obstruction in individual guinea pigs. *Neurourol Urodyn* **20**:699-713, 2001.
- 6 Kok DJ, Wolffenbuttel KP, Minekus JP, van Mastrigt R, Nijman JM. Changes in bladder contractility and compliance due to urethral obstruction: A longitudinal followup of guinea pigs *J Urol* **164**:1021-1024, 2000.
- 7 Ghafar MA, Shabsigh A, Chichester P, Anastasiadis AG, Borow A, Levin RM, Buttyan R. Effects of chronic partial outlet obstruction on blood flow and oxygenation of the rat bladder. *J Urol* **167**:1508-1512, 2002.
- 8 Levin RM, O'Connor LJ, Leggett RE, Whitbeck C, Chichester P. Focal hypoxia of the obstructed rabbit bladder wall correlates with intermediate decompensation. *Neurourol Urodyn* **22**:156-163, 2003.
- 9 Kato K, Lin AT, Haugaard N, Longhurst PA, Wein AJ, Levin RM. Effects of outlet obstruction on glucose metabolism of the rabbit urinary bladder. *J Urol* **143**:844-847, 1990.
- 10 Lin AT, Monson FC, Kato K, Haugaard N, Wein AJ, Levin RM. Effect of chronic ischemia on glucose metabolism of rabbit urinary bladder. *J Urol* **142**:1127-1133, 1989.
- 11 Brading A, Pessina F, Esposito L, Symes S. Effects of metabolic stress and ischaemia on the bladder, and the relationship with bladder overactivity. *Scand J Urol Nephrol Suppl* **215**:84-92, 2004.
- 12 de Jong BW, Bakker-Schut TC, Coppens J, Wolffenbuttel KP, Kok DJ, Puppels GJ. Characterization of collagen infiltration by Raman spectroscopy. *Vibrational Spectrosc* **32**: 57-65, 2003.

- 13 Migally N, Tucker A, Zambarnard J. Glycogen localization in pulmonary vascular smooth muscle of chronically hypoxic rats. *J Submicrosc Cytol* **14**:247-252, 1982.
- 14 De Jong BWD, Wolffenbuttel KP, Arentshorst ME, Lodder P, Kok DJ. Detrusor glycogen reflects the functional history of bladders with partial outlet obstruction. *BJU Int* **100**:846-852, 2007.
- 15 Park JM, Bauer SB, Freeman MR, Peters CA. Oxybutynin chloride inhibits proliferation and suppresses gene expression in bladder smooth muscle cells. *J Urol* **162**:1110-1114, 1999.
- 16 Pessina F, Solito R, Maestrini D, Gerli R, Sgaragli G. Effect of anoxia-glucopenia and re-perfusion on intrinsic nerves of mammalian detrusor smooth muscle: importance of glucose metabolism. *Neurourol Urodyn* **24**:389-396, 2005.
- 17 Johansson R, Pandita RK, Poljakovic M, Garcia-Pascual A, De Vente J, Persson K. Activity and expression of nitric oxide synthase in the hypertrophied rat bladder and the effect of nitric oxide on bladder smooth muscle growth. *J Urol* **168**:2689-2694, 2002.
- 18 Adam RM, Eaton SH, Estrada C, Nimgaonkar A, Shih SC, Smith LE, Kohane IS, Bägli D, Freeman MR. Mechanical stretch is a highly selective regulator of gene expression in human bladder smooth muscle cells. *Physiol Genomics* **20**:36-44, 2004.
- 19 Park JM, Borer JG, Freeman MR, Peters CA. Stretch activates heparin-binding EGF-like growth factor expression in bladder smooth muscle cells. *Am J Physiol* **275**:C1247-C1254, 1998.
- 20 Mitterberger M, Pallwein L, Gradl J, Frauscher F, Neuwirt H, Leunhartsberger N, Strasser H, Bartsch G, Pinggera GM. Persistent detrusor overactivity after transurethral resection of the prostate is associated with reduced perfusion of the urinary bladder. *BJU Int* **99**:831-835, 2007.

A grayscale microscopic image of tissue, likely bladder tissue, showing a complex network of cells and fibers. The image is used as a background for the chapter title and author information.

Prevention of obstruction induced bladder damage by Acetylsalicylic acid

D.J. Kok
B.W.D. de Jong
K.P. Wolffenbuttel
M.E. Arentshorst
P. Lodder
J.R. Scheepe

Chapter

5

Submitted

Abstract

Objective: Obstruction induced high-pressure bladder causes bladder wall ischemia. During the periods of reduced perfusion and reperfusion structural damage can occur that enhances loss of bladder function. Acetylsalicylic acid (ASA) may protect against this damage by improving tissue perfusion and interfering with the damaging processes during reperfusion. We tested the *in vivo* effect of ASA on the deterioration of bladder function and structure in animals with urethral obstruction.

Methods: In guinea pigs with urethral obstruction urine flow, bladder pressure, detrusor overactivity (DO), compliance and contractility were measured weekly. Bladder tissue was obtained at end point. Glycogen accumulation, a marker for ischemia, was quantified with a PAS stain, collagen infiltration into the detrusor muscle with an Elastic von Gieson stain. Eight animals received ASA, 4 mg/kg b.w./day, during 9 weeks of obstruction. Their data was compared to obstructed (n=93) and sham operated animals (n=13).

Results: In the obstructed bladder contractility increases to generate the high pressure needed to overcome obstruction. This yields ischemia indicated by glycogen accumulation and a sharp loss in compliance. Under ASA treatment the obstructed bladder generates significantly more force and higher pressures but compliance remains normal and less glycogen accumulates. Collagen infiltration and DO are the same in both groups.

Conclusion: The data indicates that in the obstructed bladder ASA increases perfusion and thereby contractility and prevents ischemia related damage. Considering the lack of effect on DO it seems worthwhile to further investigate a combination of ASA with compounds that aim to reduce DO like Oxybutynin.

Introduction

Both in structural (urethral valves, BPH) and functional (neurogenic bladder dysfunction) bladder outlet obstruction (BOO) the bladder can deteriorate through a cascade of events that includes increases in bladder contractility and pressure, detrusor overactivity (DO) and loss of compliance [1-3]. After surgical treatment of the original problems, management of bladder pressure and bladder overactivity may preserve bladder and renal function. For this anticholinergics with or without clean intermittent catheterisation (CIC) are the main entities used [1,4]. Although antimuscarinic drugs like Tolterodin or Oxybutynin do lower intravesical pressure, further unexplained deterioration of bladder function combined with progression of smooth muscle cell hypertrophy and bladder wall fibrosis still occurs.

We have shown in our guinea pig model of urethral obstruction [2,3] that in addition to the known collagen infiltration [5], strong accumulation of glycogen is found in long-term obstructed bladder [6]. In fact the level of glycogen accumulation in an individual bladder is directly related to the degree of instability, the increase in voiding pressure and the increase in bladder pressure during filling (loss of compliance) that occurred previously. Glycogen accumulation marks previous hypoxia. In acute ischemia glycogen is used for anaerobic energy production and its concentration locally decreases. When the appearance of ischemia becomes chronic an organ can adapt by building stores of glycogen. This has been shown to occur in the brain [7]. There the glycogen level decreases during an acute period of ischemia and returns to supranormal levels thereafter. This increase in glycogen appears to induce tolerance to repeat episodes of ischemia. In the bladder hypoxia occurs when high pressure reduces the blood flow in the bladder wall [8-11]. Oxidative stress during the periods of reduced perfusion and re-perfusion may excite the afferent nerves in the bladder wall what triggers DO [11, 12]. *In vitro* hypoxia causes less nerve damage in bladder strips where glycogen is accumulated [12]. We showed previously that Oxybutynin prevents glycogen accumulation as long as it can maintain a low pressure and normal compliance and that DO is concurrently suppressed [13]. However, under Oxybutynin treatment bladder contractility did still increase. This may explain why in individual animals transient failure of Oxybutynin to inhibit detrusor contraction led to immediate DO and glycogen accumulation at end-point. Apparently in the setting of increased contractility a bladder is prone to cause ischemic damage the moment the suppression of bladder pressure for some reason fails.

Prevention of this local hypoxia and the related nerve damage may be a second handle to attack the bladder problems in urethral obstruction.

Acetylsalicylic acid (ASA) has been applied to prevent ischemic nerve damage in the bladder [14]. That study applied an *in vitro* approach looking at the contractility of strips of detrusor muscle. Strips from obstructed rabbit bladder produced less contractile force as a whole and expressed per cross-sectional area [15] as compared to

strips from non-obstructed rabbit bladder. Bladder strips from animals that were treated with a low dose of ASA, 2 mg/kg b.w./day, retained their electrical field induced contractility [14].

Here we examined whether ASA can preserve *in vivo* measured bladder function in a model of urethral obstruction where bladder function is monitored longitudinally. The changes in bladder function were related to the accumulation of glycogen, a measure for ischemic nerve damage, and to the degree of collagen infiltration in the detrusor muscle.

Materials and Methods

We used a model for gradual urethral obstruction where a silver ring around the urethra induces urethral obstruction in immature male albino Guinea pigs (Hartley strain) [2,3]. Bladder function was measured weekly and the bladder was removed at end point for tissue analysis.

Study design

The ASA group contained 8 animals. They were measured and obstructed at week 0 and followed with weekly measurements for 10 weeks. One animal died at week 6 due to anaesthesia problems. Their data was compared to obstructed (n=93) and to sham-operated (n=11) animals. Two sham-operated and 8 obstructed animals were analysed concurrent with the ASA group. To minimize animal use sham-operated and obstructed animals from other studies were added to increase the numbers to 11 respectively 93. In all these animals urodynamic investigations were performed weekly. The week of sacrifice was varied to obtain bladder material at all time points. Thus the number of animals and consequently the number of urodynamic tests in these groups decreases from week to week. The absolute changes and the time path of changes in bladder function were similar in the sham and obstruction groups from the ASA study as compared to the additional control groups, allowing combination of the data. Sham-operated animals were followed up to 9 weeks. The number of animals in this group from day 0 to week 9 was: 11 (day 0, before obstruction), 10 (first week of obstruction), 10, 8, 3, 3, 6, 7, 4, 2 (week 9). In the obstructed group the numbers were: 93 (day 0), 66 (week 1), 76, 61, 55, 47, 46, 26, 14, 14 (week 9).

The applied dosage of ASA was 4 mg /kg/ day divided over 2 doses.

Urodynamic Procedure [2,3]

The animals were anaesthetized using ketamine (43 mg/kg i.m.) and xylazine (0.9 mg/kg i.m.). Through a 24-gauge suprapubic catheter bladder pressure was measured and the bladder was filled continuously with sterile saline at a rate of 0.23 ml per minute. Flow rate was measured with an ultrasound transducer (T106 small animal

Flow meter, Transonic Systems, Ithaca, NY) around the penis. The volume voided was collected in tubes and used to calibrate the flow-rate signal of each voiding. After the last voiding the residual fluid was measured.

Operative Procedure

Under ketamine/xylazine anaesthesia the peritoneal cavity was accessed via a lower vertical midline abdominal incision. A silver jeweler's jump ring, internal diameter 2.2 mm, was placed around the bladder neck above the prostate.

End-Point Procedure

After the final urodynamic study the animal was sacrificed and the bladder was removed immediately. Part was snap-frozen and stored at -80°C , part was fixated in 10% buffered formalin (pH 7.4) and embedded in paraffin. Tissue sections for histology were taken opposite to the site of catheterisation.

Calculations

Detrusor overactivity (DO) was assessed as the number of detrusor contractions of 10 cm H₂O (one third of the mean voiding pressure for unobstructed animals) without urine-flow during the filling phase. The maximum flow rate [Q_{\max}], the associated bladder pressure [$p_{\det Q_{\max}}$], bladder compliance [ml/ cm H₂O] and bladder contractility [W_{\max}] were calculated as described previously [2,3].

PAS-stain and PAS-score

Paraffin-embedded cross-sections of 4 μm covering all bladder wall layers were stained with the periodate acid Schiff's protocol (PAS). This procedure stains sugar moieties to visualize the general structure. At what we defined as score 0 linear structures like cell membranes are visible. At higher scores granular staining appears inside the muscle cells. These granules are glycogen accumulations. Biochemical analysis has shown that a high count of PAS stained granules in tissue correlates to high glycogen content [12]. We have shown with Raman spectroscopy that the granules contain large amounts of glycogen [5]. Three investigators scored the number of these granules and the increasing number was defined as score 1, 2 or 3. We observed that concomitant with the increase in number of granules their location spread. At score 1 the granules were located near the adventitium. At score two they were also found in the middle of the muscle layer and at score 3 they were throughout the muscle up to the urothelium.

Elastic von Gieson stain (EVG)

In the EVG procedure collagen stains red, elastin black and the rest of the tissue yellow. Three investigators have visually assessed the degree of red within the muscle layer and scored this from 1 to 3.

Statistics

All values are expressed as the mean \pm SEM. Statistical significance was determined by two-sided unpaired Student's *t*-tests with $p < 0.05$ considered statistically significant. Note that because of our specific study protocol the numbers of animals in the comparison changes from week to week (as explained above).

The protocol was approved by the institutional animal care and use committee of the Erasmus University and was in line with guidelines by the EU.

Results

Bladder pressure ($p_{\det Q_{\max}}$)

Compared to both the sham group and the obstruction group ($p < 0.01$) the $p_{\det Q_{\max}}$ increased significantly in the ASA group, Figure 1.

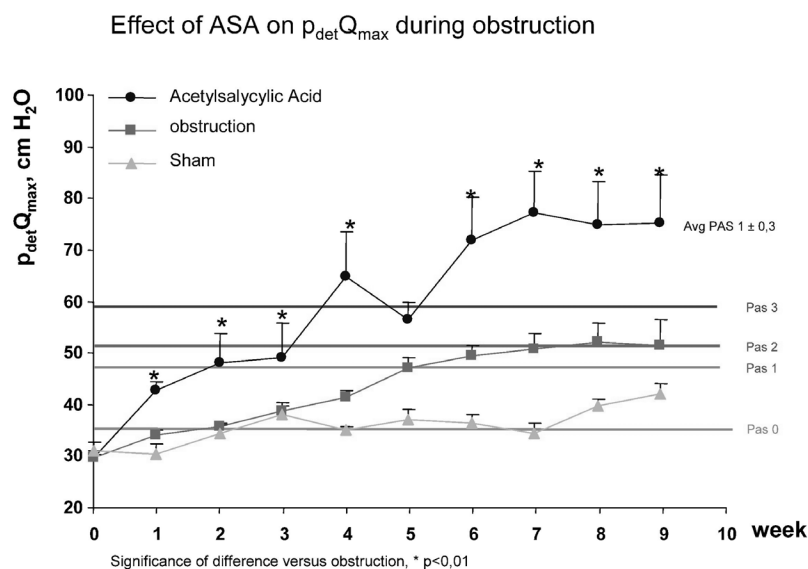


Figure 1

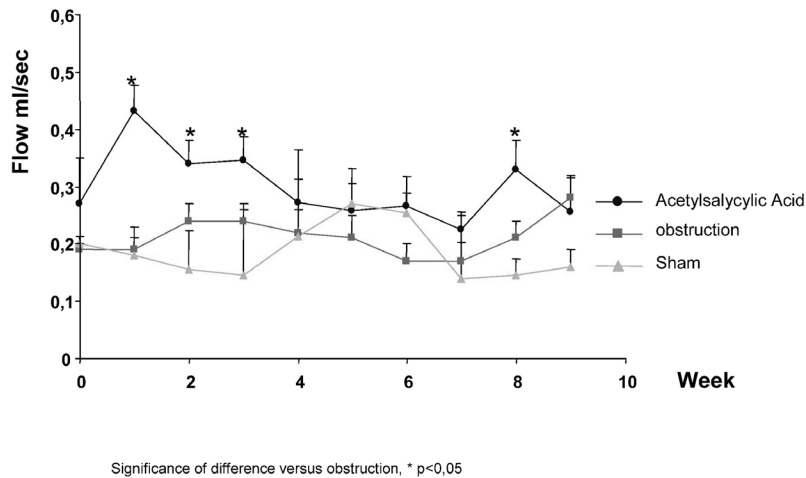
Effect of acetylsalicylic acid (ASA) on $p_{\det Q_{\max}}$ during 9 weeks of obstruction. The triangles represent the sham group, squares the obstruction group and filled circles the ASA group. The solid lines represent the average $p_{\det Q_{\max}}$ for animals with a PAS score of respectively 0, 1, 2 and 3. The values on which these lines are based were taken from ref [14]. * significance of difference versus obstructed group, $p < 0.01$.

In a previous publication [6] we have shown that the PAS score of a bladder tissue correlates closely to the highest pressure that specific bladder has generated during its life time. In Figure 1 the solid lines represent the average highest pressure for groups of obstructed animals with respectively a PAS score of 0, 1, 2 or 3. A PAS score of 3 that represents the highest degree of glycogen accumulation and the most ischemic damage is associated with the highest bladder pressure. The ASA group had an average pressure well above that for the PAS 3 score but its average PAS score was 1. This indicates less ischemic damage.

Urine flow rate

Compared to the obstruction group, the urine flow-rate was higher ($p < 0.05$) in the ASA group during the first three weeks and at week 8, Figure 2.

Effect of ASA on flow rate during obstruction

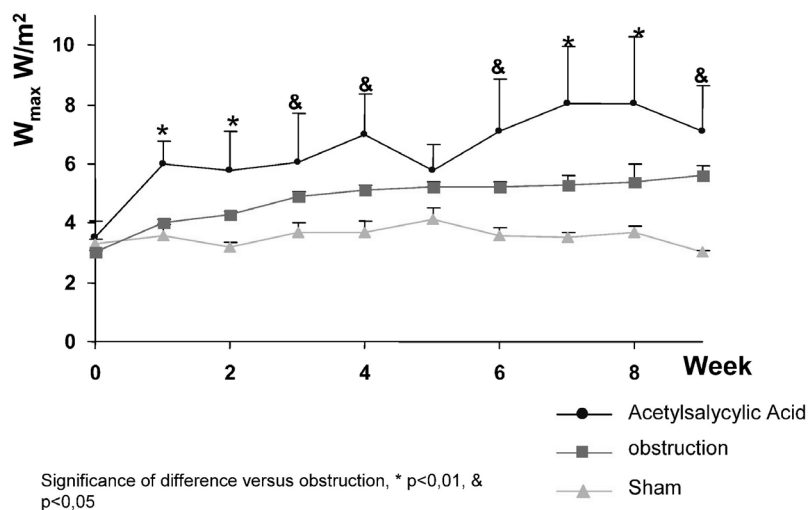
**Figure 2**

Effect of ASA on the flow rate during 9 weeks of obstruction. The triangles represent the SHAM group, squares the obstruction group and the filled circles the ASA group. * significance of difference versus SHAM group, $p < 0,05$.

Contractility

Compared to both the sham group and the obstruction group bladder contractility increased significantly ($p < 0,01$) in the ASA group during all weeks, Figure 3.

Effect of ASA on contractility during obstruction

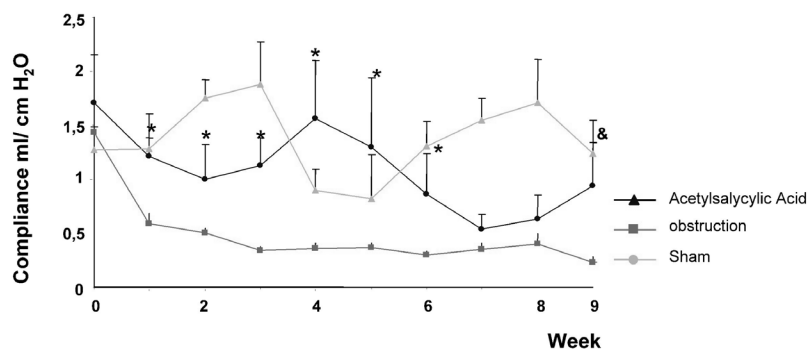
**Figure 3**

Effect of ASA on contractility during 9 weeks of obstruction. The triangles represent the SHAM group, squares the obstruction group and filled circles the ASA. * significance of difference versus obstruction group, $p < 0,01$.

Compliance

Bladder compliance in sham-operated animals fluctuated around 1 during the whole study period, Figure 4. In the obstructed animals compliance decreased significantly ($p < 0,05$) compared to the sham group. In the ASA treated animals compliance remained normal and was significantly higher ($p < 0,01$) compared to the obstruction group.

Effect of ASA on compliance during obstruction

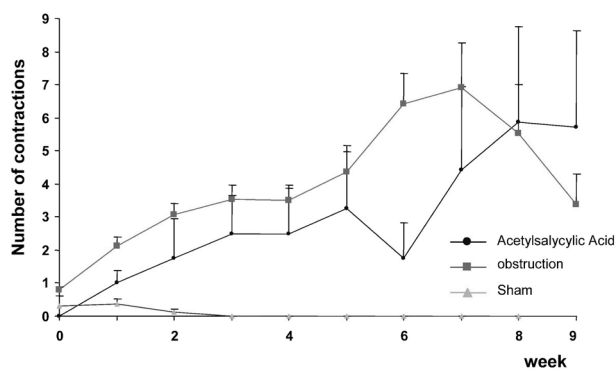
Significance of difference versus obstruction, * $p < 0,01$, & $p < 0,05$ **Figure 4**

Effect of ASA on compliance during 9 weeks of obstruction. The triangles represent the SHAM group, squares the obstruction group and filled circles the ASA group. * and & significance of difference versus obstruction group $p < 0,01$ respectively $p < 0,05$.

Detrusor overactivity

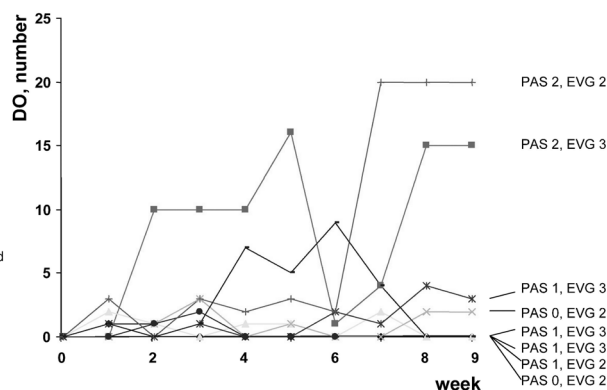
In sham-operated animals DO was rare, in obstructed animals it was common. This started the first week of obstruction and increased in severity the following weeks. For the groups as a whole DO in the obstructed animals that received ASA did not differ from DO in untreated obstructed animals, Figure 5. However, 5 out of the 8 animals had less DO than the obstruction group, Figure 6, while three had an intermediate to very high degree of DO. The 2 animals with the most severe DO also showed the most glycogen accumulation at end point, as indicated by the PAS score of 2.

Effect of ASA on detrusor overactivity

**Figure 5**

Effect of ASA on detrusor overactivity during 9 weeks of obstruction. The triangles represent the SHAM group, squares the obstruction group and filled circles the ASA group.

Detrusor overactivity and bladder structure in individual ASA treated animals

**Figure 6**

Effect of ASA on detrusor overactivity in the individual animals. In the two animals where DO was high, the tissue obtained at week 10 showed much glycogen deposition (PAS score of 2). The degree of collagen infiltration into the muscle was similar in all animals (EVG score).

EVG

The EVG score, indicating collagen infiltration into the detrusor muscle, for the ASA treated animals, $2,5 \pm 0,2$, was significantly ($p < 0,01$) higher than the score for the SHAM group, $1,1 \pm 0,1$, and equal to the score for animals that were obstructed for 9 weeks or more without treatment, $2,4 \pm 0,2$.

Discussion

Both animal [8] and human studies [9] show that the perfusion of the bladder wall is reduced by DO and high bladder pressure. In unobstructed conscious pigs the bladder blood flow decreases on average 50% during voiding and up to 67% at peak pressure [8]. Perfusion almost completely stops when intravesical pressure exceeds 41 cm H₂O [11] and already starts to decrease appreciably when bladder pressure rises during filling in a bladder rendered non-compliant by propofol [8]. The resulting focal hypoxia forces detrusor muscle cells to an anaerobic metabolism [8, 10]. During the period of reduced perfusion and re-perfusion the afferent nerves present in the bladder wall become excited or even damaged [11, 12]. Glycogen deposits are used to counteract this damage [12]. In a rabbit model the bladder was shown to respond to this by increasing small vessel density [16]. After long-term obstruction in the mini pig the increase in total blood flow for the bladder thus matches the increase in bladder mass. However, the new vessels in the obstructed bladder will still be susceptible to closure by high bladder pressure, which is even increased. In addition, the hypertrophied obstructed bladder wall appears even more vulnerable to disturbance of the blood flow. In mini-pigs applying an intravesical pressure of 20-30 cm H₂O greatly decreased the blood flow in obstructed bladders while it had no effect on the blood flow in non-obstructed bladder. [17].

We have previously shown that during obstruction glycogen accumulates in the detrusor cells. The degree of accumulation is proportional to the increase in bladder pressure during miction during the obstructive period [5,6]. It seems likely that this glycogen accumulates in response to recurrent hypoxia both to accommodate anaerobic muscle function and to protect nerves during reperfusion. Glycogen deposits can protect afferent nerves from the oxidative damage that can occur during re-perfusion, as was shown for bladder strips from Guinea pig, man and monkey [12]. Something comparable happens in the brain. While the acute situation of hypoxia causes a drop in glycogen as it is being consumed, the glycogen content is actually supra-normal shortly there-after and is permanently increased when repeated situations of hypoxia occur [7]. Glycogen accumulation in the bladder muscle most likely reflects adaptation to repeated periods of hypoxia induced by high bladder pressure. The ultimate proof will be to measure blood flow in normal and obstructed bladder at different time points during obstruction. This has not been performed yet.

We have previously shown that when obstructed guinea pigs are treated with oxybutynin, the bladder pressure remains low, no DO occurs and no glycogen is accumulated [13]. However, in some animals there was transient loss of Oxybutynin action. In these animals bladder pressure increased significantly, DO started and significant glycogen accumulation was found at end-point. Both in obstructed animals and obstructed animals treated with oxybutynin glycogen accumulation thus coincided with increased voiding pressure and in fact occurred when voiding

pressure increased above 95% upper limit of the normal range in our guinea pigs, 41 cm H₂O. In contrast, ASA treatment prevents glycogen accumulation in obstructed animals while voiding pressure is well above this limit. Apparently ASA decreases the detrimental effects of the high voiding pressure. This protection by ASA could be due to anti-thrombotic and vasodilatory effects [14]. This hypothesis was tested in an *in vitro* study with strips of rabbit bladder muscle. Strips from obstructed bladders showed reduced contractility upon electric stimulation while those from ASA treated obstructed animals showed less reduction in contractility [14]. The loss of response to electric stimulation was thought to result from afferent nerve damage. It was also noted that total bladder mass in both obstructed and ASA treated obstructed rabbits showed a comparable 4-fold increase. This increase is not as much a sign of damage but more a sign of adaptation to the high pressure. We also find no change in our parameter for fibrosis. Collagen infiltration into the detrusor increased to the same extent in both obstructed and ASA treated obstructed animals. In seeming contrast to the *in vitro* data obtained with acute experiments with bladder strips we find an increase of total bladder contractility in our chronic *in vivo* study. Apparently the increase in muscle mass outweighs the decrease in intrinsic contractility of the individual fibres. In addition it may be that ASA maintains a better perfusion *in vivo* what enables the increased muscle mass to produce even more force than the same amount of muscle mass in obstructed bladder without ASA. The extra collagen reflects adaptation to that high pressure. It is very likely that during the peak voiding pressure blood flow through the bladder wall is also reduced under ASA treatment. A vasodilatory effect of ASA during the period of re-perfusion filling phase could act to prevent nerve damage. This protection, however, appears incomplete. The unstable contractions that we see suggest that some nerve excitement does occur. However, the fact that compliance remains good and only moderate glycogen accumulation occurs indicate that no permanent damage occurs. The maintenance of a good compliance could be related to a second effect that has been ascribed to ASA, inhibition of prostanoids synthesis [18]. Cyclooxygenase enzymes in the bladder wall produce prostanoids in response to stretch [19]. The prostanoids modulate afferent nerve activity and contribute to the basal detrusor muscle tone [20, 21]. The strong decrease in bladder compliance that we witness directly after obstruction [3] can probably be ascribed to prostanoids production by the detrusor smooth muscle cells and ASA appears to inhibit this.

A possibility that was not explored in our study is that chronic administration of ASA effects the bladder function also in the unobstructed state, for instance by changes in diuresis. Chronic increased diuresis may affect bladder function. It is not known if chronic administration of ASA causes chronic diuresis. The acute response to a therapeutic dose of ASA is a decrease in diuresis [22]. This makes a chronic increase in diuresis unlikely.

In conclusion ASA appears to protect the obstructed bladder against high pressure induced ischemic damage. The protection is not complete as DO does occur. An interesting study will be to combine ASA with a compound like oxybutynin that interferes with the generation of high bladder pressure and DO. In addition it will be worth studying whether a bladder that has been treated with ASA during obstruction shows a better regain in bladder function after de-obstruction.

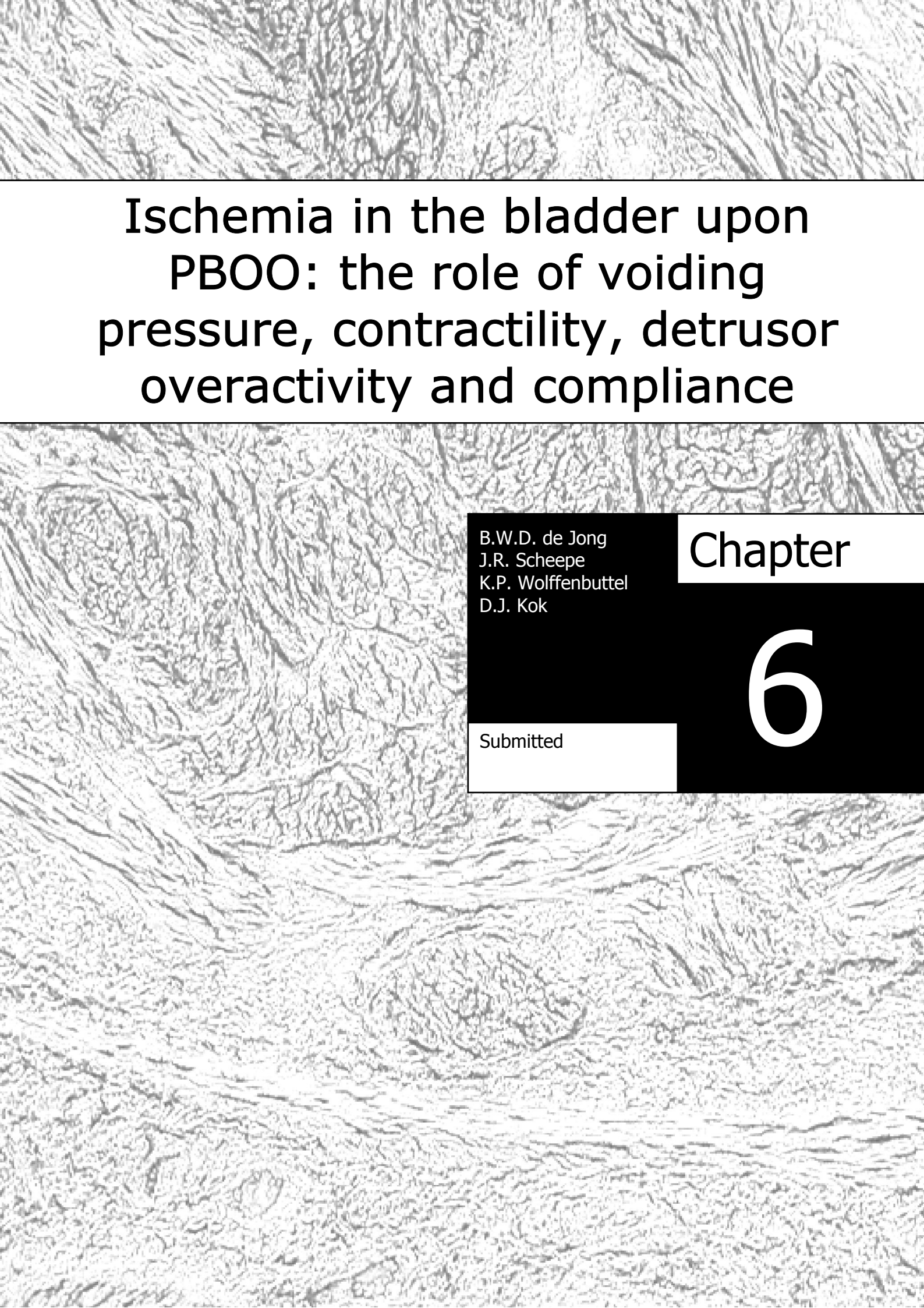
Acknowledgements

This study was supported by the Dutch Kidney Foundation, grant C03.2070.

References

- 1 Snodgrass WT, Adams R. Initial urologic management of myelomeningocele. *Urol Clin North Am* **31**: 427-434, 2004.
- 2 Wolffenbuttel KP, Kok DJ, Minekus JP, van Koevinge GA, van Mastrigt R, Nijman JM. Longitudinal urodynamic follow-up of experimental urethral obstruction in individual guinea pigs. *Neurourol Urodyn* **20**: 699-713, 2001.
- 3 Kok DJ, Wolffenbuttel KP, Minekus JP, van Mastrigt R, Nijman JM. Changes in bladder contractility and compliance due to urethral obstruction: A longitudinal followup of guinea pigs *J Urol* **164**: 1021-1024, 2000.
- 4 Kasabian NG, Bauer SB, Dyro FM, Colodny AH, Mandell J, Retik AB. The prophylactic value of clean intermittent catheterization and anticholinergic medication in newborns and infants with myelodysplasia at risk of developing urinary tract deterioration. *Am J Dis Child* **146**: 840-843, 1992.
- 5 de Jong BW, Bakker-Schut TC, Coppens J, Wolffenbuttel KP, Kok DJ, Puppels GJ. Characterization of collagen infiltration by Raman spectroscopy. *Vibrational Spectrosc* **32**: 57-65, 2003.
- 6 de Jong BWD, Wolffenbuttel KP, Arentshorst ME, Lodder P, Kok DJ. Detrusor glycogen reflects the functional history of bladders with partial outlet obstruction. *BJU Int* **100**: 846-52, 2007.
- 7 Otori T, Friedland JC, Sinson G, McIntosh TK, Raghupathi R, Welsh FA. Traumatic brain injury elevates glycogen and induces tolerance to ischemia in rat brain. *J Neurotrauma* **21**: 707-718, 2004.
- 8 Greenland JE, Brading AF. Urinary bladder blood flow changes during the micturition cycle in a conscious pig model. *J Urol* **156**: 1858-1861, 1996.
- 9 Mitterberger M, Pallwein L, Gradl J, Frauscher F, Neuwirt H et al.. Persistent detrusor overactivity after transurethral resection of the prostate is associated with reduced perfusion of the urinary bladder. *BJU Int* **99**: 831-835, 2007.
- 10 Kato K, Lin AT, Haugaard N, Longhurst PA, Wein AJ, Levin RM. Effects of outlet obstruction on glucose metabolism of the rabbit urinary bladder. *J Urol* **143**: 844-847, 1990.
- 11 Brading A, Pessina F, Esposito L, Symes S. Effects of metabolic stress and ischaemia on the bladder, and the relationship with bladder overactivity. *Scand J Urol Nephrol Suppl* **215**: 84-92, 2004.
- 12 Pessina F, Solito R, Maestrini D, Gerli R, Sgaragli G. Effect of anoxia-glucopenia and re-perfusion on intrinsic nerves of mammalian detrusor smooth muscle: importance of glucose metabolism. *Neurourol Urodyn* **24**: 389-396, 2005.

- 13 Scheepe JR, de Jong BWD, Wolffenbuttel KP, Arentshorst ME, Lodder P, Kok DJ. The Effect of Oxybutynin on Structural Changes of the Obstructed Guinea Pig Bladder. *J Urol* **178**: 1807-1812, 2007.
- 14 Schroder A, Levin RM, Kogan BA, Longhurst PA. Aspirin treatment improves bladder function after outlet obstruction in rabbits. *Urology* **58**: 608-613, 2001.
- 15 Cher ML, Kamm KE, McConnell JD. Stress generation and myosin phosphorylation in the obstructed bladder. *J Urol* **143**: 355, 1990.
- 16 Chichester P, Lieb J, Levin SS, Buttyan R, Horan P, Levin RM. Vascular response of the rabbit bladder to short term partial outlet obstruction. *Mol Cell Biochem* **208**: 19-26, 2000.
- 17 Nielsen KK. Blood flow rate and total blood flow related to length density and total length of blood vessels in mini-pig urinary bladder after chronic outflow obstruction and after recovery from obstruction. *Neurourol Urodynam* **14**: 177-186, 1995.
- 18 Tsukimi Y, Mizuyachi K, Matsumoto H, Sato M, Ng B, Tajimi M. Mechanism of action by which aspirin alleviates detrusor hyperactivity in rats. *J Pharmacol Sci* **95**: 101-107, 2004.
- 19 Gilmore NJ, Vane JR. Hormones released into the circulation when the urinary bladder of anesthetized dogs is distended. *Clin Sci* **41**: 69-83, 1971.
- 20 Poggesi L, Nicita G, Castellani S, Selli C, Galanti G, Turini D, et al. The role of prostaglandins in the maintenance of the tone of the rabbit urinary bladder. *Invest Urol* **17**: 454-458, 1980.
- 21 Maggi CA. Prostanoids as local modulators of reflex micturition. *Pharmacol Res* **25**: 253-308, 1992.
- 22 Berg KJ. Acute effects of acetylsalicylic acid on renal function in normal man. *Eur J Clin Pharmacol* **11**: 117-123, 1977.

The background of the entire page is a grayscale microscopic image showing a dense network of elongated, fibrous structures, likely representing muscle or connective tissue. The fibers are oriented in various directions, creating a complex, textured pattern.

Ischemia in the bladder upon PBOO: the role of voiding pressure, contractility, detrusor overactivity and compliance

B.W.D. de Jong
J.R. Scheepe
K.P. Wolffenbuttel
D.J. Kok

Chapter

6

Submitted

Abstract

Aims: We have examined whether voiding pressure, contractility, detrusor overactivity, compliance and combinations of these variables correlates to glycogen deposition as a measure for ischemia in guinea pigs with BOO under different medications.

Methods: In a guinea pig model for BOO flow rate, detrusor overactivity (DO), voiding pressure at maximum flow ($pDET_{max}$), contractility and compliance were assessed weekly in each animal for up to 16 weeks. We applied oxybutynin and aspirin to reduce ischemic changes upon PBOO. After sacrifice, bladder wall cross-sections were stained to score granular glycogen deposits in the detrusor from 0 (no glycogen) to 3 (most intense).

Results: In obstructed animals, $pDET_{max}$, contractility and DO increased, compliance decreased and the glycogen score (GS) was 2.2. In BOO with oxybutynin $pDET_{max}$ remained low, compliance normal and GS was 1.0. In 2 animals $pDET_{max}$ rose transiently and the GS was 2.5. In BOO with aspirin, $pDET_{max}$ and contractility were increased even more than with BOO alone while DO was the same but compliance remained normal and GS was 1.0.

Conclusion: Glycogen deposition is mostly related to reduced compliance and DO. More emphasis on changes in bladder compliance and insight into parameters reflecting reduced bladder perfusion like glycogen deposition could benefit the follow-up of patients with obstruction.

Introduction

The cause of bladder outlet obstruction (BOO) varies from prostate enlargement in adult men to neurogenic bladder disorders or posterior urethral valves (PUV) in children. The consequence of a partially closed urethra is that the bladder pressure during voiding increases and the bladder muscle has to work harder. Over time a bladder that experiences obstruction will show structural changes that include an increase in muscle mass and collagen deposition [1]. These changes may serve the purpose of ensuring good bladder emptying but unfortunately they negatively effect the elastic properties of the bladder and thereby its storage function.

Which exact mechanisms couple the BOO to the structural and functional changes is not clear yet. Obviously, the increased voiding pressure may be suspected to play an initiating role. Indeed there is evidence that bladder urothelial and muscle cells are mechano-sensitive and react to stretch and pressure on the urothelium. The role of bladder detrusor cells stress have been well described with in vitro studies in which detrusor strips en cell cultures on stretchable media were stretched. It was found that the cells showed gene expression and protein synthesis related to the complex pathway that leads to adaptations needed for increased resistance against higher pressures [1, 2]. This mechanism may apply for a dysfunctional bladder nervous system, e.g. spina bifida, where overfilling is a common problem. However, with BOO it is not clear whether the bladder is actually overfilled. Therefore the question remains whether if this adaptation mechanism in the bladder with BOO is actually triggered by tissue stretch. An alternative cause for triggering this mechanism may be the compression of tissue, urothelium in particular, caused by increased intravesical pressures.

Another event related with functional and structural changes is the occurrence of ischemia, as blood flow is decreased during increased bladder pressures [3, 4]. The cyclic episodes of ischemic conditions followed by reperfusion, created by filling and emptying of the bladder, lead to generation of free radicals of reactive oxygen and nitrogen species [5]. Recent studies have shown that such ischemia related oxidative stress causes mitochondrial DNA deletions in detrusor cells [6]. It also causes membrane and sub-cellular organelle damage, to which intrinsic nerve cells are the most susceptible [7]. Nerve damage in turn is believed to cause bladder overactivity, thereby enlarging the periods of ischemic conditions.

In the human, monkey and guinea pig bladder ischemia has been linked to glycogen accumulation within the detrusor [8]. In addition, we have shown that the amount of glycogen accumulation follows the progression in decreasing bladder function in our guinea pig model for partial BOO (PBOO). In this model the bladder function was measured weekly under anaesthetics in all individual animals with urodynamic measurements [9]. Using this same model we also applied medical intervention with oxybutynin and aspirin respectively to limit the progression of bladder dysfunction

during PBOO [10, 11]. As was expected oxybutynin limited the increase in bladder pressures during voiding but aspirin allowed bladders to develop very high pressures during voiding. In contrast the effect of both regimens on bladder compliance was similar. Compliance remained good with oxybutynin and decreased only slightly with aspirin. DO was suppressed only with oxybutynin but contractility raised despite intervention with both anticholinergics.

In this paper we further explore this seeming contradiction that compliance remains good both under low and high voiding pressures. For this we have re-evaluated the previously published [9, 10, 11] data on changes in bladder function and bladder structure under four conditions: no obstruction, obstruction only, obstruction plus oxybutynin and obstruction plus aspirin. The outcome of this study, better insight into the interplay between structural and functional changes in the detrusor during BOO, may help to focus research and clinical efforts for optimal prevention of (further) bladder functional deterioration or even regeneration of function.

Materials and Methods

All data used here was derived from studies described in previous publications [9, 10, 11]. In this paper we combine this data into a new interpretation.

Animal model and animal groups

All data are based on urodynamic measurements and bladder tissues that were obtained from a guinea-pig model for PBOO; to allow for urodynamic follow-up from the start of PBOO, and be able to surgically apply PBOO, the guinea pigs had to weigh ≈ 300 g (≈ 6 weeks old). The model was extensively described previously [12, 13]. In addition, this model was further developed for medical intervention, as recently published [10, 11]. Briefly, bladder pressure was measured in each guinea pig through a suprapubic bladder catheter, and the urinary flow rate was measured using an ultrasound flow probe attached loosely around the penis. This was done weekly, starting just before imposing PBOO and ending just before the animal was sacrificed. Six animals (OTO) were obstructed and received Oxybutynin, 0.4 mg/kg body weight/day administered orally twice a day in equal portions, for a total period of 10 weeks. Oxybutynin was acquired as syrup (Dridase).

Seven animals (ATO) were obstructed and received aspirin, 4 mg/kg body weight/day, also administered orally twice a day in equal portions, for 10 weeks (acetyl salicylic acid, Sigma, Zwijndrecht, The Netherlands). Sixteen animals were obstructed and followed for 7 to 10 weeks and ten animals were sham operated and followed for up to 9 weeks (in all 39 in total).

Urodynamic data

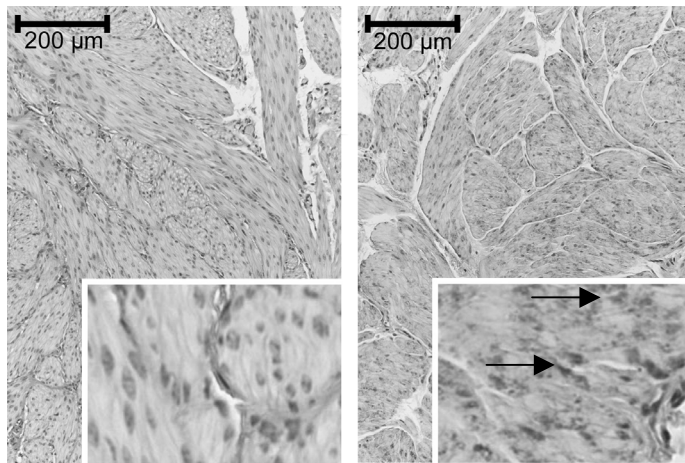
For all animals we obtained the bladder pressure at maximum flow rate (pQ_{\max}), contractility (W_{\max}), compliance ($\text{mL}/\text{cmH}_2\text{O}$) calculated as Δ infused volume/ Δ bladder pressure and the number of unstable contractions (NUC) as a measure for detrusor overactivity (DO).

Tissue structure

All animals were sacrificed directly after the last measurement and the bladder was taken out. Bladder tissues were snap-frozen in liquid nitrogen-cooled isopentane and stored at -80°C until use. About half of each bladder tissue sample was later fixed in 10% buffered formalin (pH 7.4) and embedded in paraffin wax for sectioning. Cross-sections of $4\text{ }\mu\text{m}$ covering all bladder wall layers were made for staining with periodic acid Schiff's protocol (PAS stain). As described in our previous work [9] we used the PAS stain to score the number of glycogen granules staining in the detrusor layer within the cross-sections of bladder wall tissues. Using light microscopy, three researchers scored the cross-sections while unaware of origin, with scores of 0 (minimal staining) to 1 (little staining), 2 (strong staining) and 3 (maximum staining). The abundance of the staining correlated with the site of glycogen deposition; a score of 1 represented light glycogen granule staining only at the serosal side; a score of 2 represented more intense staining, where glycogen granules were found deeper into the muscle layer; a score of 3 represented strong staining of glycogen granules that were present throughout the muscle layer. With four scoring groups we could combine good differentiation of the amount of glycogen with group sizes that allow statistical analysis.

Results

The results for glycogen scoring on obstructed and sham / controls tissue sections are derived from our previous work on glycogen scoring [9, 14]. We found a clear correlation between the site of glycogen deposition and the amount of stained granules. A glycogen score 0 represented no visible glycogen granules. For glycogen score 1 there were a few glycogen granules only close to the serosa. For glycogen score 2 the amount of staining was clearly greater and granules appear deeper into the muscle layer towards the urothelium. Tissues with glycogen score 3 had the most stained granules, which were visible throughout the whole detrusor layer. Glycogen granules always appeared within the cytoplasm of muscle cells. Tissue sections with PAS stains from the animals treated with aspirin and oxybutynin were evaluated in the same way. Figures 1a and 1b show examples of respectively a glycogen score 1 and a glycogen score 3 from ATO animals. These examples are also representative for the obstructed, sham / controls and OTO animals.

**Figure 1**

Example of PAS stains of bladder detrusor layer with scores 0 and 3. Bar = 200 µm. Inserts are 4x enlargements. Some glycogen granules are denoted with arrows. Color image: see appendix.

The inter-observer differences for one tissue sample were < 1 score value; the results of the three observers were averaged to obtain the mean score for each tissue. Table 1 shows the distribution of glycogen scoring in tissues along the obstructed, sham / controls, aspirin and OTO animals.

Glycogen score	0	1	2	3	Number of animals
BOO	1	1	6	8	16
Control / sham	7	2	1	0	10
Aspirin & BOO	2	3	2	0	7
Oxybutynin & BOO	0	4	1	1	6
Total	10	10	10	9	39

Table 1

All animals from the ATO group and some of the animals from the other groups were not measured in week 1. These animals did not completely recover yet from the operation for placing the silver ring. Therefore a suprapubic catheter could not be installed. Two weeks after the operation all animals had recovered well.

In figure 2a the averaged pressure for each group as function of the time is plotted. Error bars represent the standard error of the mean, SEM (SD/\sqrt{n}). A significant difference compared to the sham / controls group is annotated by * ($p < 0.05$). A significant difference between the obstructed group and the ATO and OTO groups is annotated by † ($p < 0.05$). In week 9 only one sham-operated animal was measured, in week 10 no data from sham / controls was available. This accounts for all urodynamic variables.

There is a distinct increase in pressure from the ATO group compared to the sham / controls group, with significance on week 2 to 8. Also compared to the obstructed group the increase is obvious, with significance on weeks 5, 8 and 10. Note the large spread; at several weeks some ATO animals reached pressures above 100 cm H₂O. Pressures in the OTO group were almost identical to the sham / controls group, only in weeks 4 ($p < 0.05$), 8 and 9 some differences occurred. Compared to the obstructed group, it seemed lower, although only significant at weeks 3 and 7. The pressures

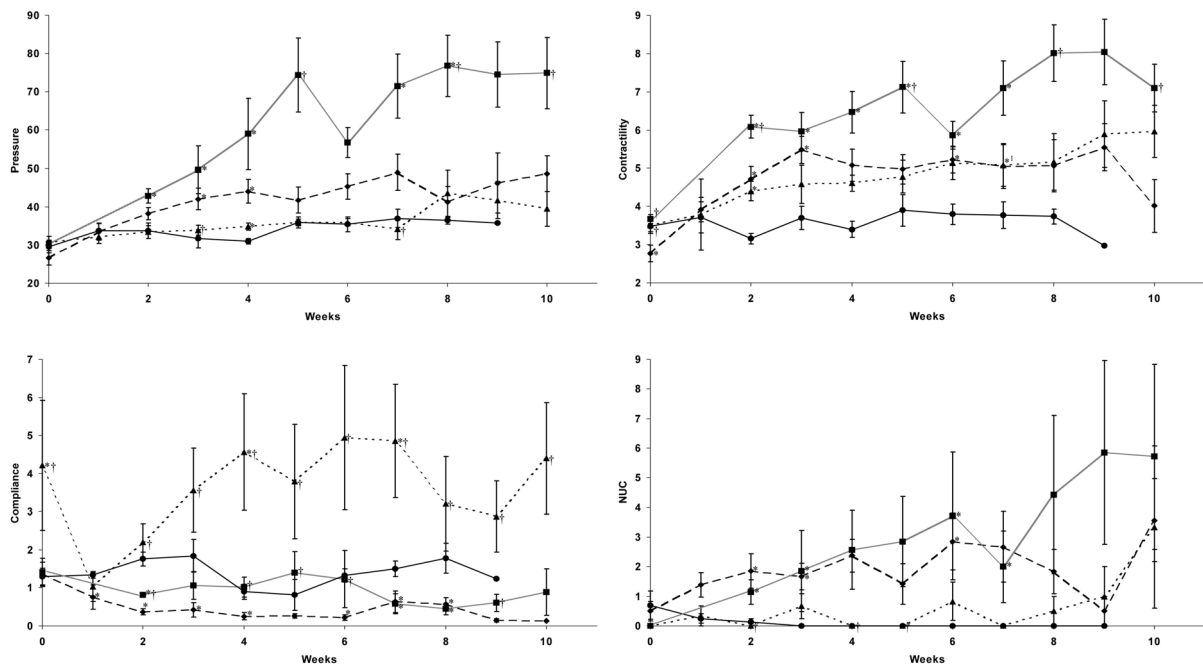


Figure 2

For all graphs: 10 weeks follow-up of bladder urodynamic variables pressure at maximum flow (A), contractility (B), compliance (C) and number of unstable contractions (D). Solid black lines with round points = control animals (week 10 not present), striped lines with checker points = obstructed animals, solid grey lines with square points = ATO animals, dotted lines with triangle points = OTO animals.

from the obstructed group was higher than from the sham / controls group, however only significant at weeks 3 and 4.

Figure 2b shows the contractility of all groups as function of the time. The obstructed, ATO and OTO groups all seemed to have a higher contractility after 2 weeks onwards. The ATO group differed significantly from weeks 2 to 8, the OTO group only at week 2, 4, 6 and 7 and the obstructed group only at weeks 2, 3 and 6. The contractility from OTO and obstructed group were quite similar. The ATO group had even higher contractility than from the obstructed group, with significance at weeks 2, 5, 8 and 10. The contractility from the obstructed group in week 0 (before placement of PBOO) was lower than in all other groups ($p < 0.05$). There is no clear explanation for this event.

Figure 2c shows the compliance as function of the time. The compliance of the OTO group appears to be higher than that of the sham / controls group, though only significance appeared at weeks 4 and 7. The SEM is large shows a large spread and is due to the manner in which compliance is calculated. Still, there is a significant difference with the obstructed group along the whole time-span, except at week 1. At week 0, before placement of PBOO and treatment, no difference between the groups is expected, so for the increase of the OTO there is no clear explanation. Compliance of the obstructed group is significantly lower than the sham / controls at almost all weeks and the ATO seemed to be intermediate between the sham / controls and the obstructed group.

In Figure 2d the NUC as function of the time is plotted. Both the sham-operated as the OTO group had almost no unstable contractions, although at week 10 the NUC of the OTO group rapidly increased. The obstructed and ATO groups have more unstable contractions, sometimes significant, but the spread is large and averages seem to fluctuate.

In table 2 the average glycogen scores with the SEM between brackets per group are given. All differences between sham / controls and the other groups were significant. Furthermore, only ATO was significantly different from the obstructed group.

Animal Group	Averaged glycogen score (SEM)	P value vs. Sham / controls	P value vs. Obstructed	P value vs. OTO
ATO	1.0 (0.31)	0.007	0.005	0.347
OTO	1.5 (0.34)	0.012	0.051	
Obstructed	2.3 (0.22)	0.000		
Sham / controls	0.40 (0.22)			

Table 2

Group of animals	Urodynamic variable	Percentage outside range of 2SD Sham / controls (weeks & glycogen)											Glycogen score
		0	1	2	3	4	5	6	7	8	9	10	
Obstructed	Pressure	0	8	7	31	44	42	47	57	36	40	57	88
	Contractility	0	10	40	56	60	42	47	29	40	60	33	
	Compliance	0	9	14	13	56	25	64	0	11	57	40	
	NUC	13	38	57	47	63	25	43	44	42	17	57	
	Animals (n)	16	12	14	16	16	12	14	8	11	6	6	16
ATO	Pressure	0	-	29	57	57	100	100	100	100	100	83	29
	Contractility	0	-	86	71	83	100	83	83	100	86	100	
	Compliance	0	-	0	14	0	0	0	0	0	0	17	
	NUC	0	-	29	14	43	43	43	43	57	57	57	
	Animals (n)	7	-	7	7	7	6	6	6	7	7	6	7
OTO	Pressure	0	0	0	0	0	0	0	0	33	17	33	33
	Contractility	0	33	17	50	0	60	67	50	40	67	67	
	Compliance	0	0	0	0	0	0	0	0	0	0	0	
	NUC	0	17	0	33	0	0	17	0	17	17	17	
	Animals (n)	6	6	6	6	6	6	6	6	6	6	6	6

Table 3

For most of the variables used in the clinic, such as bladder pressure, the normal range of measured values is denoted as the confidence interval (2SD) of the mean of normal values. Values outside the normal range indicate abnormal conditions. This approach was also tested for all urodynamic variables and the glycogen scores for each week. Data of all weeks from the sham / controls group were averaged and 2SD was determined, assumed that the normal value was constant during the 9 weeks. The results are plotted in table 3.

Discussion

In order to assess insight on the relationship between muscle function and ischemic conditions, we applied a bilateral approach. In one approach the forming of ischemic conditions is limited by aspirin. Recently we have shown that aspirin maintains blood flow during BOO [11]. Aspirin also has a role in the breakdown of prostaglandins. [15] Prostaglandin levels, in particular PGE2 seem to be increased during BOO, causing bladder over activity [16]. However, our results do not confirm this finding. Without ischemic conditions the detrusor can work under optimal aerobic conditions because the oxygen supply is intact. We then compared the bladder function during obstruction with and without intervention with aspirin. In the other approach the detrusor is actually suppressed by oxybutynin. Oxybutynin binds primarily to muscarinic receptors in the bladder, though binding to other receptors leading to unwanted side effects are well known [17]. In this way the signal transfer from the efferent nerves to the detrusor cells is (partially) blocked. The bladder is then limited to produce high pressures during voiding. Arteries within the bladder wall are not compressed and blood flow is preserved. Also detrusor overactivity, which may also result in partially compressed arteries, is suppressed. Again we compared the bladder function during obstruction with and without intervention with oxybutynin. The glycogen scores as a measure for the amount of ischemic conditions are representative for the whole time-path of changes in urodynamic variables. We have shown this relation between bladder structure and the importance of insight on how each bladder has reached the end-stage using the time-path of urodynamic measurements previously [9, 14]. In this work we have shown that intervention with both aspirin and oxybutynin reduces the amount of ischemic conditions (aspirin significant, table 2). Still, the averaged glycogen scores of these interventions show that they do not completely prevent ischemia when compared to sham-operated and controls animals. Table 1 shows that in general the glycogen scores are around 1 but a few individuals have higher scores. It is likely to assume that intervention in these individuals did not occur, e.g. no effective oral intake, rather than that it did not work, although a larger number of animals is needed to emphasize this proposition. Animals with only obstruction showed a clear increase in average glycogen score.

Two animals had low scores and all urodynamic variables were inside the normal range. It could be that the placement of a silver ring in these animals was not effective to cause PBOO. One sham-operated animal had a glycogen score of 2, combined with a slight increase in pressure and contractility during weeks 1 and 2.

A prominent finding in the compliance is the high averaged values and large spread of OTO animals. Sham / controls animals have considerable lower values. Since oxybutynin relaxes the detrusor, this suggests that the detrusor in a normal functional bladder might still be under slight tension. The compliance in ATO animals fluctuates between normal and obstructed values. Aspirin does not influence detrusor activity directly but its supposed inhibitory role in prostanoids synthesis [18] may enhance relaxation of the detrusor after voiding. Aspirin also has a vasodilatory effect [19], preserving the blood flow and thereby reducing nerve damage [11]. The apparent shift of ATO compliance from normal to obstructed values might be related to decreased effectiveness in combination with increasing voiding pressures over time. As shown before [20] the compliance of obstructed animals immediately reduces and remains low during the whole period of obstruction. Both the sham / controls and the OTO group have almost no detrusor overactivity, as was expected. The obstructed bladders showed an increased NUC, in which the spread was large.

Detrusor overactivity may be generated as a consequence of nerve damage, which in turn is caused by ischemia [7]. However, in the ATO group with significant less ischemic conditions as determined with the glycogen scores the NUC are also markedly increased, though again with a large spread. This indicates another cause for detrusor overactivity.

The contractility of ATO animals increases the most because the detrusor can work under aerobic conditions. The high averaged pressures from the ATO group confirm this. Though the detrusor in obstructed animals is also triggered to work harder, it must deal with ischemic conditions and therefore works less efficient. Future studies on the ratio of myosin subtypes SM1/SM2 and other related biochemical changes upon ischemia might emphasize this. The increased resistance from PBOO demands more force to empty the bladder, thus contractility is also increased in the OTO group. But the averaged pressures in this group remain the same as the sham / controls group. We postulate that the increase in contractility comes from the longer durations of voiding time (data not shown). An interesting finding was that the pressures in the obstructed group showed a trend of increase compared to sham / controls but only at a few weeks it was significant. In the clinic voiding pressure at maximum flow rate is an important variable to assess whether bladder function is normal or not. The criterion for an abnormal value is that it is outside the 95% confidence interval of normal values (2SD). In table 3 we have shown that a minimum of 43% of bladders with PBOO will be missed when using this approach while structural analysis on detection of ischemia missed 12%. Glycogen scores of 0 and 1 are defined as normal glycogen amount and scores 2 and 3 defined as increased glycogen linked to ischemic

conditions. With 12.5% (2 out of 16) of the obstructed animals determined as normal, the 95% confidence interval is correct in this matter. We have the idea that the use of voiding pressures as variable to determine bladder dysfunction is questionable. Furthermore, the other urodynamic variables for obstructed animals in table 3 showed similar percentages, though the spread is large. Controversially, with this same approach on voiding pressures all ATO bladders were determined as dysfunctional at several weeks, while the confidence interval on the glycogen score revealed only 29%. Again, this is exactly according to our definitions on glycogen scoring for ischemia with 2 out of 7 animals that are higher than score 1. Percentages on contractility are similar but for NUC these percentages were lower, mainly because of the large spread. Almost no values of compliance were outside the normal range, due to the relative large spread in the values of the sham / controls group.

In the OTO group it is obvious that the use of pressure and NUC as variables for detecting bladder dysfunction is not appropriate. Since the compliance in the OTO group is increased compared to the sham / controls group as explained earlier, this variable neither is of any use. The contractility from this group is comparable to the obstruction group and also the percentages in table 3 are comparable. Comparable to the ATO group 2 out of 6 animals had a glycogen score of 2 respectively 3, thus having ischemic periods. The percentage of glycogen scores outside the confidence interval confirmed this.

Conclusion

In conclusion, PBOO leads to an increased level of glycogen storages, representative for ischemic conditions. Intervention with both oxybutynin and aspirin reduced this glycogen accumulation significantly. Bladder functional variables that correlated the most with this decreased glycogen accumulation upon intervention were compliance and to a lesser degree detrusor overactivity. Bladder pressure at voiding in OTO animals and control animals were very similar, yet in ATO animals the pressure was markedly increased, even higher than in obstructed animals. Bladder contractility showed no correlation with reduced ischemic conditions.

Moreover, as medical intervention may prevent further loss or even improve the conditions for bladder function, it may also mislead the interpretation of urodynamic variables. We therefore emphasize the need to focus on monitoring bladder structure. In particular the ability to determine the level of ischemic conditions may be successful.

However, when using histochemistry in a clinical application, biopsies of bladder wall tissues are needed. To overcome this problem we are studying the possibilities of non-destructive optical techniques to detect biochemical changes that are related to bladder dysfunction. Previously we published a study using Raman spectroscopy in which collagen infiltration and glycogen accumulation within muscle fibres of the detrusor layer was detected [21]. Non-destructive techniques that can monitor

ischemic conditions more directly such as differential pathlength spectroscopy are also in focus for research [22].

Acknowledgements

This study was supported by the Dutch Kidney Foundation, grant C03.2070.

References

1. Mirone V, Imbimbo C, Longo N, Fusco F. The detrusor muscle: an innocent victim of bladder outlet obstruction. *Eur Urol* **51**:57-66, 2007.
2. McVary K. Lower urinary tract symptoms and sexual dysfunction: epidemiology and pathophysiology. *BJU Int* **97**:23-28, 2006.
3. Azadzo KM, Pontari M, Vlachiotis J, Siroky MB. Canine bladder blood flow and oxygenation: changes induced by filling, contraction and outlet obstruction. *J Urol* **155**:1459-1465, 1996.
4. Greenland JE, Brading AF. The effect of bladder outflow obstruction on detrusor blood flow changes during the voiding cycle in conscious pigs. *J Urol* **165**:245-248, 2001.
5. Connors W, Whitebeck C, Chicester P, Legget R, Lin AD, Johnson A, Kogan B, Levin R, Mannikarottu A. L-NAME, a nitric oxide synthase inhibitor, diminishes oxidative damage in urinary bladder partial outlet obstruction. *Am J Physiol Renal Physiol* **290**:F357-F363, 2006.
6. Lu SH, Chang LS, Yang AH, Lin AT, Chen KK, Wei YH. Mitochondrial DNA deletion of the human detrusor after partial bladder outlet obstruction-correlation with urodynamic analysis. *Urology* **55**:603-607, 2000.
7. Brading A, Pessina F, Esposito L, Symes S. Effects of metabolic stress and ischaemia on the bladder, and the relationship with bladder overactivity. *Scand J Urol Nephrol Suppl* **215**:84-92, 2004.
8. Pessina F, Solito R, Maestrini D, Gerli R, Sgaragli G. Effect of anoxia-glucopenia and re-superfusion on intrinsic nerves of mammalian detrusor smooth muscle: importance of glucose metabolism. *Neurourol Urodyn* **24**:389-396, 2005.
9. De Jong BWD, Wolffenbuttel KP, Arentshorst ME, Lodder P, Kok DJ. Detrusor glycogen reflects the functional history of bladders with partial outlet obstruction. *BJU Int* **100**:846-852, 2007.
10. Scheepe JR, de Jong BWD, Wolffenbuttel KP, Arentshorst ME, Lodder P, Kok DJ. The Effect of Oxybutynin on Structural Changes of the Obstructed Guinea Pig Bladder. *J Urol* **178**:1807-1812, 2007.
11. Kok DJ, de Jong BWD, Wolffenbuttel KP, Arentshorst ME, Lodder P, Scheepe JR. Prevention of obstruction induced bladder damage by Acetylsalicylic acid. Submitted, chapter 6 of this thesis.
12. Kok DJ, Wolffenbuttel KP, Minekus JP, van Mastrigt R, Nijman JM. Changes in bladder contractility and compliance due to urethral obstruction: a longitudinal follow-up of guinea pigs. *J Urol* **164**:1021-1024, 2000.
13. Wolffenbuttel KP, Kok DJ, Minekus JP, van Koeveeringe GA, van Mastrigt R, Nijman JM. Urodynamic follow-up of experimental urethral obstruction in individual guinea pigs. *Neurourol Urodyn* **20**:699-713, 2001.
14. De Jong BWD, Wolffenbuttel KP, Scheepe JR, Kok DJ. The detrusor glycogen content of a de-obstructed bladder reflects the functional history of that bladder during PBOO. *Neurourol Urodyn*, accepted for publication, 2008, chapter 4 of this thesis.

15. Khan MA, Thompson CS, Angelini GD, Morgan RJ, Mikhailidis DP, Jeremy JY. Prostaglandins and cyclic nucleotides in the urinary bladder of a rabbit model of partial bladder outlet obstruction. *Prostaglandins Leukot Essent Fatty Acids* **61**:307-314, 1999.
16. Schroder A, Newgreen D, Andersson KE. Detrusor responses to prostaglandin E2 and bladder outlet obstruction in wild-type and Ep1 receptor knockout mice. *J Urol* **172**:1166-1170, 2004.
17. Oki T, Kageyama A, Takagi Y, Uchida S, Yamada S. Comparative evaluation of central muscarinic receptor binding activity by oxybutynin, tolterodine and darifenacin used to treat overactive bladder. *J Urol* **177**:766-770, 2007.
18. Tsukimi Y, Mizuyachi K, Matsumoto H, Sato M, Ng B, Tajimi M. Mechanism of action by which aspirin alleviates detrusor hyperactivity in rats. *J Pharmacol Sci* **95**:101-107, 2004.
19. Schroder A, Chichester P, Kogan BA, Longhurst PA, Lieb J, Das AK, Levin RM. Effect of chronic bladder outlet obstruction on blood flow of the rabbit bladder. *J Urol* **165**:640-646, 2001.
20. Wolffenbuttel KP, de Jong BWD, Scheepe JR, Kok DJ. Potential for recovery in bladder function after removing a urethral obstruction. *Neurourol Urodyn*, accepted for publication, 2008.
21. De Jong BWD, Bakker Schut TC, Coppens J, Wolffenbuttel KP, Kok DJ, Puppels GJ. Raman spectroscopic detection of changes in molecular composition of bladder muscle tissue caused by outlet obstruction. *Vibrational Spectroscopy* **32**:57-65, 2003.
22. Amelink A, Sterenberg HJ, Bard MP, Burgers SA. In vivo measurement of the local optical properties of tissue by use of differential path-length spectroscopy. *Opt Lett* **29**:1087-1089, 2004.

The background of the entire page is a grayscale microscopic image showing the complex, layered structure of bladder wall tissue. The image displays various cellular and fibrous components, with some areas appearing more densely packed than others.

Identification of bladder wall layers by Raman spectroscopy

B.W.D. de Jong
T.C. Bakker Schut
K.P. Wolffenbuttel
J.M. Nijman
D.J. Kok
G.J. Puppels

Journal of Urology
168:1771-1778, 2002

Chapter

7

Abstract

Purpose: To explore the applicability of Raman spectroscopy for *in situ* investigation of bladder wall tissue.

Materials and methods: Bladder wall tissue was obtained from a guinea pig model. Frozen sections were used for Raman spectroscopic investigations. Of each section, 500-700 spectra were obtained in a 2-dimensional grid, spanning an area that included the urothelium, lamina propria and muscle layer. The data set of spectra was subdivided into groups of similar spectra by means of a cluster analysis algorithm. With each group assigned a different color, Raman maps of the frozen sections were constructed based on group membership of the measured spectra. These maps were then compared with histological and histochemical data obtained from haematoxylin-eosin (HE) staining and immunohistochemical staining for collagen I and III and for smooth muscle actin, in order to correlate Raman spectral features with bladder wall structure and molecular composition.

Results: The urothelium, lamina propria and muscle layer can be clearly distinguished based on their Raman spectra. The lamina propria spectra are dominated by signal contributions of collagen, the smooth muscle layer shows strong signal contributions of actin. The urothelium has a relatively strong lipid signal contribution.

Conclusions: These results and the fact that Raman spectroscopy is rapidly evolving into a technology that can be applied *in vivo*, by means of thin flexible fiber optic catheters, indicate that the prospects are good for *in vivo* analysis of the molecular composition of the normal and pathologic bladder, without the necessity of taking biopsies.

Introduction

Bladder outlet obstruction (BOO), like posterior urethral valves (PUV) in children and benign prostate hypertrophy in adults, causes changes in bladder function and structure ^{1,2}. Functional changes are reflected by urodynamic abnormalities as: increased bladder pressure, instability, changed flow rate, in- or decreased bladder contractility and decreased bladder compliance ^{3,4}. The end stage varies, in boys with PUV from a de-compensated bladder to a contracted non-compliant bladder ². Structural changes include increased bladder wall thickness, muscle cell hypertrophy, extra-cellular matrix deposition and changes in collagen types ^{5,6}. Many questions remain regarding BOO. It is not clear yet if obstructed bladders follow a specific path of functional and structural deterioration and the exact relations between functional and structural changes are as yet undetermined. Also the response of a bladder to relief of the obstruction is unpredictable. Clinically this information is hard to gain as the early stages of deterioration are usually missed in patients. Animal models, like guinea pigs, showing all features encountered in the human situation ^{7,8}, are used to study the whole sequence from onset of the obstruction onwards. In this model we demonstrated that the changes in bladder function followed a specific path in which two phases were recognized. Bladder pressure, maximum urine flow rate and contractility first increased in response to the induced increase in urethral resistance then stabilized and decreased. There was an initial decrease in compliance that was ascribed mainly to increased muscle tension. After the other parameters reached their plateau value compliance decreased further, now related to changes in bladder matrix structure ^{7,8}. We hypothesized that the different degrees of structural changes in these two phases may co-determine recovery or further deterioration, upon removal of the obstruction.

Therefore we need techniques that enable monitoring of changes in bladder structure, related to concomitant changes in bladder function. The classical means for this, histochemical analysis of biopsy material, has the important drawback that it only allows for a limited number of focal measurements at a single point in time. We are therefore developing a method that can be repeatedly applied *in vivo*, at multiple sites and without a need for taking biopsies. Raman spectroscopy promises to become such a technique ⁹⁻¹¹.

Raman spectroscopy

Interaction with molecules in the tissue leads to scattering of the incident light. A small fraction of the light is scattered at wavelengths different from the wavelength of the incident light, because some of the energy of the incident photon is transferred to the molecule, in which a vibration is excited. The amount of energy that is transferred in such a Raman scattering event is sharply defined by the masses of the atoms involved in the vibration, the type of chemical bond between them, the chemical

(micro)environment of the vibrating molecular group and the molecular conformation^{9,10}. Therefore, Raman spectra are highly molecule specific¹². The Raman spectra obtained from complex molecular mixtures such as cells or tissues will contain signal contributions from all molecules present and are in fact a representation of the overall molecular composition of the tissue. Depending on the specific application this information can either be explicitly extracted from the spectra, or the spectra can be used as highly specific optical spectroscopic fingerprints, by which a cell or tissue can be identified. This is possible since in principle different types of tissues or cells will always differ in their overall molecular composition and therefore will have different Raman spectra. Raman spectroscopy has been successfully applied for the *in vivo* determination of the molecular composition of arterial tissue¹³ and skin¹⁴, for the identification of micro-organisms¹⁵ and for the *in vivo* classification of different stages in malignant transformation¹⁶.

With the ultimate goal in mind, to apply Raman spectroscopy to monitor and relate changes in bladder wall structure and molecular composition to changes in bladder function, we have investigated the possibility to identify the different tissue layers in cross sections of bladder wall tissue on the basis of their *in vitro* Raman spectrum and we have identified the sources of the main signal contributions in each tissue layer.

We also have performed preliminary *in vivo* Raman spectroscopy on bladders. *In vivo* Raman spectra contain signal from all layers, contrary to *in vitro* Raman spectra which are measured separately in each layer. We have determined the signal contributions of each layer to the *in vivo* Raman spectra of bladders in both filled and emptied conditions.

Our goal is to identify damage in bladders, related to differences in layer contributions and molecular changes in the *in vivo* Raman spectra as the ultimate clinical application.

Materials and methods

Immunohistochemistry

Immunohistochemistry was used to locate smooth muscle actin (mouse anti-human smooth muscle actin, Biogenex, San Ramon, CA), collagen I (mouse anti-human collagen I, Novus Molecular Inc.) and collagen III (mouse anti-human collagen III, Biogenex, San Ramon, CA). Detection of the primary antibodies was done with the StrAviGen MultiLink[®] Kit from Biogenex which contains a biotinylated multilinker against all rodents and a horseradish peroxidase-conjugated streptavidin label. DAB was used together with H₂O₂ as substrate. The collagen I primary antibody was developed for use on frozen sections but could be applied to paraffin sections after a 0,1% pronase treatment, 15 min. at 37°C.

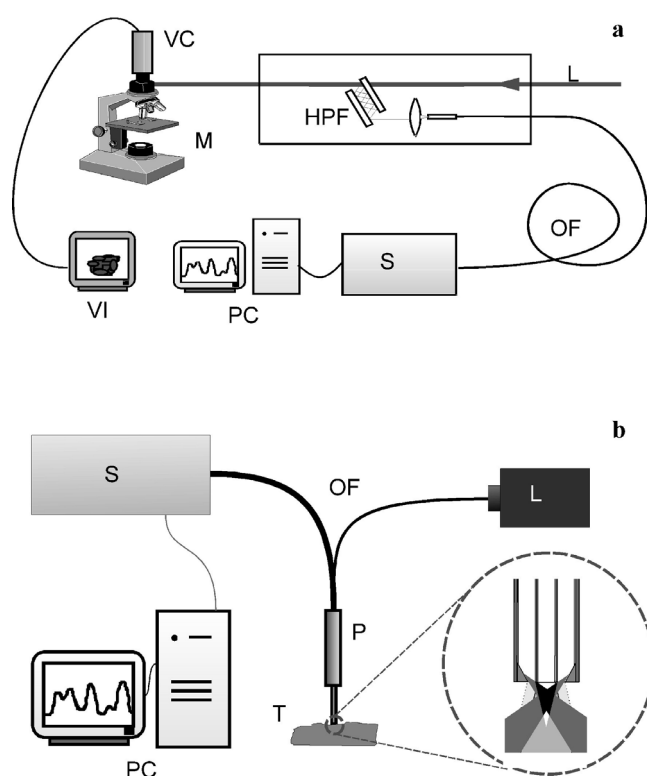


Figure 1

Schematic presentation of in vitro (a) and in vivo (b) Raman spectroscopic setups. Fiberoptic probe tip is enlarged. Black area represents tissue volume from which Raman signal is most efficiently collected. L, laser beam. HPF, high pass filter. M, microscope. OF, optical fiber. S, spectrometer. PC, personal computer. VC, video camera. VI, video imaging. P, probe. T, tissue.

In vitro Raman spectroscopy

Bladder tissue was collected from guinea pigs, used in our model for partial urethral obstruction⁷. Part of the tissue was snap frozen in liquid nitrogen cooled isopentane, stored at -80°C and used for Raman spectroscopic analysis. Frozen sections of 40–50 μm in thickness were cut and air-dried several hours prior to Raman spectroscopy. Formalin (10%) fixed tissue was embedded in paraffin and 5 μm thick sections were used for immunohistochemistry.

Frozen sections were placed under a microscope (DM-RXE, Leica, Cambridge, UK) that was interfaced to a Raman microspectrometer setup (figure 1a) built in-house. To collect Raman spectra, near infrared laser light ($\sim 847\text{ nm}$) from an Argon-ion pumped Titanium: Sapphire laser system (Spectra Physics, Mountain View, CA) was coupled into a microscope (DM-RXE, Leica, Cambridge, UK) via a single mode optical fiber ($\varnothing 0.1\text{ mm}$) and a high pass filter (HPF). An 80x NIR optimized objective (Olympus, Japan) was used to focus the laser light onto the tissue sample, and to collect light that was scattered by the sample. The HPF (a chevron type dielectric filter set) was used for optical coupling of the laser, the microscope and the spectrometer, and for suppression of the laser light that was scattered back by the tissue sample¹⁷. The inelastically scattered Raman light was focused onto the 100 μm \varnothing core of an optical fiber, which coupled the light into a spectrometer (System 100, Renishaw, Wotton under Edge, UK), equipped with a thermoelectrically cooled deep-depletion CCD camera. The CCD camera was connected to a personal computer where data were stored and analyzed.

Four frozen sections of bladder wall tissue on individual calciumfluoride (CaF_2) windows were placed on the motorized, computer controlled sample stage of the microscope (Leica DM STC, Cambridge, UK). Acquisition of Raman spectra and microscope stage movement were controlled by Grams/32 Spectral Notebook Software (Galactic Industries Corp., Salem, NH). Tissue areas containing urothelium, lamina propria and muscle layer were selected and Raman maps of these areas were constructed. For these maps, 500-700 spectra were obtained representing 500-700 elements of a 2-dimensional grid. The individual grid elements spanned tissue areas of 30 by 30 μm up to 90 by 90 μm . Signal collection time for each grid element was 60 seconds, during which time the grid element was scanned through the laser focus so as to obtain an area-averaged Raman spectrum. After measuring, the tissue was stained with haematoxylin/eosin (HE) and a digital photograph of the measured location was taken. For compositional analysis, spectra from collagen I, collagen III and actin were measured.

In vivo Raman spectroscopy

To study the possibilities for *in vivo* Raman spectroscopy on bladder wall tissue, bladders from guinea pigs undergoing operations for urodynamic studies^{4,7,8} were measured. No extra surgery or adjustments to the protocol were needed, additional operation time was 5 to 10 minutes. A detailed description of *in vivo* Raman setup (figure 1b) has been given elsewhere^{13,16,18}. A Visionex Gaser 10 forward viewing fiber optic probe was used to illuminate the bladder with laser light (wavelength 830 nm; laser power ~170 mW at the tissue; Process Instruments diode laser, Salt Lake City, UT) and to collect Raman signal from the tissue. The probe consists of a central 400 μm \varnothing illuminating fiber and 7 surrounding 300 μm \varnothing collecting fibers inside a metal case (8F, ~ 2.5 mm \varnothing). Signal detection was done with a spectrometer (System 100, Renishaw, Wotton under Edge, UK) with a spectral interval from 800 - 1800 cm^{-1} and a collection time of 10 seconds.

The probe was placed on the outside of the bladder wall measuring towards the urothelium. Bladders were measured in both filled and emptied conditions.

Data analysis

Wavenumber calibration and correction for the wavenumber dependent signal detection efficiency for both setups were carried out as described earlier^{9,18}. In addition to this, the emission lines of neon and neon-argon lamps were also used. Spectra were corrected for background signals and normalized, according to a procedure described by Wolthuis *et al.*¹⁸. *In vitro* measurements were carried out in the 400 - 1800 wavenumber interval, *in vivo* measurements in the 800 - 1800 cm^{-1} range. Spectral resolution of the *in vitro* and *in vivo* setup was approximately 8 - 10 cm^{-1} .

Cluster analysis. *In vitro* data were processed with Principal Component Analysis (PCA), an unsupervised mathematical method that finds combinations of variables which describe the major spectral trends in the integer data set and making it orthogonal. I.T. Jolliffe ¹⁹ has defined the applications of PCA in more detail. PCA processed data were analyzed by means of cluster analysis. Cluster analysis is used to find groups of spectra that have resembling spectral characteristics. Several sophisticated clustering methods exist ²⁰. Here we applied a simple method called K-means clustering (KCA), which can easily handle large amounts of PCA processed data like the Raman maps presented here ²⁰. With KCA, the spectra are grouped in a predetermined number of clusters. In short the procedure is as follows. For each cluster a spectrum is randomly chosen from the spectra in the data set, to act as initial cluster center. All spectra in the data set are then compared to these cluster centers and assigned to the center that they most resemble. After all spectra are assigned to a certain cluster, the new cluster centers are calculated by averaging all spectra assigned to a certain cluster. This procedure is repeated until a stable solution is reached.

Four clusters are used for bladder wall tissue analysis, based on the assumption that spectra could describe the three bladder layers and the absence of tissue in the measuring volume (holes in the tissue sections or tissue section edges). The clusters that were formed by means of KCA were assigned a color. Each grid element of the Raman map was then assigned the color of the particular cluster to where its spectrum belonged. In this way a color-map of the frozen section was obtained, in which areas with similar spectra have the same color. This color-map was then compared with the HE stained tissue digital photo of the frozen section.

These procedures of data analysis have been performed on four frozen sections of bladder wall tissue obtained from different animals.

Non-Negative Least Squares fitting procedure. For the determination of the signal contributions of the different bladder wall layers to the total *in vivo* bladder wall spectrum, a non-negative least squares (NNLS) fitting procedure was performed ²¹. With NNLS the proportions of multiple spectra from different sources (i.e. chemicals, tissues) in one total spectrum can be determined. NNLS uses a database of spectra to construct a spectrum that has the highest possible similarity to the total spectrum to be fitted. Spectra in the database can only have a positive contribution to the fit. In order to determine the signal contributions of individual bladder wall layers to the *in vivo* total bladder wall spectra, a database was created consisting of *in vitro* spectra obtained from isolated tissue layers (urothelium, lamina propria and muscle) and guinea pig urine. The spectra of these layers were obtained by means of the same setup as used for the *in vivo* measurements. From the fit coefficients the relative signal contribution of the individual tissue layers to the *in vivo* bladder wall spectrum were determined.

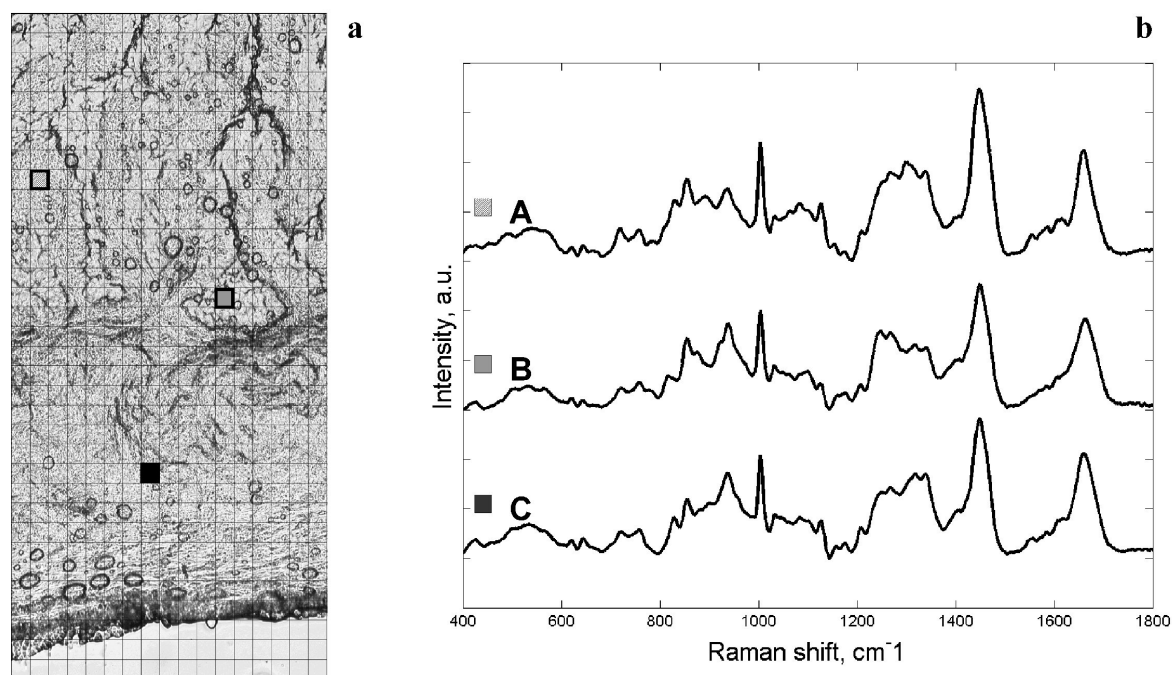


Figure 2

Examples of measurement area on bladder wall tissue, divided in grid elements (a) and Raman spectra measured in 3 grid elements (b). Dashed grid elements in a represent locations of these measured spectra. A, urothelium. B, lamina propria. C, muscle layer.

Results

Raman spectroscopy results

Figure 2a shows the area of one of the four bladder wall cross-sections that were analyzed with Raman spectroscopy. After calibration and correction for background signal, a Raman spectrum was obtained for each grid element, as shown in figure 2b. For each tissue section 500-700 spectra were obtained in a 2-dimensional grid as described in the section on materials and methods. The spectra were grouped using K-means cluster analysis and each group was assigned a color after which a color-map of the tissue section was constructed. These Raman-based color-maps were compared with the bright field microscopic image photographs of each of the measured tissues before and after HE-staining. As is evident from figure 3, the Raman maps closely corresponded to the bladder wall structure as seen in the photographs.

The Raman map shows the urothelium in black, the lamina propria in dark and the smooth muscle layer in light gray. Locations in the image where no tissue was present and where accordingly only Raman signal from the support material was obtained are shown in white. Some areas within the muscle layer gave rise to spectra that ended up in the same cluster as the spectra from the lamina propria. These areas correspond to bundles of collagen fibers between the muscle fibers. As is shown below the main signal contribution to the lamina propria spectra is also due to collagen.

Apart from this, the three bladder layers produce Raman spectra that differ sufficiently to distinguish between them.

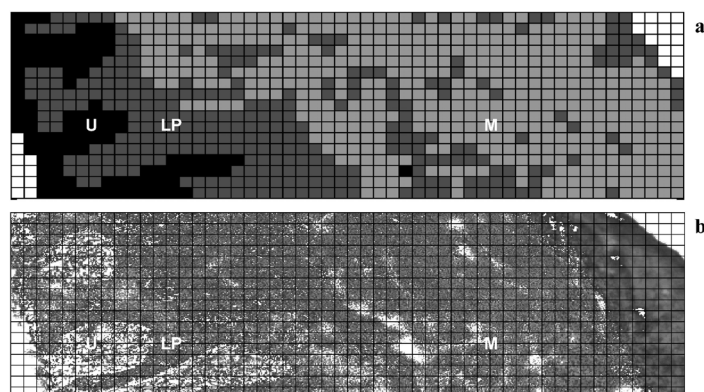


Figure 3

Comparison of Raman map of semi-section of bladder wall (a) with microscopic image of same section after hematoxylin and eosin staining (b). Urothelium (U) is black, lamina propria (LP) is dark gray and muscle layer (M) is light gray. Dark gray areas throughout light gray muscle layer are collagen fibers, which clustered with lamina propria, and mainly consist of collagen. White areas represent areas without tissue Raman signal.

Compositional analysis

The averaged spectra of the muscle layer cluster and the lamina propria cluster were compared with reference spectra of respectively actin and collagen, because these components are known to be abundant in these layers. Figure 4 illustrates that the spectrum of the muscle layer is dominated by signal contributions from actin. Both actin and myosin are two major intracellular muscle proteins. The spectra of these proteins are very similar²²⁻²⁵.

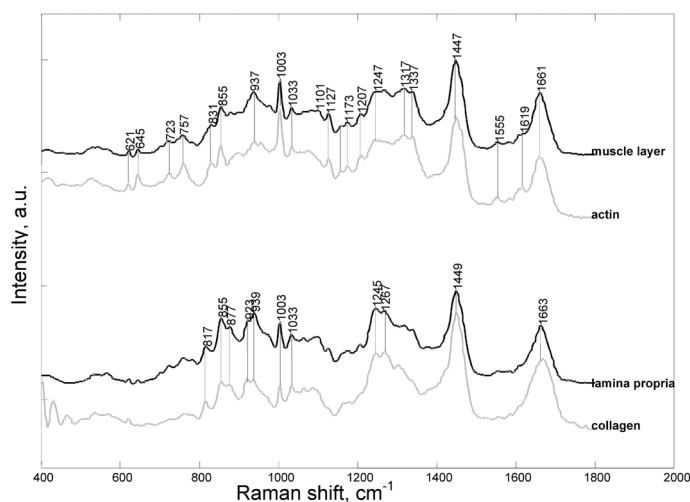


Figure 4

Raman spectrum of muscle layer compared to actin spectrum and Raman spectrum of lamina propria compared to collagen spectrum. Small vertical lines between tissue spectra (black) and pure compound spectra (gray) highlight similarities.

Likewise, figure 4 shows that the main signal contributions to the lamina propria spectrum come from collagen. The vertical lines together with peak positions emphasize correlation of tissue spectra and reference spectra^{26,27}. All band positions that are characteristic for collagen are also found in the spectrum of the lamina propria. The presence of the highest concentration of collagen in lamina propria was confirmed by immunohistochemical analysis (figure 5).

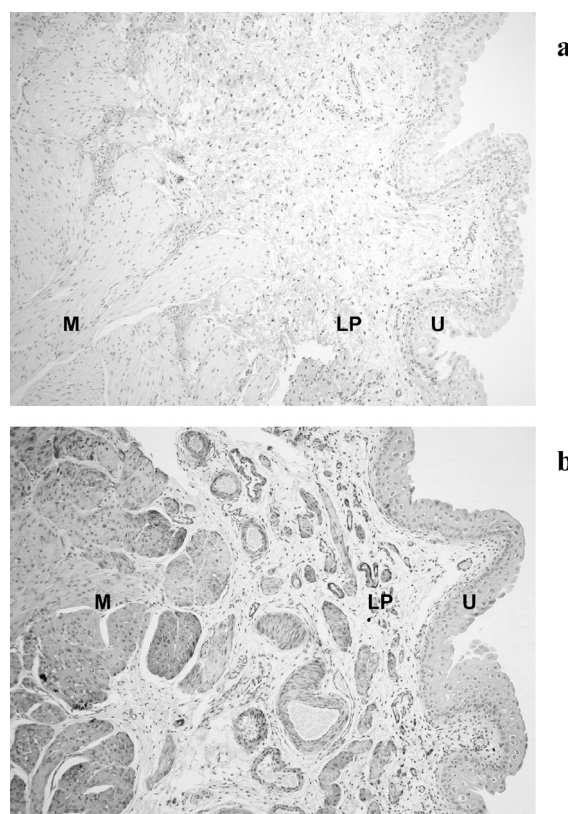


Figure 5

Immunohistochemical staining of collagen (a) and smooth muscle actin (b) in bladder wall with diaminobenzidine tetrahydrochloride and Mayer's hematoxylin background staining. Collagen is mainly present in lamina propria (LP) and in smaller amount between muscle fibers (M). Actin is mainly present in the muscle layer and around blood vessels in the lamina propria. U, urothelium.

Color version: see appendix.

The urothelium contains stronger signal contributions from fatty acids than the spectra of the lamina propria or the muscle layer. This becomes clear when a difference spectrum is calculated (figure 6B, urothelium spectrum minus muscle layer spectrum), which enhances the differences between these spectra. Positive features in this spectrum correspond to molecular species present in a relatively higher concentration in the urothelium. A comparison with a typical fatty acid spectrum (oleic acid) shows that fatty acid concentration is higher in the urothelium. In figure 5 the vertical lines at 1081 cm^{-1} , 1261 cm^{-1} , 1299 cm^{-1} , 1439 cm^{-1} and 1659 cm^{-1} show the correlation between the urothelium residue spectrum and a spectrum of fatty acids.

HE stained bladder wall sections reveal the typical bladder-wall layers, muscle, lamina propria and urothelium. Immunohistochemistry revealed the location of collagen I (figure 6a) and III (not shown) throughout the whole lamina propria and around the muscle fibers. There was no expression of either collagen I or III in the urothelium. Smooth muscle actin stained in the whole muscle layer and in small amounts around blood vessels in the lamina propria (figure 6b).

In vivo Raman spectroscopy

In figure 7 a typical example of a fit procedure on an *in vivo* bladder spectrum is shown. In this example the bladder was filled, which means that signal from urine was measured as well. Therefore a spectrum of guinea pig urine was added to the

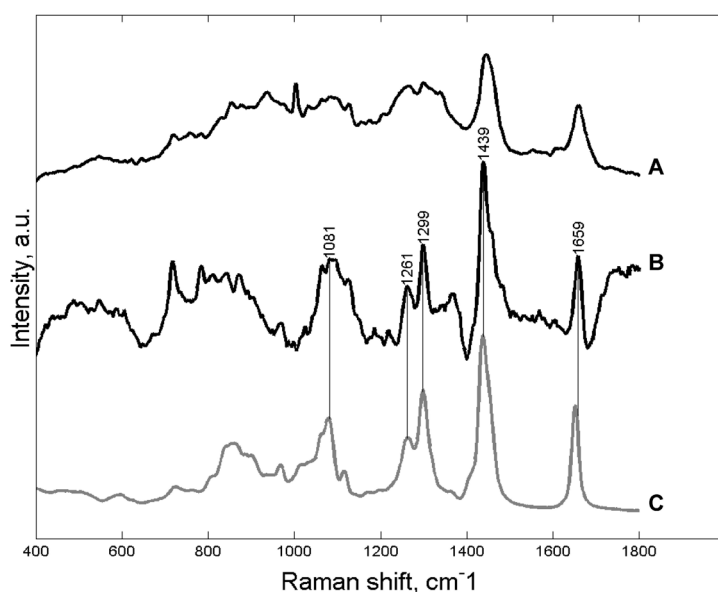


Figure 6

Raman spectrum of urothelium (a), difference of Raman spectrum urothelium minus muscle layer (b) and spectrum of fatty acids (c). Urothelium contains relatively more lipids compared to other layers. These lipid characteristics are enhanced when muscle spectrum is subtracted, forming a different spectrum. Similarities are clearly shown between different spectrum and spectrum of pure fatty acids, indicated by thin vertical lines.

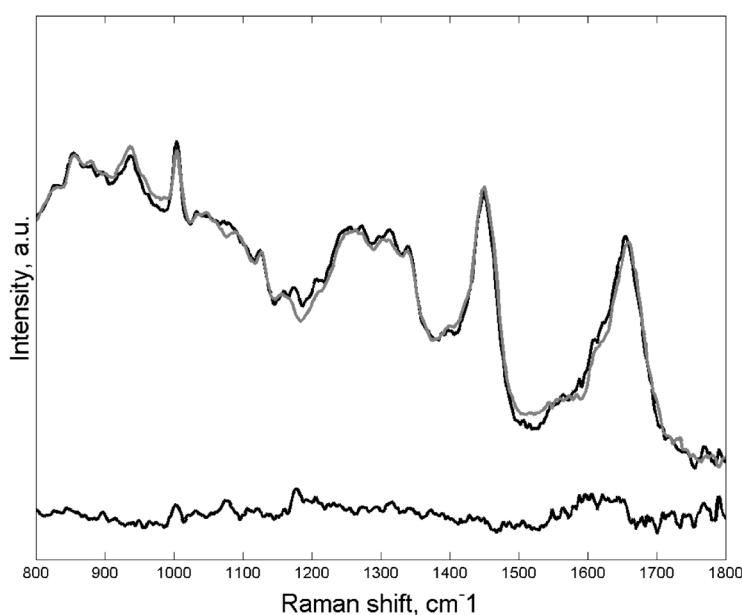


Figure 7

In vivo Raman spectroscopy of bladder wall shows whole bladder Raman spectrum (a), result of fit procedure of spectrum a with spectra of isolated bladder wall layers (urothelium, lamina propria and muscle layer) and fit result of a-b (c).

bladder spectral database, explained in materials and methods. The contribution of urine signal, first determined from the total bladder spectrum, is 51 %. The remaining of the fit result, consisting of purely tissue signal, is set to 100%. From this, the contributions of the individual bladder wall layers are determined; 65 % is from muscle layer, 16 % from lamina propria and 19 % from urothelium.

A fit residual is produced by subtracting the total fit result from the whole bladder wall spectrum. The fit residual indicates where and to what extent the fit result still differs from the whole bladder spectrum. The fit procedure gives a good match but needs optimization.

Discussion

The results of this work show that Raman spectroscopy has great potential for investigations of bladder pathologies in general, and for *in vitro* and *in vivo* monitoring of bladder wall structure and molecular composition of bladder wall layers in particular. It was shown by means of Raman microspectroscopic mapping and clustering analysis, that the spectra of the urothelium, the lamina propria and the smooth muscle layer are easily distinguishable.

Moreover, as an initial comparison with reference spectra of pure compounds already makes clear, information can be obtained about the molecular composition of the different tissue layers. The lamina propria spectrum is characterized by strong signal contributions from collagen, as would also be expected, from a comparison with a collagen I immunohistochemical staining (figure 3). Not surprisingly, the smooth muscle layer has strong signal contributions from actin and myosin. Figure 6 shows that in comparison to the other tissue layers the lipid concentration is significantly higher in the urothelium. Urothelium cells are relatively small compared to lamina propria cells, have a higher concentration of intracellular free fatty acids²⁸ and there are no extra-cellular components such as collagen fibers between the cells. Therefore, the amount of cell membrane (which contain a high amount of fatty acids) per measured grid element is also increased. At the luminal side the urothelium also contains lipid-based plaques, which are impermeable for urine²⁸.

We are currently working to refine the analysis of the spectra from single bladder samples to obtain more detailed information about the molecular composition of the different tissue layers. Maps will be made at higher spatial resolution (in principle a sub-micron resolution can be obtained, as in any optical microscope). Spectra will be fitted with an extensive database of spectra of pure compounds, known or assumed to be present in a concentration that would lead to a measurable contribution to the Raman spectrum, analogous to previous work on arterial wall and skin^{13,14}. This would enable us to extend the research to series of samples, e.g. comparing normal bladder to obstructed bladder. It is well known that several changes take place in molecular composition of the bladder wall tissue layers as a result of urethral obstruction in specific regions. Moreover, bladder function loss is known to be related to changes in collagen deposition.

Our preliminary *in vivo* measurements show that in a single bladder spectrum the contributions of each bladder wall layer can be determined. Therefore we used a non-negative least squares (NNLS) fitting procedure. For NNLS we have used a database consisted of spectra from the separated individual tissue layers (urothelium, lamina propria and muscle) and guinea pig urine to construct a spectrum that has the highest possible similarity to the total spectrum to be fitted. The total tissue contribution, obtained by excluding the urine signal from the fit result, has been set to 100%, from which we determined the contributions of each bladder wall layer. In the example,

half of the total signal is due to urine. In other bladder measurements in which the bladder was filled to a different extent, a different urine signal contribution was observed due to variation in the thickness of bladder wall samples. The fit residual, obtained by subtracting the fit result from the measured whole bladder wall spectrum, is an indicator to observe the accuracy of the fit procedure. Bands in the residual may be explained as molecular residues, not present in the fit spectra of the database, or that the fit spectra were not adequate enough.

The quality of the bladder spectral database spectra can be improved by increasing the number of measurements on isolated bladder wall layers. With this in mind we will further develop *in vivo* Raman spectroscopy for determining specific alterations of bladder wall layer contribution due to obstruction. Based on the results of the *in vitro* studies, we will also explore if differences in molecular composition can be detected with *in vivo* measurements.

On the one hand, the information obtained in such studies will provide valuable information that may help to further unravel the processes and events that lead to restoration of normal bladder function or irreversible loss of function, regarding the overall changes in molecular composition of bladder wall layers. On the other hand it may prove possible to use the changes in the Raman spectra that result from the changes in molecular composition to develop a diagnostic tool that will predict reversibility/irreversibility response to treatment. This may ultimately reduce the need for taking bladder biopsies and open the way for monitoring changes in bladder wall structure in a longitudinal fashion.

Acknowledgement

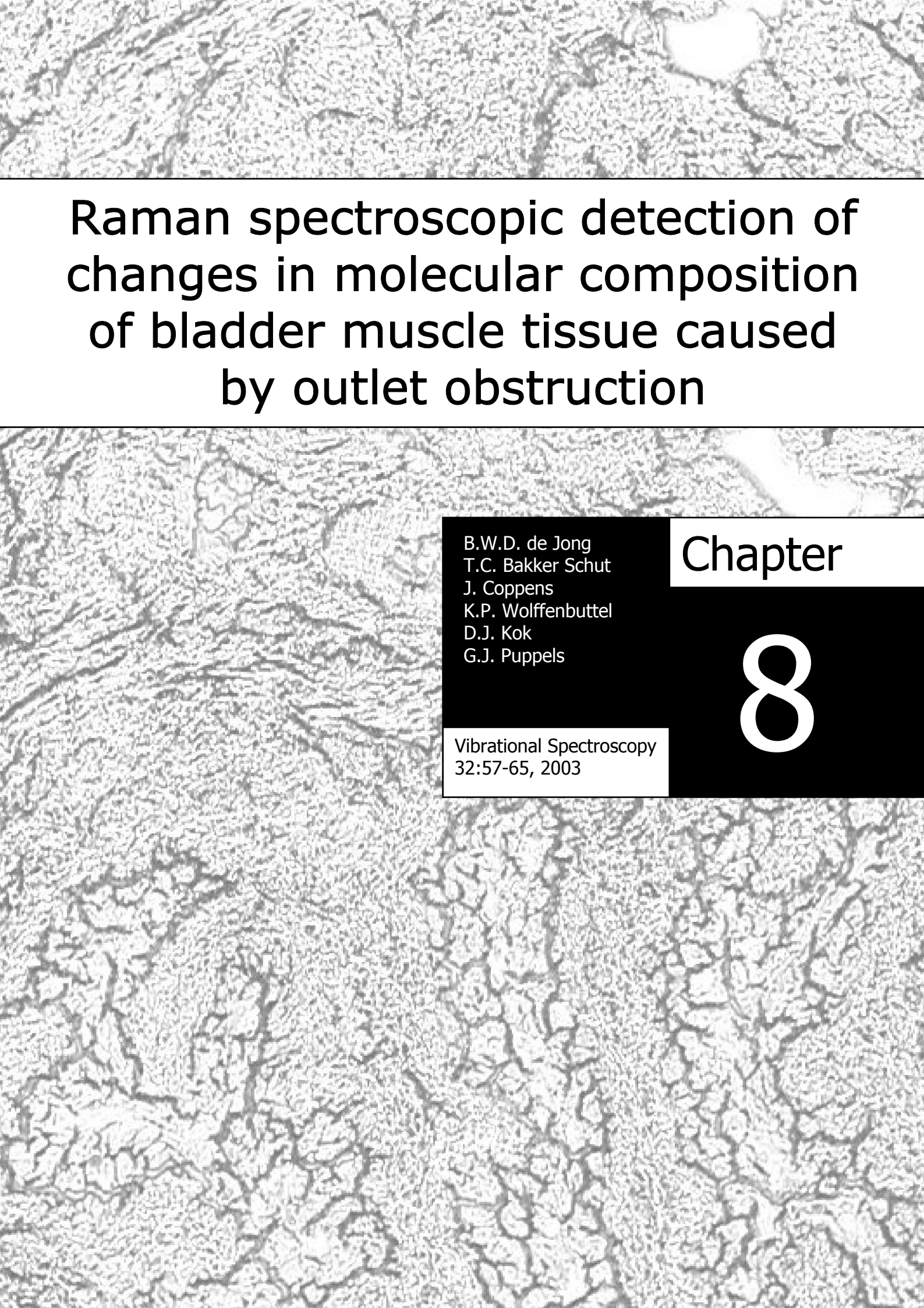
This work was supported by the SUWO (Society for Urological Research, The Netherlands)

References

1. Zderic SA, Wein A, Rohrman D, Gong CL, Nigro D, Haugaard N and Levin R.: Mechanisms of bladder smooth-muscle hypertrophy and decompensation: lessons from normal development and the response to outlet obstruction, *World J Urol*, **16**: 350-358, 1998.
2. Holmdahl G: Bladder dysfunction in boys with posterior urethral valves. *Scand J Urol & Nephrol, Supplementum* **188**: 1-36, 1997.
3. Van Mastrigt R and Griffiths DJ: An evaluation of contractility parameters determined from isometric contractions and micturition studies. *Urol Res*, **14**: 45-52, 1986.
4. Groen J, van Mastrigt R, van Asselt E, van Koeveeringe GA and Bosch R: Contractility parameters of the guinea pig bladder in situ: Similarity to human bladder contractility. *J Urol*, **151**: 1405-1410, 1994.
5. Freedman AL, Qureshi F, Shapiro E, Lepor H, Jacques SM, Evans MI, Smith CA, Gonzalez R and Johnson MP: Smooth muscle development in the obstructed fetal bladder. *Urology*, **49**: 104-107, 1997.
6. Deveaud CM, Macarak EJ, Kucich U, Ewalt DH, Abrams WR and Howard PS: Molecular analysis of collagens in bladder fibrosis. *J Urol*, **160**: 1518-1527, 1998.

7. Wolffenbittel KP, Kok DJ, Minekus JPJ, van Koeveringe GA, van Mastrigt R and Nijman JM: Urodynamic follow-up of experimental urethral obstruction in individual guinea pigs. *Neurourol Urodyn*, **20**: 699-713, 2001.
8. Kok DJ, Wolffenbittel KP, Minekus JP, van Mastrigt R and Nijman JM: Changes in bladder contractility and bladder compliance upon urethral obstruction: a longitudinal follow-up of individual guinea pigs. *J Urol*, **164**: 1021-1024, 2000.
9. Puppels GJ: Confocal Raman Microspectroscopy, in Mason WT: *Fluorescent and Luminescent Probes for Biological Activity*. San Diego, Academic Press, 1999, pp 377-406.
10. Hanlon EB, Manoharan R, Koo TW, Shafer KE, Motz JT, Fitzmaurice M, Kramer JR, Itzkan I, Dasari RR and Feld MS: Prospects for in vivo Raman spectroscopy. *Phys Med Biol*. **45**: R1-59, 2000.
11. Manoharan R, Wang Y and Feld MS: Histochemical analysis of biological tissues using Raman spectroscopy. *Spectrochimica Acta Part A*. **52**: 215-249, 1996.
12. Tu AT: Basic concept and elementary theory: *Raman Spectroscopy in Biology*. New York, John Wiley & Sons; Ltd., 1982.
13. Buschman HP, Marple ET, Wach ML, Bennett B, Bakker Schut TC, Bruining HA, Bruschke AV, van der Laarse A and Puppels GJ: *In vivo* determination of the molecular composition of artery wall by intravascular Raman spectroscopy. *Anal. Chem.* **72**: 3771-3775, 2000.
14. Caspers PJ, Lucassen GW, Wolthuis R, Bruining HA and Puppels GJ: *In vitro* and *in vivo* Raman spectroscopy of human skin. *Biospectroscopy*. **4**: S31-39, 1998.
15. Maquelin K, Choo-Smith LP, van Vreeswijk T, Endtz HP, Smith B, Bennett R, Bruining HA and Puppels GJ: Raman spectroscopic method for identification of clinically relevant microorganisms growing on solid culture medium. *Anal. Chem.* **72**: 12-19, 2000.
16. Bakker Schut TC, Witjes JH, Sterenberg HJCM, Speelman OC, Roodenburg JLN, Marple ET, Bruining HA and Puppels GJ: *In vivo* detection of dysplastic tissue by Raman spectroscopy. *Anal. Chem.* **72**: 6010-6018, 2000.
17. Puppels GJ, de Grauw CG, Plate MBJT, and Greve J: Chevron-type dielectric filter set for efficient narrow-band laser line rejection in Raman microspectrometers. *Appl Spectrosc* **48**:1399-1402, 1994.

18. Wolthuis R, Bakker Schut TC, Caspers PJ, Buschman HPJ, Römer TJ Bruining HA and Puppels GJ: Raman spectroscopy methods for *in vitro* and *in vivo* tissue characterization, in Mason WT: *Fluorescent and Luminescent Probes for Biological Activity*. San Diego, Academic Press, 1999, pp 433-455.
19. Jolliffe IT: *Principal Component Analysis*. New York, Springer-Verlag, 1986
20. Jain AK and Dubes RC: *Algorithms for clustering data*. Englewood Cliffs, Prentice Hall, 1988.
21. Brennan JF, Römer TJ, Lees RS, Tercyak AM, Kramer JR and Feld MS: Determination of human coronary artery composition by Raman spectroscopy. *Circulation* **96**: 99-105,1997.
22. Kishi K and Noda H: Laser Raman studies on myosin, C-protein and myosin-C-protein complex. *J Biochem (Tokyo)*. **94**: 353-9, 1983.
23. Barrett TW, Peticolas WL and Robson RM: Laser Raman light-scattering observations of conformational changes in myosin induced by inorganic salts. *Biophys J*. **23**: 349-58, 1978.
24. Pezolet M, Pigeon-Gosselin M, Nadeau J and Caille JP: Laser Raman scattering. A molecular probe of the contractile state of intact single muscle fibers. *Biophys J*. **31**: 1-8, 1980.
25. Caille JP, Pigeon-Gosselin M and Pezolet M: Effects of organic solutes on the Raman spectra of barnacle muscle fibers. *Can J Physiol Pharmacol*. **65**: 1416-20, 1987.
26. Frushour BG and Koenig JL: Raman scattering of collagen, gelatin, and elastin. *Biopolymers* **14**: 379-91, 1975.
27. Goheen SC, Lis LJ and Kauffman JW: Raman spectroscopy of intact feline corneal collagen. *Biochim Biophys Acta*. **536**: 197-204, 1978.
28. O'Conner LJ, Nicolas T and Levin RM: Subcellular distribution of free fatty acids, phospholipids, and endogenous lipase activity of rabbit urinary bladder smooth muscle and mucosa. *Adv Exp Med Biol* **462**: 265-73, 1999.

A grayscale microscopic image of bladder muscle tissue, showing a complex, textured pattern of muscle fibers and connective tissue. The image is used as a background for the chapter title and author information.

Raman spectroscopic detection of changes in molecular composition of bladder muscle tissue caused by outlet obstruction

B.W.D. de Jong
T.C. Bakker Schut
J. Coppens
K.P. Wolffenbuttel
D.J. Kok
G.J. Puppels

Chapter

8

Vibrational Spectroscopy
32:57-65, 2003

Abstract

Bladder outlet obstruction leads to loss of bladder function as a result of structural damage. Functional parameters of an obstructed bladder do not enable a prediction of the clinical outcome of removal of the obstruction. Therefore other diagnostic methods are needed. This study presents first results of an approach based on Raman spectroscopy, which aims to detect changes in molecular composition of the bladder wall that may have diagnostic value. Raman spectroscopic mapping of unfixed sections of damaged and undamaged bladder wall from a guinea pig model of bladder obstruction was used to detect changes in composition of bladder muscle tissue. Collagen infiltration in muscle fibers was clearly visualized. Other compositional changes that are revealed include the accumulation of glycogen in obstructed bladder wall as well as an apparent but as yet unknown change in protein composition. *In vivo* Raman spectroscopic application may enable determination of bladder structure without the need for biopsies. These initial findings show that Raman spectroscopy can be a valuable diagnostic tool for evaluation of the extent of bladder structure loss.

Introduction

Bladder outlet obstruction affects both pediatric and adult populations [1]. It leads to loss of bladder function and may affect kidney function. At present urodynamic parameters are used to diagnose bladder dysfunction. With this approach the chances for restoration of function upon removal of the obstruction cannot be predicted. Bladder dysfunction is characterized by increased bladder pressure, changed flow rates, instability, in- or decreased bladder contractility and decreased bladder compliance [2]. The rate at which these parameters deteriorate varies between individuals. Furthermore, for some parameters the direction of the change reverses over time. For instance, bladder contractility first increases, then stabilizes and finally may decrease again. It is difficult to establish the degree of bladder deterioration at a single time point from the urodynamic parameters unless the complete urodynamic history is also known. Clinically, the functional history of a specific bladder is usually unknown at the time a patient presents. In most cases only a single time point urodynamic evaluation is available. It is even more difficult to predict how a bladder will react to removal of the obstruction. Patients presenting with similar bladder function can either improve or further deteriorate. Additional diagnostic measures are needed to establish both the progression of deterioration for a specific bladder and its chances of functional recovery.

The functional changes are accompanied by clear changes in bladder structure. In short, the bladder wall consists of three internal layers. The urothelium, the innermost layer, is an epithelium that is resistant to the urine it faces. A middle layer, the lamina propria, consists mainly of connective tissue (collagen) that smoothly stretches to a certain maximum and at that moment inhibits further stretching of the bladder. On the outside lies the muscle layer that, upon activation, provides the contraction to empty the bladder. Known structural changes due to obstruction are thickening of the total bladder wall, smooth muscle cell hypertrophy, extra-cellular matrix deposition in the lamina propria as well as collagen infiltration within muscle fibers [3, 4, 5]. It has been proposed that the collagen depositions in the lamina propria and collagen infiltration into the muscle layer are related to the decreasing compliance. Collagen infiltration in addition is thought to decrease bladder contractility by hindering proper muscle contraction, caused by local ischemia (improper blood perfusion) [6] or by separating the cells of the nervous system from the muscle fibers, which will interrupt activation of muscle contraction.

Raman spectroscopic mapping can detect small changes in tissue structure, as was shown for various other tissues like brain tumors and basal cell carcinomas [7, 8].

Recently, we have shown that Raman spectroscopic mapping allows clear identification of the urothelium, lamina propria and muscle layer [9].

In this study we show that more detailed Raman spectroscopic mapping could be a diagnostic tool to characterize changes in composition of bladder wall.

Materials and methods

Bladder tissue was obtained from guinea pigs used in our model for partial urethral obstruction [2, 10]. Normal and damaged tissues were selected based on urodynamic as well as histological observations.

Raman spectroscopy

For Raman mapping, frozen sections of 20–25 μm in thickness from four normal bladders and three obstructed bladders were individually mounted on CaF_2 windows and air-dried several hours prior to Raman spectroscopy. The bladder wall samples were placed on the motorized, computer controlled sample stage of a microscope (DM-RXE, Leica, Cambridge, UK) that was interfaced to a Raman microspectrometer setup (figure 1) built in-house. Acquisition of Raman spectra was controlled by the WiRE 1.2 software (Renishaw) using Grams/32 Spectral Notebook Software (Galactic Industries Corp., Salem, NH, USA). Stage movement was programmed in Array Basic (the internal software platform of Grams). To collect Raman spectra, near infrared laser light (845 nm) from a Spectra Physics 3900S Titanium Sapphire laser system (Spectra Physics, Mountain View, CA) pumped with a Coherent Innova 300 Argon-ion laser (Coherent, Palo Alto, CA) was used. The laser light was coupled into the microscope via a single mode optical fiber and a chevron type dielectric short pass filter set. An 80x NIR optimized objective (Olympus, Tokyo, Japan) was used to focus the laser light onto the tissue sample, and to collect light that was scattered by the sample. The chevron filter was used for optical coupling of the laser, the microscope

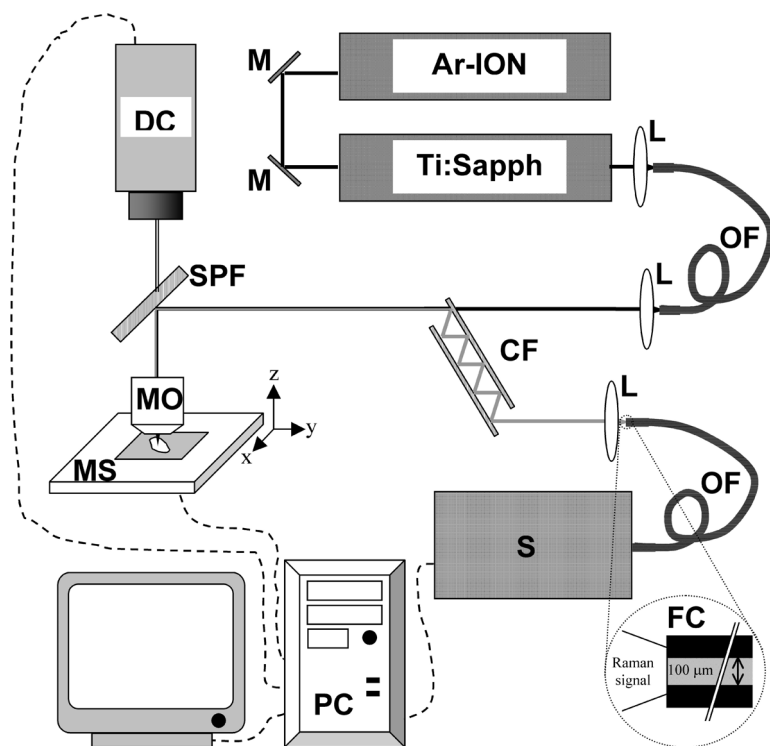


Figure1: Schematic overview of Raman mapping system; Ar-ION: argon ion laser, Ti:Sapph: titanium sapphire laser, tunable, set at ~ 845 nm, M: mirror, L : lens, OF: optical fiber 100 μm diameter core, SPF: short pass filter $< \sim 700$ nm, CF: Chevron filter, made of two dielectric short pass filters < 850 nm, MO: microscope objective 80x NA 0.75 NIR, MS: computer controlled x-y-z microscope stage, FC: detail of fiber optic core, S: spectrometer with back depletion CCD, PC: computer, DC: digital video camera.

and the spectrometer, and for suppression of the laser light that was scattered back by the tissue sample. The inelastically scattered and filtered Raman light was focused onto the 100 μm diameter core of an optical fiber. The optical fiber was coupled into a spectrometer (System 100, Renishaw, Wotton under Edge, UK), equipped with a thermoelectrically cooled deep-depletion CCD camera. The CCD camera was connected to a personal computer where data were stored.

Data acquisition and analysis

Tissue areas in the normal and damaged bladder wall sections containing sharply defined muscle fibers were selected and Raman maps of these areas were constructed. The individual grid elements spanned tissue areas of 2-3 square microns. Signal collection time for each grid element was 20 seconds, during which time the grid element was scanned through the laser focus so as to obtain an area-averaged Raman spectrum. We have focused this study on the bladder muscle layer.

All data processing software was programmed in Matlab 6.1 (Mathworks, Natick, MA), using the PLS-toolbox (Eigenvector Research Inc., Manson, WA). Wavenumber calibration and correction for the wavenumber dependent signal detection efficiency was carried out as described earlier [11]. All measurements were carried out in the 400 - 1800 wavenumber interval with a spectral resolution of 8 cm^{-1} . After correction and interpolation, first derivatives of all spectra were calculated, using the Savitzky-Golay to minimize the effect of a slightly varying background to the spectra, probably due to small contributions of tissue-auto-fluorescence.

Raman mapping data were processed with Principal Component Analysis (PCA) for data reduction and orthogonalization. PCA-scores were analyzed by means of cluster analysis. Cluster analysis is used to find groups of spectra that have resembling spectral characteristics. Several sophisticated clustering methods exist. Here we applied a simple method called K-means clustering (KMC), which is best suited to handle large amounts of data. With KMC, the spectra are grouped in a predetermined number of clusters. In short the procedure is as follows. For each cluster a spectrum is randomly chosen from the spectra in the data set, to act as an initial cluster center. All spectra in the data set are then compared to these cluster centers and assigned to the center that they most resemble. After all spectra are assigned to a certain cluster, the new cluster centers are calculated by averaging all spectra assigned to a certain cluster. This procedure is repeated until a stable solution is reached. To compare the molecular composition of both tissues, the KMC was performed on the data sets obtained from the unobstructed and the obstructed bladder together. In this way, both differences and similarities in molecular composition and variance in the locations of clusters in the maps are detected. The clusters that were formed by means of KMC were assigned a color. Each grid element of the Raman map was then assigned the color of the particular cluster to which its spectrum belonged. In this way Raman maps of the frozen sections were obtained, in which areas with similar spectra have

the same color. The Raman maps were then compared with images of the same tissues after histological staining that was performed after the Raman measurements.

Histochemistry

The elastic Von Gieson (EVG) was used to stain the measured frozen sections after the measurements. The frozen sections were fixed in 4% buffered formalin for 1 minute prior to staining. With the EVG stain, the collagen fibers are stained red, whereas the rest of the tissue is stained yellow. In addition, the elastin fibers are stained black/dark blue. Images of the Raman mapped areas were taken with a Sony DXC-950P digital camera (Sony Corporation, Tokyo, Japan) mounted on top of the microscope and interfaced with the computer (figure 1).

Results and discussion

Raman spectroscopic mapping

The examples that are presented here of both normal and damaged bladder tissue are representative for the results in all maps. The normal bladder tissue map contained 9720 spectra and the damaged bladder tissue map 8555 spectra. Examples of maps

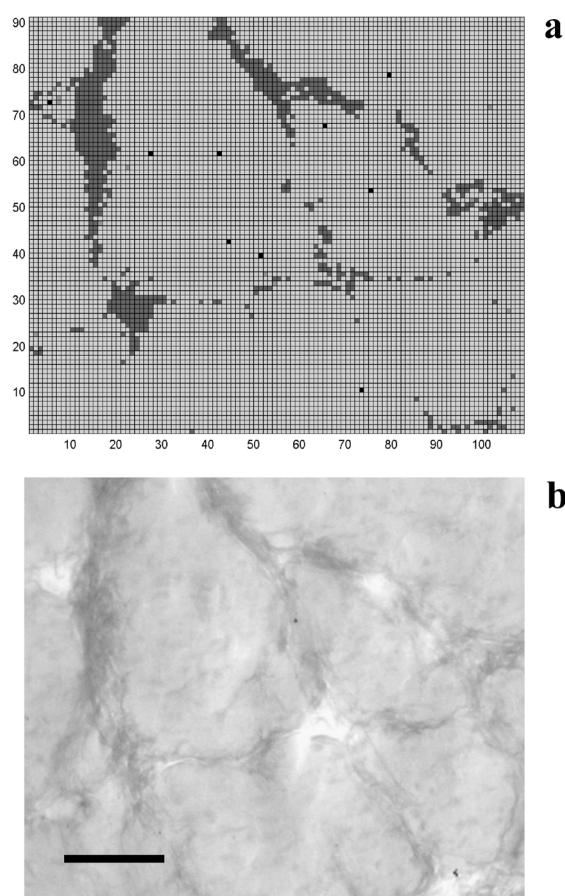


Figure 2:

Raman spectroscopic maps of normal (a) and damaged (c) bladder muscle tissues. In the normal tissue map, cluster III represents the muscle tissue. Cluster V represents the collagen fibers. The Raman map clearly matches the photograph taken from the EVG stained normal bladder tissue section (b). Collagen stains dark gray and muscle tissue stains light gray. Scale bar is 100 μm.

The collagen cluster of the normal tissue map also appears in the damaged tissue map (c) (cluster V). Furthermore in the damaged tissue map, cluster IV represents the collagen infiltration, cluster I and II both represent muscle tissue. Due to destruction during staining of the damaged bladder wall slide, a photograph of an EVG stained adjacent slide is shown (d).

obtained from normal and obstructed tissue, accompanied with images of the EVG stains, are shown figure 2. The number of clusters was determined by repeatedly performing the KMC, adding one extra cluster with every new clustering analysis. The spectral differences between clusters were clearly related to differences in Raman signal contributions when the number of allowed clusters was limited to 5. When more than 5 clusters were allowed, differences in spectral characteristics of the broad relatively featureless background to the Raman signal clearly contributed to the clustering. Therefore the number of clusters was limited to 5. The contours of the normal tissue map (figure 2a) perfectly match the image taken from the area of the tissue on which the Raman map was measured (figure 2b). For the damaged tissue section an adjacent tissue section had to be used for the EVG-stain, since the section used in the Raman experiments was lost during the staining procedure. For this reason the contours of the stained section and the Raman map do not perfectly match (figure 2d). Cluster-averaged spectra belonging to the maps of figure 2a and c are plotted in figure 3.

The map of the normal bladder tissue (figure 2a) contains only two clusters; one mainly showing spectral characteristics of collagen and the other mainly showing spectral characteristics of actin and myosin [9]. The muscle and collagen clusters are clearly separated. There is no indication of collagen infiltration. The same collagen cluster also occurred in the map of damaged tissue (figure 2c) and was assigned to the surrounding collagen fibers. However, an additional cluster was observed in the data set of the damaged tissue, containing spectral characteristics of both collagen and muscle. It was found within and directly surrounding the muscle fibers. As comparison with histology revealed (figure 2d), this cluster seems to be associated with collagen infiltration. Thin infiltrating collagen fibers in the bladder wall tissue of our model have a maximum diameter of 10 μm . Since the tissue sections used for

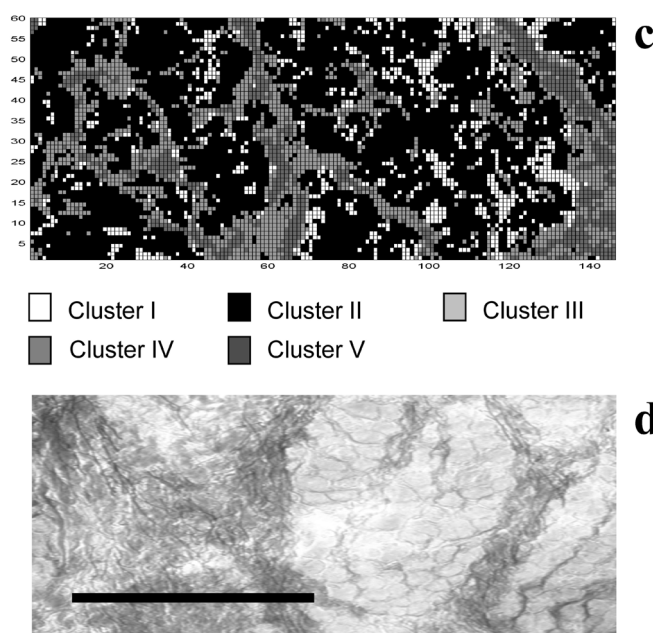


Figure 2 (Continued)

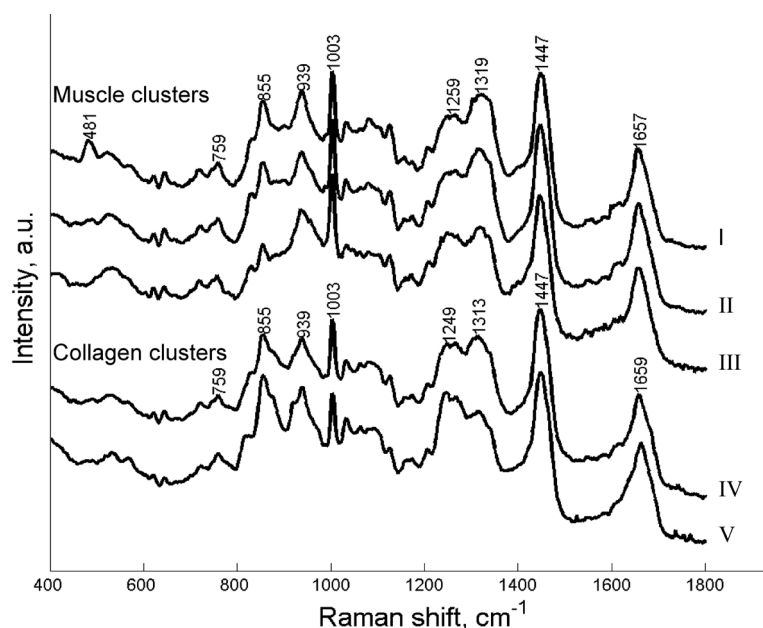
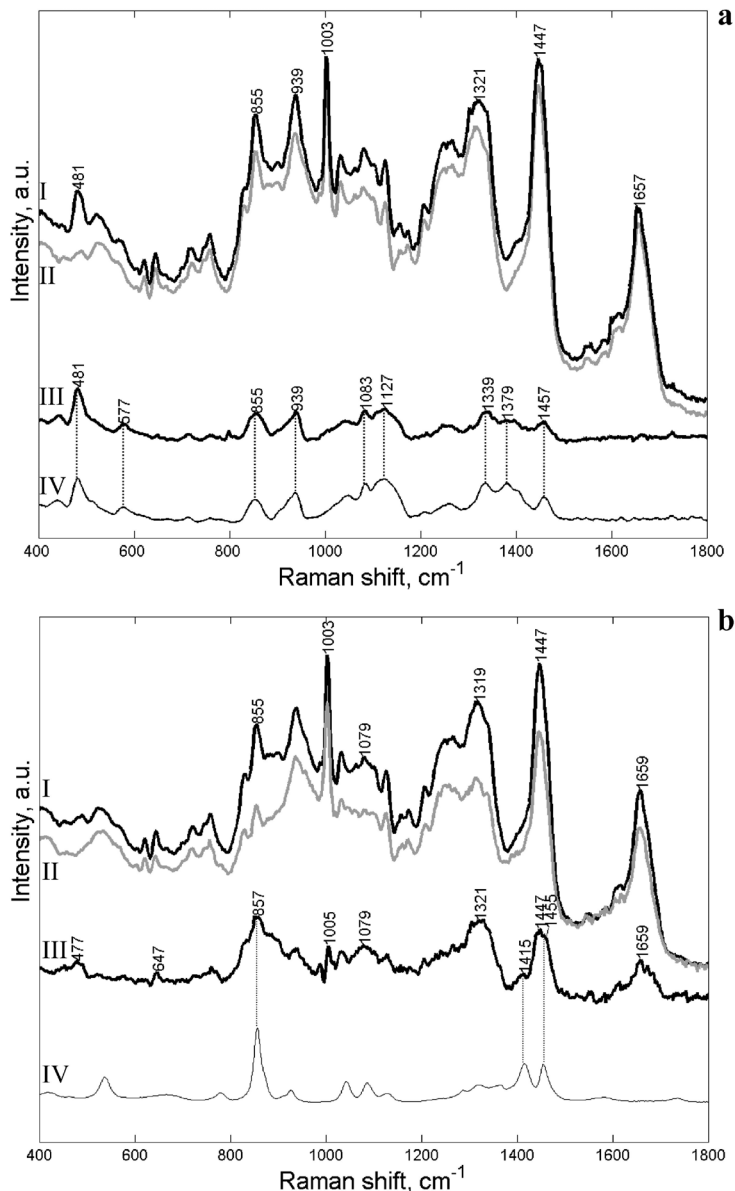


Figure 3: Averaged spectra of all clusters, divided in collagen and muscle characteristics. I: muscle cluster of damaged tissue (white areas in Raman map), II: muscle cluster of damaged tissue (black areas in Raman map), III: muscle cluster of normal tissue, IV: collagen infiltration cluster in damaged tissue, V: collagen fiber cluster in both normal and damaged tissue.

Raman mapping are 20 μm in thickness, the measuring volume always contains muscle tissue surrounding these collagen fibers which contributes to the Raman signal at the location of these infiltrating collagen fibers. Therefore in each grid element that comprises thin collagen fibers, signal from muscle tissue is also included. The same happens at the edges of muscle fibers where grid elements overlap both muscle tissue and a surrounding collagen fiber. To determine collagen infiltration only within the muscle fibers, the collagen directly surrounding the muscle fibers must be excluded.

In contrast to the collagen clusters, the muscle tissue of both maps was clustered separately. One cluster contained all spectra assigned to normal muscle tissue. Two other clusters contained spectra of muscle tissue in the damaged map. The difference spectrum of these two clusters (spectrum III in figure 4a) revealed an almost pure spectrum of glycogen. Below the difference spectrum a reference spectrum of glycogen (measured in-house, Sigma, Zwijndrecht, The Netherlands) is plotted, band position similarities are emphasized with dotted vertical lines. The muscle/glycogen cluster was dispersed in small units all over the damaged muscle layer, indicating glycogen accumulations. The origin of this is unclear and needs to be elucidated but the glycogen accumulations may be related to an inactive state of parts of the bladder muscle. To our knowledge, no other reports have appeared so far about glycogen accumulation in obstruction-damaged bladder muscle.

The difference between the 'muscle cluster' of the normal map and the 'muscle cluster' of the map of damaged tissue without glycogen gives a protein-like spectrum with bands at 857 cm^{-1} , 1005 cm^{-1} , 1079 cm^{-1} , 1321 cm^{-1} , 1447 cm^{-1} and 1659 cm^{-1} (figure 4b). It is well known that a number of proteins is up-regulated upon damage such as growth factors [12, 13]. Some of the spectral features may also be indicative of increased lactate in the damaged tissue, such as bands at 857 cm^{-1} , 1415 cm^{-1} and 1455 cm^{-1} . A reference spectrum of lactate (measured in house, Sigma, Zwijndrecht, The

**Figure 4:**

(a) Difference spectrum (III) of damaged muscle tissue spectrum of cluster II subtracted from damaged muscle tissue spectrum of cluster I. IV is a reference spectrum of glycogen. (b) Difference spectrum (III) of normal muscle tissue (II) subtracted from damaged muscle tissue spectrum of cluster II. IV is a reference spectrum of lactate.

Netherlands) is plotted below. The latter two peaks however are fairly weak compared to the intensity at 857 cm⁻¹. Therefore, we assume that lactate is not the major contributor to the difference spectrum. Lactate indicates an anaerobic metabolic condition. As mentioned in the introduction, ischemia may be related to collagen infiltration because blood supply can be hindered. This may also explain glycogen accumulation, since this molecule is not used in the anaerobic metabolic pathway. Other changes in molecular composition in response to possible ischemia, such as the content of phosphocreatine [14], are also likely to be reflected in the spectra. The exact nature of the compounds, responsible for this difference spectrum, remains to be established.

The results prove that Raman spectroscopic mapping can be successfully applied to determine collagen infiltration within bladder muscle fibers. Collagen infiltration has been described before with histochemical techniques [3, 4, 5]. An interesting question

for further Raman spectroscopic studies would be the quantification of collagen infiltration using Raman maps. As shown in the examples, accumulation of glycogen in damaged bladder muscle tissue was observed. However, differences in composition and structure between normal and damaged bladder wall tissue, such as glycogen accumulation and protein-like changes, need to be further investigated in studies on a larger number of bladder samples. Raman spectroscopic mapping excludes the need for using (immuno)-physiochemical reagents. Therefore it may reveal more markers related to damage than conventional methods and may even uncover unanticipated components. The data in this study are used as an example for the possibilities of Raman mapping in conjunction with investigation of bladder wall composition.

We expect that this line of research, aimed at analyzing the changes in overall bladder wall biochemical composition and identifying their Raman spectral signatures, will enable development of an *in vivo* Raman spectroscopic method for determination of the degree of damage in the bladder wall, without the need for taking biopsies.

Acknowledgements

This work was supported by the Dutch Kidney Foundation (NSN), project no. PC 162.

References

1. Dinneen MD, Duffy PG. Posterior urethral valves. *Br J Urol* **78**:275-281, 1996.
2. Wollfenbuttel KP, Kok DJ, Minekus JPJ, van Koevinge GA, van Mastrigt R, Nijman JM. Urodynamic follow-up of experimental urethral obstruction in individual guinea pigs. *Neurourol Urodynam* **20**:699-713, 2001.
3. Kim JC, Yoon JY, Seo SI, Hwang TK, Park YH. Effects of partial bladder outlet obstruction and its relief on types I and III collagen and detrusor contractility in the rat. *Neurourol Urodynam* **19**:29-49, 2000.
4. Charlton RG, Morley AR, Chambers P, Gillespie JI. Focal changes in nerve, muscle and connective tissue in normal and unstable human bladder. *BJU International* **84**:953-960, 1999.
5. Kim KM, Kogan BA, Massad CA, Huang YC. Collagen and elastin in the obstructed fetal bladder. *J Urol* **146**:528-531, 1991.
6. Gosling JA, Kung LS, Dixon JS, Horan P, Whitbeck C, Levin RM. Correlation between the structure and function of the rabbit urinary bladder following partial outlet obstruction. *J Urol* **163**:1349-1356, 2000.
7. Nijssen A, Bakker Schut TC, Heule F, Caspers PJ, Hayes DP, Neumann MHA, Puppels GJ. Discriminating basal cell carcinoma from its surrounding tissue by Raman spectroscopy. *J Invest Dermatol* **119**:64-69, 2002.
8. Koljenović S, Choo-Smith L-P, Bakker Schut TC, Kros JM, van den Berge HJ, Puppels GJ. Discriminating vital tumor from necrotic tissue in human glioblastoma tissue samples by Raman spectroscopy. *Lab Invest* **82**:1265-1277, 2002.
9. de Jong BWD, Bakker Schut TC, Wollfenbuttel KP, Nijman JM, Kok DJ, Puppels GJ. Identification of bladder wall layers by Raman spectroscopy. *J Urol* **168**:1771-1778, 2002.

10. Kok DJ, Wolffenbuttel KP, Minekus JPJ, van Mastrigt R, Nijman JM. Changes in bladder contractility and bladder compliance upon urethral obstruction: a longitudinal follow-up of individual guinea pigs. *J Urol* **164**:1021-1024 2000.
11. Wolthuis R, Bakker Schut TC, Caspers PJ, Buschman HPJ, Römer TJ, Bruining HA, Puppels GJ. in W.T. Mason, *Fluorescent and Luminescent Probes for Biological Activity*, Academic Press, San Diego, 1999, p. 433.
12. Chen MW, Levin RM, Buttyan R. Peptide growth factors in normal and hypertrophied bladder. *World J Urol* **13**:344-348, 1995.
13. Flynn BJ, Mian HS, Cera PJ, RL Kabler RL, Mowad JJ, Cavanaugh AH, Rothblum LI. Early molecular changes in bladder hypertrophy due to bladder outlet obstruction. *Urology* **59**:978-982, 2002.
14. Lin AT, Chen KK, Yang CH, Chang LS. Effects of outlet obstruction and its reversal on mitochondrial enzyme activity in rabbit urinary bladders. *J Urol* **160**:2258-2262, 1998.

Discrimination between nontumor bladder tissue and tumor by Raman spectroscopy

B.W.D. de Jong
T.C. Bakker Schut
K. Maquelin
T. van der Kwast
C.H. Bangma
D.J. Kok
G.J. Puppels

Analytical Chemistry
78:7761-7769, 2006

Chapter

9

Abstract

We have applied Raman spectroscopy to discriminate between non-tumor and tumor bladder tissue and to determine the biochemical differences therein.

Tissue samples from 15 patients were collected and frozen sections were made for Raman spectroscopy and histology. Twenty-five pseudo-color Raman maps were created in which each color represents a cluster of spectra measured on tissue areas of similar biochemical composition. For each cluster the cluster-averaged spectrum (CAS) was calculated and classified as tumor and non-tumor in accordance to pathology. Unguided hierarchical clustering was applied to display heterogeneity between and within groups of non-tumor and tumor CAS. A linear discriminant analysis model was developed to discriminate between CAS from tumor and non-tumor. The model was tested by a leave-one-patient-out validation, 84 of the 90 CAS (93%) were correctly classified with 94% sensitivity and 92% specificity. Biochemical differences between tumor and non-tumor CAS areas were analyzed by fitting spectra of pure compounds to the CAS. Non-tumor CAS showed higher collagen content while tumor CAS were characterized by higher lipid, nucleic acid, protein and glycogen content.

Raman spectroscopy enabled effective discrimination between tumor and non-tumor bladder tissue based on characterized biochemical differences, despite heterogeneity expressed in both tumor and non-tumor CAS.

Introduction

In the urinary tract, urothelial cell carcinoma of the urinary bladder is the most common malignancy. In 2005, over 63,000 new cases of bladder cancer are expected in the US [1]. In Western Europe over 66,000 new cases were diagnosed in 1990. [2].

Much research is aimed at developing and optimizing techniques for diagnosing bladder cancer. Fluorescent cystoscopy [3, 4, 5], electrical impedance spectroscopy [6] and virtual cystoscopy with CT and MRI [7] improve the real time localization of tumor sites. Urine analysis using protein and DNA markers [8, 9, 10] are of help in detecting tumor presence and support the analysis of changes in tissue morphology and composition. However, none of these techniques can both localize suspect areas and characterize the morphological and compositional changes in a single measurement without the use of contrast agents.

Raman spectroscopy will provide detailed information about the biochemical composition of tissue. This allows identification of the tissue, including tumors and other abnormalities, and also gives insight into biochemical alterations in the tissue that may throw light on pathogenesis. Raman spectroscopy can be applied *in vivo* using fiber optic probes [11, 12, 13, 14]. Raman spectroscopy inside the bladder would allow for nondestructive detection and characterization of diseased tissue areas during cystoscopy. The only limit on the number of suspect sites that is investigated will be the time allowed during cystoscopy although a single spectrum can be obtained in a matter of seconds. This is all the more important because the initial phase of bladder cancer, carcinoma *in situ* (CIS), is difficult to recognize with cystoscopy. Non-destructive screening around suspect and clear tumor sites may increase the chance of CIS detection.

In order to develop *in vivo* Raman spectroscopic applications to classify tissues as being healthy or not, Raman spectral databases have to be created that reflect the detailed biochemical changes. It is needed to identify these biochemical changes within the Raman spectra and to understand the influence of heterogeneity in between as well as within healthy and diseased tissues on Raman spectral models. Raman spectroscopic maps, made up of grid-wise measured spectra on untreated frozen tissue sections, allow for both spectral characterization for specific tissue areas and insight in heterogeneity in tissues.

Here we present a study in which Raman spectroscopic maps are made on bladder tissues containing non-tumor and tumor areas of different stages and grades. Histology was applied to classify spectra measured on these specific areas within each map as non-tumor or tumor. Unguided hierarchical cluster analysis is used to identify heterogeneity between spectra measured on non-tumor and tumor bladder tissue but also the spectral heterogeneity within non-tumor and tumor bladder tissue. LDA was used to produce a model that differentiated classified spectra into a non-tumor and a tumor group. Validation of this model was done by leaving out all spectra measured

on tissues of one patient, and predict these as non-tumor and tumor in comparison to the original classification. In addition we determined which biochemical differences underlie the spectral differences between non-tumor and tumor tissues and the heterogeneity within both groups by comparing tissue spectra to spectra measured on pure compounds.

Experimental section

Tissues

Fifteen snap-frozen and liquid nitrogen stored bladder specimens were obtained from the tissue bank of the Department of Pathology, Erasmus MC, Rotterdam. They included non-tumor bladder tissue, tissues with carcinoma in situ (CIS), Ta, T2 and T3 tumor tissue, staged according to WHO/ISUP guidelines [15]. From each specimen thin sections were cut of alternately 20 μm and 10 μm thickness. The 20 μm tissue sections were mounted on a calcium fluoride window and dried in ambient air for Raman spectroscopic mapping. The adjacent 10 μm tissue sections were stained with hematoxylin eosin (HE) and evaluated by a pathologist.

Raman spectroscopy

Tissue Raman spectra data were acquired using a Raman-microspectrometer that has been built in-house, and which has been described in detail previously [16]. In short, air-dried tissue sections, mounted on calcium-fluoride windows, were placed on a computer controlled motorized sample stage of a microscope (DM-RXE, Leica, Cambridge, UK). Near infrared laser light (845 nm, ~100 mW) from a titanium-sapphire laser (Spectra Physics 3900S, Mountain View, CA) pumped by an argon ion laser (Coherent Innova 300, Palo Alto, CA) was coupled into the microscope. An 80x NIR optimized objective (Olympus MIR plan 80x/0.75, Tokyo, Japan) with a working distance of approximately 1,6 mm was used to focus the laser light on the tissue sample, and to collect Raman scattered light from the sample. After passing through a chevron type laser suppression filter the Raman signal was measured by means of a multichannel Raman spectrometer (a modified System 100 spectrometer, Renishaw, Wotton under Edge, UK). Data acquisition from the spectrometer was controlled by Grams/32 Spectral Notebook Software (Galactic Industries Corp., Salem, NH), into which control software for the microscope sample stage (Leica DM STC, Cambridge, UK) has been integrated to enable automated mapping of the sample.

Raman mapping experiments were carried out to determine the heterogeneity in molecular composition especially in and around tumor tissue. Areas containing tumor tissue were selected for mapping based on evaluation of the adjacent section that had been HE-stained. Each selected area was divided in small squares, hereafter referred to as grid elements. In each grid element one Raman spectrum was taken. The laser

light was focused 2 μm beneath the tissue surface with a spot size of less than 1 μm^2 . To obtain a Raman spectrum representative for the whole grid element the sample stage was moved randomly within the grid element boundaries during the 20 seconds of signal collection time. In the Raman mapping experiments carried out for this study the size of the grid elements within each map was homogeneous but varied between maps from 16 μm^2 to 100 μm^2 . For each map the grid element size was chosen, taking the total map area and measurement time into account.

Data pre-processing

All spectral data processing software was programmed in Matlab 6.5 (Mathworks, Natick, MA), using the PLS-toolbox 2.0 (Eigenvector Research Inc., Manson, WA). Instrument calibration was performed as described previously [12, 16]. Briefly, the wavenumber-axis (400 – 1800 cm^{-1}) was calibrated using the known wavelengths of the emission lines of a neon-argon calibration lamp, and the relative peak positions of cyclohexane. Background signal, originating from the calcium-fluoride window and optical instrument components was subtracted from the tissue spectra. Spectra were corrected for the wavelength dependent signal detection efficiency of the setup, using a tungsten light source with a known emission spectrum [17].

Raman spectroscopic maps

Further analysis was carried out on the first derivatives of the pre-processed spectra after smoothing with an 11-point Savitsky-Golay filter. A Principal component analysis (PCA) was applied to the spectral dataset of the Raman map [12, 18]. The principal components (PC's) that accounted for 99% of the variance served as input for a hierarchical cluster analysis (HCA), using Ward's clustering algorithm and the Euclidean distance measure [19]. The dissimilarity level, below which spectra were grouped in one cluster, was chosen such that the cluster-averaged spectra displayed spectral differences above the noise level and that clusters could be related to the histologically distinct areas that were visible after HE-staining of the tissue section. In this way the variation in spatial resolution does not affect clustering results.

The clusters were assigned a color, and each grid element of the Raman map was then given the color of the cluster to which its spectrum belonged. The resulting pseudo-color-map, in which tissue areas with similar spectra, and therefore similar molecular composition, have the same color, was compared to histology. Each tissue section was HE-stained after the Raman mapping experiments and bright-field images were taken. A pathologist analyzed the stained tissue sections, and classified each tissue area, corresponding to a Raman cluster, as tumor or non-tumor. In the non-tumor group, normal and inflamed areas were distinguished. This procedure was performed for all 25 Raman maps.

Linear discriminant Discriminant Analysis, LDA

An unsupervised cluster analysis as described above serves to analyze the spectral variance in a dataset. Such spectral variance is present in datasets obtained of non-tumor tissue, in datasets of tumor tissue and in datasets containing both spectra of tumor and non-tumor tissue. The aim is to find within all this spectral variance the spectral features that can be used to discriminate between non-tumor and tumor tissue. The algorithm underlying a Linear Discriminant Analysis is taught to pick out these spectral features, which are then used to discriminate between normal tissue and tumor. It is therefore a supervised method in which examples of spectra of normal tissue and of tumor tissue are given in the form of their PC-scores.

It finds the combination of variables that give the best discrimination between the non-tumor and tumor spectra [20]. The maximum number of PCs in this LDA was kept at least two times smaller than the number of spectra in the smallest group, to prevent overfitting of the dataset. The second restriction was that from the total list of PC's only those PCs were selected that significantly contribute to the discrimination between tumor and non-tumor tissues.

To test how well the LDA model predicts the type of tissue of an unknown sample we applied a "leave-one-patient-out" cross-validation. In this procedure an LDA model is built from the spectra of all but one patient and then used to predict the tissue class of the tissue samples of the patient that was left out. This procedure was repeated for all 15 patients, leading to independent predictions per patient. For each predicted spectrum a so-called probability of prediction is calculated. This probability is determined by the Euclidean distances to the class means in the model (i.e. tumor and non-tumor). Each distance was then normalized by dividing by the sum of all distances, resulting in a summed probability of 1. Hereafter, these values are converted to percentages (multiplying by 100).

Diagnostic accuracy, ROC curves

The diagnostic accuracy of the predictions was quantified by constructing a receiver operating characteristic (ROC) curve. This represents the relationship between sensitivity and specificity at different cut-off values of the probability [21]. When the features of a single spectrum completely fit the characteristics of a tumor spectrum as described by the LDA model and are in complete disagreement with the characteristics of non-tumor, the spectrum is classified as tumor with a 100% probability. This probability of the classification decreases as the fit to the tumor characteristics decreases and that to the non-tumor characteristics increases. At 50% probability the spectra can be termed tumor and non-tumor with equal probability. Below 50% the spectra will be classified as non-tumor.

In the calculations a probability above 50% was used as cut-off between tumor and non-tumor. For the ROC curve this cut-off value is varied from 0% probability, where every spectrum is predicted as tumor (no false negative results), to 100% probability,

where every spectrum is predicted as non-tumor (no false positive results). The area under the curve is a measure for the diagnostic accuracy.

Data analysis: Spectral characterisation

All non-tumor cluster-averaged spectra and all tumor cluster-averaged spectra were combined into two groups. From both groups the overall averages were calculated yielding an overall non-tumor and an overall tumor spectrum.

Each non-tumor cluster-averaged spectrum was then fitted with the overall tumor spectrum plus a dataset of reference spectra and a first order polynomial, using a least squares fit procedure. Similarly, each tumor cluster-averaged spectrum was fitted with the overall non-tumor spectrum plus the database of reference spectra and a first order polynomial. In this way, the molecular differences between tumor and non-tumor tissue were analyzed. The reference dataset contained the spectra of the following pure compounds: collagen-I and -III, actin, albumin, DNA, RNA, cholesterol, β -carotene, gangliosides, glycogen, phosphatidylcholine, phosphatidylethanolamine, arachidonic acid, palmitic acid, palmitoleic acid, stearic acid, (all from Sigma-Aldrich, Zwijndrecht, The Netherlands), oleic acid methyl-ester and linoleic acid, (ICN, Bryan, Ohio, US), all measured with the instrument described above. The pure compounds were chosen to represent the main molecular species in tissue, nucleic acids, proteins, lipids and sugars. β -Carotene was added, because of its very distinctive spectral features, which were observed in a number of tissue samples.

Results and discussion

During cystoscopy visual analysis can be insufficient to diagnose the nature of a specific tissue site. More detailed information may then be obtained by histologic analysis of the tissue. At present this requires a biopsy, which does not provide instant feedback and may be subjected to a bias of the person(s) performing the histological observation. Often these drawbacks provide enough reason to choose the option of watchful waiting, where cystoscopy is repeated after some time to monitor changes. In this approach a tumor recurrence may occur during the waiting period, pointing to possibly missed tumor sites. Though this may be an acceptable low percentage in current clinical practice, further reduction of the number of recurrences by early detection will be valuable to the individual patient.

Raman spectroscopy is evolving as a method that enables *in vitro* and *in vivo* tissue analysis. It is non-destructive, and signal collection can be in the order of seconds, [22, 23, 24]. To get to the state of *in vivo* application several criteria must be met. First, a database of spectra must be established that is representative of normal and diseased tissue that may be encountered in practice. Second, a classification model must be developed, based on this spectral database and histological analysis of the tissue of

which spectra were obtained. Third, the accuracy of this model must be tested and the biochemical basis for the classification model should be investigated. The classification model should preferably not only discriminate between non-tumor or tumor but also specify on what grounds something is called “tumor” and which compositional changes have occurred.

In this study we set out to address these points. Therefore we have created a database of Raman spectra of bladder tumors and normal bladders. Twenty-five Raman maps were measured from 15 bladder tissue sections from 15 individual patients. Nine of the tissue samples contained sites of tumors; eight were invasive tumors, and one was a carcinoma *in situ*. Four samples contained large sites of inflammation, one of which also showed invasive tumor sites. In two tissue samples no abnormalities were present.

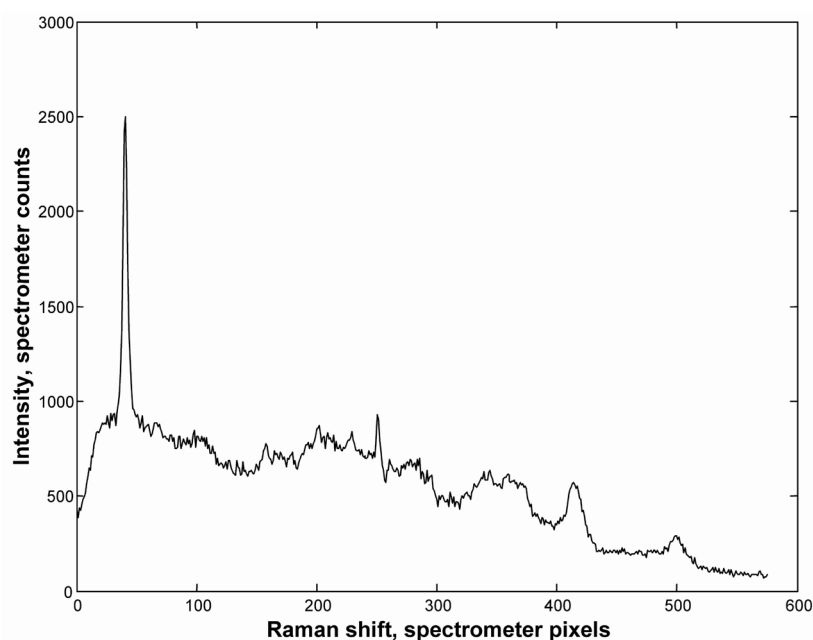


Figure 1
Raman spectrum from a single grid element without background corrections and calibration.

In figure 1 an example of a single Raman spectrum taken from a random map from a random grid element is plotted without calibration and still includes all background signal. The average signal-to-noise ratio per grid element spectrum was approx. 10. This was calculated by dividing the baseline corrected height of the CH₂-band by the width of the feature-free region between 1750-1800 cm⁻¹.

Figure 2 serves as an example of Raman spectroscopic map analysis. It shows the bright field microscopic image of an unstained bladder tissue section (A), the corresponding Raman spectroscopic map (B), an image of the same tissue section after HE-staining (C) and the cluster-averaged Raman spectra (D). In this example 5 clusters described the main histological structures of this small section, which contained both tumor and non-tumor tissue. Three clusters could directly be related to the HE stained tissue. The purple cluster represents tumor tissue, which is histologically characterized by large and abundant cell nuclei and the presence of glycogen granules, which stain dark red. For clarity this tumor area is demarcated in

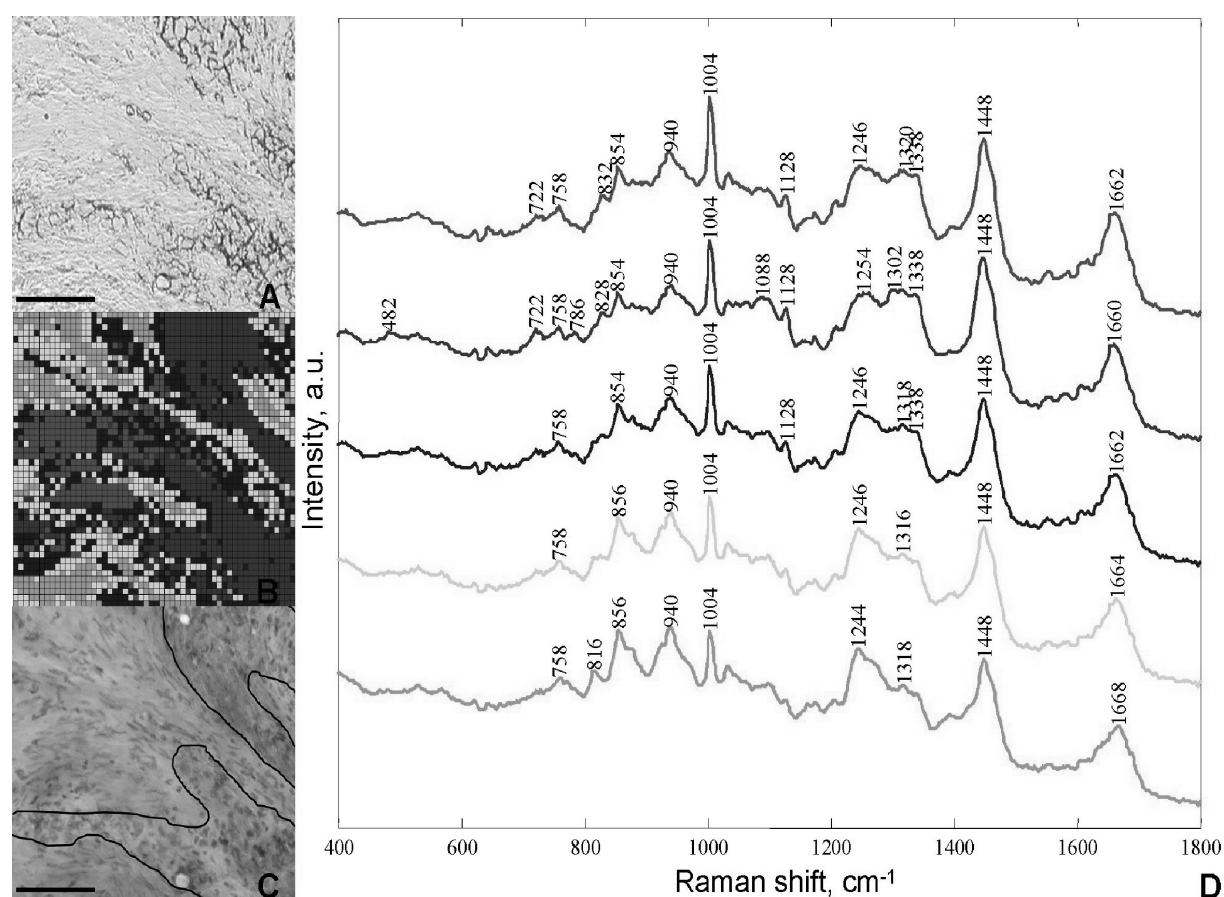


Figure 2

A: Unstained section of bladder tissue containing both non-tumor and tumor areas, 20 μm in thickness. Scalebar = 100 μm . B: Raman spectroscopic map, each grid element is 6,5 μm by 6,5 μm . Purple area is representative for tumor, red area for muscle tissue, green area for collagen fibers and blue and yellow are areas of transition between two types of tissue. C: Same section as A but HE stained after the measurements. Tissue areas are outlined. D: Averaged spectra of the clusters in B with matching colors, a.u.: arbitrary units. Color image: see appendix.

figure 2C. The red cluster represents muscle tissue, as can be concluded from the HE stained tissue section of figure 2C, and shows the presence of muscle cells with the typical stretched nuclei in this area. The green cluster represents collagen rich areas, in the HE stained tissue section visible as light red bands and areas with few cell nuclei. The yellow and blue clusters are not recognizable as specific tissue structures in the HE stained section. In the Raman map they are found at boundaries between two tissue areas containing different types of cells. This occurs in many Raman maps and is related to the fact that at these boundaries the grid elements of the Raman map represent volumes of tissue that contain both tissue types. This was verified by fitting the blue and yellow cluster-averaged spectra with the cluster-averaged spectra of the adjacent tissue types, which resulted in near-perfect fits (not shown), therefore spectra from these clusters were not further analyzed.

Analysis of the Raman maps yielded 3 to 7 spectral clusters per map. Based on pathohistological evaluation of the tissue sections after HE-staining, each cluster was classified either as non-tumor or as tumor tissue. For each cluster, a cluster-averaged spectrum (CAS) was calculated (as in figure 2D) and these were combined in one

dataset. Only those cluster averages of which the pathology by histological evaluation was unambiguous were included. This resulted in 90 CAS with histology based classification of the tissue, 29 CAS were left out because no accurate histological classification could be obtained. These CAS were mostly derived from small clusters in between larger clusters as described for the blue and yellow clusters in figure 2. The non-tumor tissue group comprised 37 CAS, representing sites of extra cellular matrix (collagen), muscle fibers and non-tumor tissue areas containing inflammation. The tumor group comprised 53 CAS measured on carcinoma *in situ* (CIS), Ta, T2 and T3 tumor tissue.

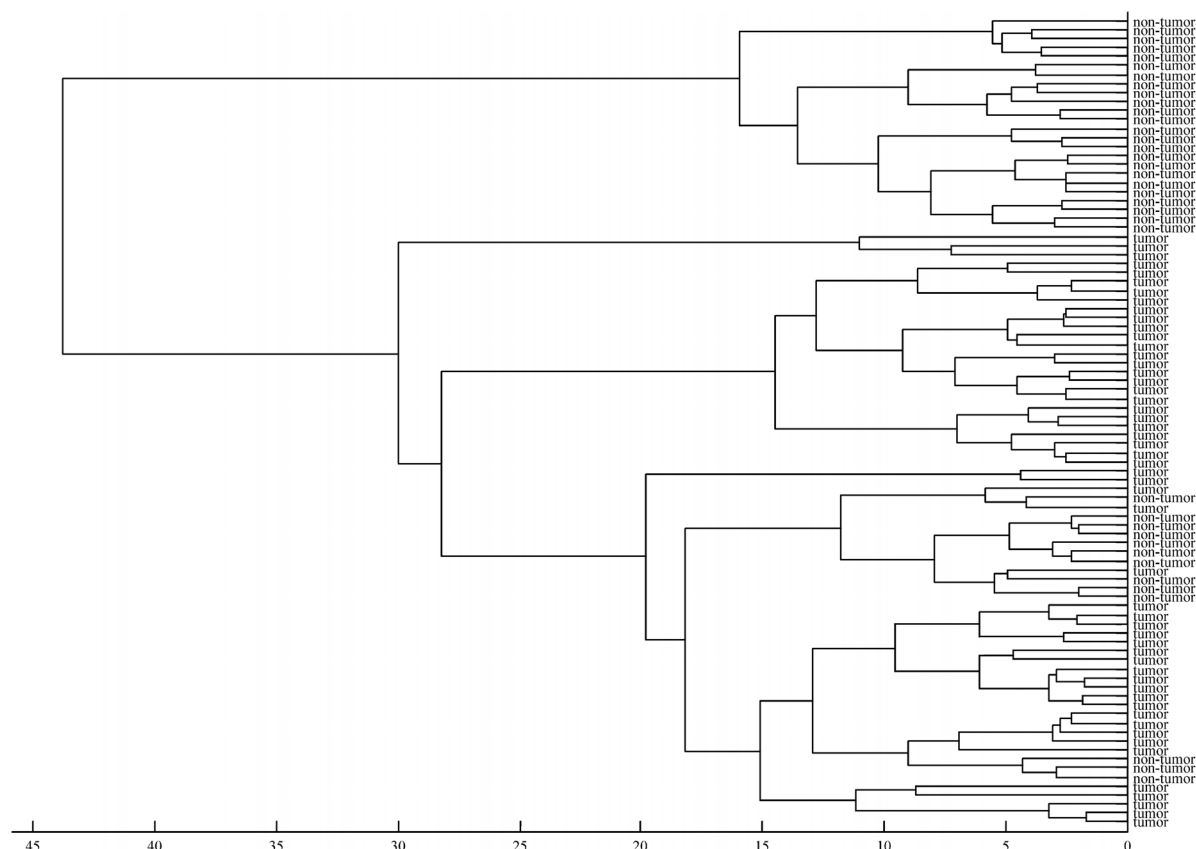


Figure 3

Dendrogram of unguided classification of 90 averaged cluster spectra from all maps combined.

The 90 CAS were subjected to an unsupervised Ward's HCA with euclidean distances. The results were plotted in a dendrogram (figure 3) in which two main clusters were formed. One cluster contained exclusively non-tumor CAS, the other contained all 53 tumor CAS plus 13 non-tumor CAS. The non-tumor CAS that clustered with the tumor CAS in the HCA were obtained from muscle and from inflammation sites. All CAS in the non-tumor cluster contained a considerable contribution of collagen whereas the non-tumor CAS, that clustered with tumor, did not. To discriminate between non-tumor and tumor bladder tissue by Raman spectroscopy effectively, a

supervised model based on pathological classification is needed, due to the large heterogeneity in the dataset.

The large heterogeneity in the non-tumor CAS, could be expected since these spectra were derived from tissue areas of connective tissues, muscle tissues and inflammation sites. Within the tumor cluster, separated sub-clusters of tumor CAS were formed. This means that there is also heterogeneity in the tumor CAS. This can be attributed to the fact that the tumor CAS were derived from tumor areas with different grades and stage, leading to molecular differences.

The dataset of 90 CAS was used to train a LDA model for the discrimination between non-tumor and tumor tissue. Despite this heterogeneity shown in the dendrogram the most consistent LDA model contained 5 variables (PCs) and discriminated between non-tumor and tumor CAS with a 97.8% (88/90) accuracy, compared to histology as classification standard. Tumor sites were detected to 100% sensitivity and 95% specificity. The two non-tumor CAS that were classified by LDA as tumor, originated from clusters of a highly inflamed tissue area. Inflammation areas are recognizable in histology due to the presence of large numbers of leucocytes and lymphocytes (showing dense nuclei). In Raman spectroscopic maps increased levels of DNA and RNA are clearly visible for these inflammation areas (data not shown). Tumor tissue also contains increased levels of DNA and RNA as is shown by the fit results in figure 5b and confirmed in literature [18]. This is most likely the reason that it was not possible in all cases to discriminate between CAS of inflammation areas and CAS from tumor areas. It will be necessary to enlarge the database with more inflammation specific Raman spectra to enable extraction of more subtle inflammation specific spectral features by means of LDA.

Our ultimate objective is *in vivo* characterization of an unknown bladder tissue as tumor or non-tumor by its Raman spectrum. When dividing the data in a training-set and a test-set, only a part of the heterogeneity (shown in figure 5b) would then be included in the training-set and is therefore not a representative validation. Expanding the dataset by measurements on new patient biopsy material and randomly selecting an independent validation set is the aim for further research. Instead the validation was performed on our present dataset by a leave-one-patient-out cross validation, using LDA models with 5 variables. In table 1 an example of the

Identity	Predicted as	Probability being	
		non-tumor	Probability being tumor
non-tumor (map1)	non-tumor	0.96	0.04
non-tumor (map1)	non-tumor	0.96	0.04
non-tumor (map1)	non-tumor	0.74	0.26
tumor (map1)	tumor	0.06	0.94
tumor (map1)	tumor	0.1	0.9
non-tumor (map2)	non-tumor	0.85	0.15
non-tumor (map2)	non-tumor	0.94	0.06
tumor (map2)	tumor	0.08	0.92
tumor (map2)	tumor	0.19	0.81

Table 1: Example of a leave-one-patient-out cross validation for 2 maps from one patient

cross validation of two maps from one patient with probability of predictions and prediction outcomes is shown. For the whole dataset 93% was predicted in accordance with the histological classification with a sensitivity of 94% and a specificity of 92%. Three tumor spectra were classified as non-tumor with a poor probability of prediction. The probability for two of these predictions were close to the cut-off value 'non-tumor – tumor' and therefore the prediction quality was poor. The third misclassified tumor spectrum had a higher probability for being non-tumor. The reason for these misclassifications was unclear. Three non-tumor spectra, all from inflammation sites, were misclassified as tumor and had a relative high probability of prediction for tumor.

The data in this work compare well to those recently reported by Crow et al. [25]. In their study Raman measurements were performed on 75 biopsy samples from 72 patients, including all types of bladder cancer gradations. From their LDA they obtained an encouraging distinction between normal bladder, inflammation and different tumor grades and even stages. Instead of applying Raman maps they opted for measuring multiple spectra on larger tissue areas resulting in an overall dataset of 1525 Raman spectra. We have chosen to measure on tissue sections with detailed Raman spectroscopic maps in order to understand the role of heterogeneity in tissue and the effect on modeling. Tumors and their surrounding tissues can be very heterogeneous as shown by Raman mapping studies e.g. on glioblastoma tissue and basal cell carcinoma [22, 23].

The diagnostic accuracy of Raman spectroscopic discrimination with LDA prediction was quantified by plotting a receiver operating characteristic (ROC) curve (figure 4).

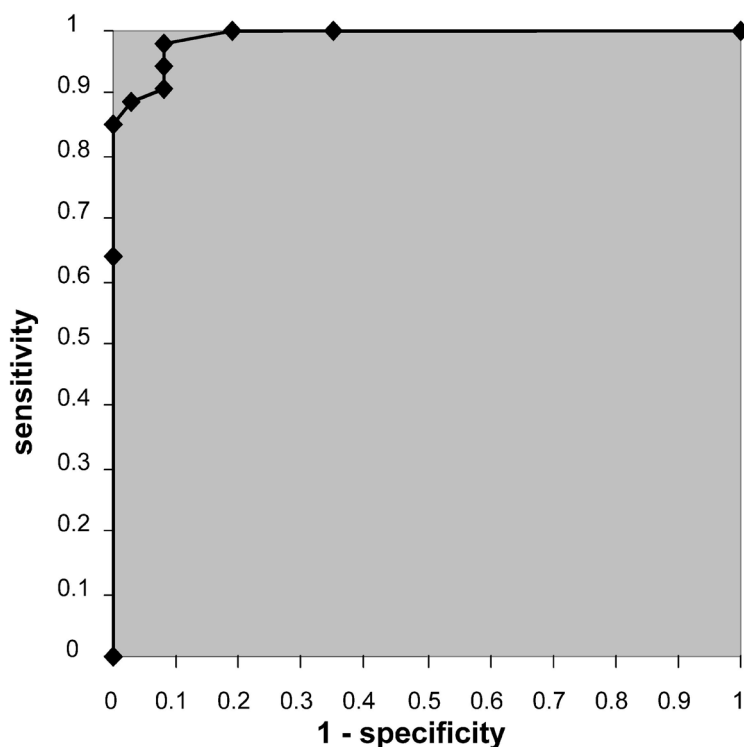


Figure 4
ROC curve representing the accuracy of Raman spectroscopic discrimination with LDA. The area under the curve is 0.99.

The plot of sensitivity against (1 – specificity) produced a curve with an area under the curve (AUC) of 0.99. Considering that an area of 1 represents a perfect test and an area of 0.5 represents a useless test, this means that the accuracy is excellent. The ROC curve also shows that it is possible to choose a desired sensitivity or specificity of detecting tumor sites by changing the cut-off probability value (determines if a spectrum is non-tumor or tumor). This is an important issue in diagnostic applications in which the balance between false negative and false positive results plays a role. We aim to increase both sensitivity and specificity by expanding the spectral database.

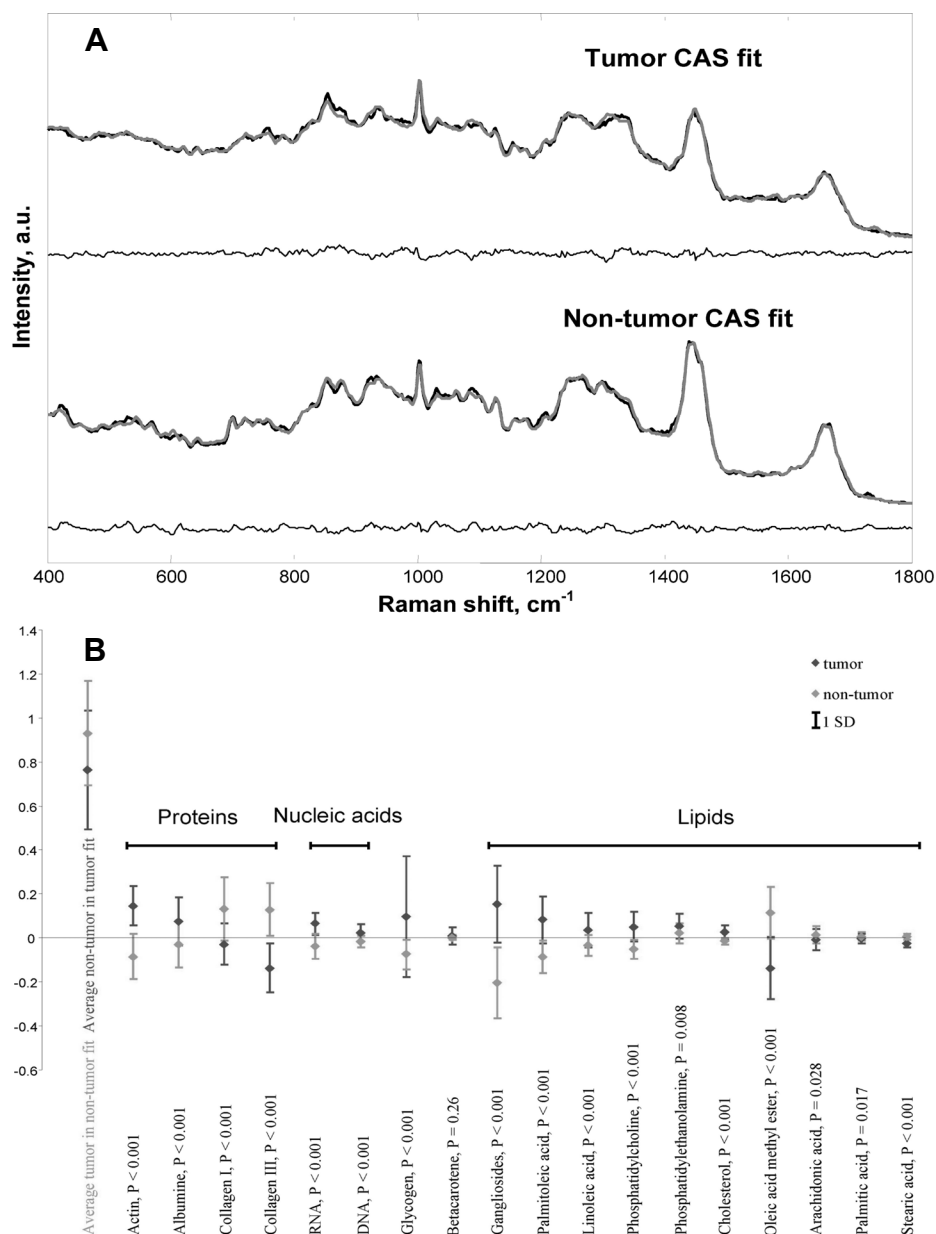


Figure 5

A: Upper plot: example of cluster averaged non-tumor spectrum in black with fit result in grey, residues plotted beneath. Lower plot: example of cluster averaged tumor spectrum in black with fit result in grey, residues plotted beneath. B: Averaged fit coefficients for each reference compound: light gray diamonds account for non-tumor and dark gray diamonds account for tumor. Both plotted with 1SD, p-values are given for significant differences.

To evaluate the main molecular differences between non-tumor and tumor tissue, we applied a fit-procedure to all CAS. This fit-procedure is performed by subjecting each of the CAS to a database of 18 reference spectra (see Materials and Methods), which were chosen to represent the main molecular species in tissue. Along with the reference compounds the averaged spectrum of all tumor CAS, hereafter referred to as the overall tumor spectrum, was included in the fit-procedure of each non-tumor CAS to enhance specific tumor – non-tumor difference features in the spectrum. In the same way the averaged spectrum of all non-tumor CAS, hereafter referred to as the overall non-tumor spectrum, was included in the fit-procedure of each tumor CAS along with the spectra of all reference compounds. In figure 5a, examples of a tumor CAS and a non-tumor CAS fit result are plotted. The black spectra are the original CAS, gray spectra are the fit results and the residues are plotted underneath.

With each fit-procedure the fit coefficients for all reference compounds, the overall tumor and non-tumor spectra are obtained, which can be positive or negative. In figure 5b, the averaged fit coefficient for each of the reference compounds in both non-tumor CAS (light gray) and tumor CAS (dark gray) are plotted along with the standard deviation of the coefficient distribution obtained. Furthermore, the overall tumor spectrum fit coefficient in all non-tumor CAS in light gray and the overall non-tumor spectrum fit coefficient in all tumor CAS in dark gray are plotted. A student T test was used to determine if the tumor CAS fit coefficient of each reference compound was significantly different ($p > 0.05$) from the non-tumor CAS fit coefficient. The compounds are grouped along the x-axis in the following order: proteins, nucleic acids, glycogen, β -carotene and lipids. As is clear, collagen I and III and some lipids are more expressed in non-tumor CAS whereas the rest is more expressed in tumor CAS. Only β -carotene was not fitted significantly differently in tumor and non-tumor CAS.

The fit results indicate that bladder tumor tissue contains a higher amount of lipids than non-tumor tissue. This is in agreement with findings published by Omberg et al. [26], who compared Raman spectral differences in tumor and non-tumor cell cultures. However, our results show that this does not hold true for all lipids. Oleic acid (methyl ester), arachidonic acid, palmitic acid and stearic acid were present in higher concentrations in non-tumor tissue than in tumor tissue. Higher amounts of arachidonic acid and stearic acid in non-tumor tissues are in agreement with findings published by Fermor et al. [27]. All lipids included in the fit procedures were chosen based on the knowledge that these lipids are located in the inner and outer membranes and cytoplasm of urothelium and carcinomas [27, 28, 29]. In one sample of tumor tissue a clear Raman signal of β -carotene was found. Carotene has been suggested to be useful in prevention of bladder cancer [30]. It was unknown whether this patient was treated with a carotene supplement. But this example suggests that there may be a role for Raman spectroscopy as a tool in follow-up studies to

determine if compounds used for treatment of various diseases are absorbed in the appropriate locations.

The ratio of total collagen content, resembled by collagen types I and III, to non-collagen content, resembled by actin and albumin, was higher in non-tumor tissue, again in agreement with Omberg et al. [26].

The overall RNA and DNA contents were higher in tumor tissue compared to non-tumor tissue. This suggests that spectral features of nucleic acids may be a sensitive marker for discrimination between tumor and non-tumor. But as mentioned earlier, inflammation areas that are classified by histology as non-tumor tissue also express abundant levels of RNA and DNA contents. Because of this, inflamed tissues could be false positively classified as tumor tissue. Therefore, further characterization of spectral differences between larger sets of spectra measured on inflamed tissues and spectra measured on tumor tissues are needed.

This work on detailed Raman maps may provide insight in different contributions of biochemical changes upon development of bladder tumor and to understand the effects of these contributions in spectral discrimination between non-tumor and tumor. The spatial and biochemical information obtained from Raman maps can be used to optimize *in vivo* detection methods using Raman spectroscopy via fiber optic probes.

Conclusion

In conclusion, detailed Raman spectroscopic mapping can be used as a tool for obtaining more information from tissue sections than present day histological techniques. We have shown heterogeneity in the spectra between non-tumor and tumor tissue but also within non-tumor and tumor spectral groups separately. Despite this heterogeneity we were able to create a Raman spectral model that discriminated between non-tumor and tumor areas in bladder tissue with high accuracy using LDA. Fit procedures on the tissue spectra with pure compounds known to be found in non-tumor and / or tumor bladder tissue revealed which tissue components contributed in the spectral discrimination. Spectra from non-tumor tissue showed higher collagen content while spectra from tumor tissue were characterized by higher lipid, nucleic acid and protein content and glycogen expression. We see this work as a fundamental step in developing Raman spectroscopy towards a diagnostic tool for *in vitro* and *in vivo* pathology.

Acknowledgements

This work was financially supported by the Schreinemaker prize 2003, The Netherlands and by a SUWO grant, Rotterdam, The Netherlands

References

1. Jemal ADV, Murray T, Ward E, Samuels A, Tiwari RC, Ghafoor A, Feuer EJ, Thun MJ. Cancer statistics, 2005. *CA Cancer J Clin* **55**: 10-30, 2005.
2. Black RJ, Bray F, Ferlay J, Parkin DM. Cancer incidence and mortality in the European Union: cancer registry data and estimates of national incidence for 1990. *Eur J Cancer* **33**: 1075-1107, 1997.
3. Tiguert R, Fradet Y. New diagnostic and prognostic tools in bladder cancer. *Curr Opin Urol* **12**: 239-243, 2002.
4. Eshan A, Sommer F, Haupt G, Engelmann U. Significance of fluorescence cystoscopy for diagnosis of superficial bladder cancer after intravesical instillation of delta aminolevulinic acid. *Urol Int* **67**: 298-304, 2001.
5. D'Hallewin M, Bezdetnaya L, Guillemin F. Fluorescence detection of bladder cancer: a review. *European Urology* **42**: 417-425, 2002.
6. Wilkinson BA, Smallwood RH, Keshtar A, Lee JA, Hamdy FC. Electrical impedance spectroscopy and the diagnosis of bladder pathology: a pilot study. *J Urol* **168**: 1563-1567, 2002.
7. Bernhardt TM, Rapp-Bernhardt U. Virtual cystoscopy of the bladder based on CT and MRI data. *Abdom Imaging* **26**: 325-332, 2001.
8. Little B. Non-invasive methods of bladder cancer detection. *Int Urol Nephrol* **35**: 331-343, 2003.
9. Sözen S, Eskicorabci S, Özen H. Urinary markers for urothelial cancer. *BJU Int* **92**: 531-533, 2003.
10. Simon MA, Lokeshwar VB, Soloway MS. Current bladder cancer tests: unnecessary or beneficial?. *Crit Rev Oncol Hematol* **47**: 91-107, 2003.
11. Bakker Schut TC, Witjes MJH, Sterenberg HJCM, Speelman OC, Roodenburg JLN, Marple ET, Bruining HA, Puppels GJ. In vivo detection of dysplastic tissue by Raman spectroscopy. *Anal Chem* **72**: 6010-6018, 2000.
12. Molckovsky A, Wong Kee Song L, Shim MG, Marcon NE, Wilson BC. Diagnostic potential of near-infrared Raman spectroscopy in the colon: differentiating adenomatous from hyperplastic polyps. *Gastrointest Endosc* **57**: 396-402, 2003.
13. Boere IA, Bakker Schut TC, van de Boogert J, de Bruin RWF, Puppels GJ. Use of fibre optic probes for detection of Barrett's epithelium in the rat oesophagus by Raman spectroscopy. *Vib Spec* **32**: 47-55, 2003.
14. Haka AS, Volynskaya Z, Gardecki JA, Nazemi J, Lyons J, Hicks D, Fitzmaurice M, Dasari RR, Crowe JP, Feld MS. In vivo margin assessment during partial mastectomy breast surgery using raman spectroscopy. *Cancer Res* **66**: 3317-3322, 2006.
15. Oosterlinck W, Lobel B, Jakse G, Malmström PU, Stöckle M, Sternberg C. Guidelines on bladder cancer. *European Urology* **41**: 105-112, 2002.
16. van de Poll SWE, Römer TJ, Volger OL, Delsing DJM, Bakker Schut TC, Princen HMG, Havekes LM, Jukema JW, van der Laarse A, Puppels GJ. Raman spectroscopic evaluation of the effects of diet and lipid-lowering therapy on atherosclerotic plaque development in mice. *Arterioscler Thromb Vasc Biol* **21**: 1630-1635, 2001.
17. Wolthuis R, Bakker Schut TC, Caspers PJ, Buschman HPJ, Römer TJ, Bruining HA, Puppels GJ. In *Fluorescent and Luminescent Probes for Biological Activity*, 2nd ed.; Mason W.T., Ed.; Academic Press: London, 1999; pp 433-455.
18. Jolliffe IT, In *Principal Component Analysis*; Springer-Verlag: New York, 1986.
19. Jain AK, Dubes RC, In *Algorithms for clustering data*; Prentice Hall: Englewood Cliffs, 1988.
20. Tabachnick B, Fidell L, In *Using multivariate statistics*; HarperCollins Publishers: New York, 1989.
21. van Erkel AR, Pattynama PMTh. Receiver operating characteristic (ROC) analysis: basic principles and applications in radiology. *Eur J Radiol* **27**: 88-94, 1998.

22. Koljenović S, Choo-Smith L, Bakker Schut TC, Kros JM, van den Berge HJ, Puppels GJ. Discriminating vital tumor from necrotic tissue in human glioblastoma tissue samples by Raman spectroscopy. *Lab Invest* **82**: 1265-1277, 2002.
23. Nijssen A, Bakker Schut TC, Heule F, Caspers PJ, Hayes DP, Neumann MHA, Puppels GJ. Discriminating basal cell carcinoma from its surrounding tissue by Raman spectroscopy. *J Invest Dermatol* **119**: 64-69, 2002.
24. de Jong BWD, de Gouveia-Brazao CA, Stoop H, Wolffenbuttel KP, Oosterhuis JW, Puppels GJ, Weber RFA, Looijenga LHJ, Kok DJ. Raman spectroscopic analysis identifies testicular microlithiasis as intratubular hydroxyapatite. *J Urol* **171**: 92-96, 2004.
25. Crow P, Uff JS, Farmer JA, Wright MP, Stone N. The use of Raman spectroscopy to identify and characterize transitional cell carcinoma in vitro. *BJU Int* **93**: 1232-1236, 2004.
26. Omberg KM, Osborn JC, Zhang SLL, Freyer JP, Mourant JR, Schoonover JR. Raman spectroscopy and factor analysis of tumorigenic and non-tumorigenic cells. *Appl Spectrosc* **56**: 813-819, 2002.
27. Fermor BF, Masters JRW, Wood CB, Miller J, Apostolov K, Habib NA. Fatty acid composition of normal and malignant cells and cytotoxicity of stearic, oleic and sterculic acids in vitro. *Eur J Cancer*, **28A**: 1143-1147, 1992.
28. O'Connor LJ, Nicholas T, Levin RM. Subcellular distribution of free fatty acids, phospholipids, and endogenous lipase activity of rabbit urinary bladder smooth muscle and mucosa. *Adv Exp Med Biol* **462**: 265-273, 1999.
29. Kawamura S, Ohyama C, Watanabe R, Satoh M, Saito S, Hoshi S, Gasa S, Orikasa S. Glycolipid composition in bladder tumor: a crucial role of GM3 ganglioside in tumor invasion. *Int J Cancer* **94**: 34-347, 2001.
30. Kamat AM, Lamm DL. Chemoprevention of urological cancer. *J Urol* **161**: 1748-1760, 1999.

The background of the entire page is a grayscale microscopic image of biological tissue. It shows various cellular structures, including elongated, spindle-shaped cells in some areas and more rounded, clustered cells in others, all with visible nuclei and complex intercellular matrices.

General discussion

Chapter

10

Normal bladder: Human and guinea pig model

A normal human bladder consists of 3 main layers: the urothelium, which is an epithelium of about 7 cell layers thick and impermeable to urine, a lamina propria that mainly consists of collagen fibers and accommodates the main blood vessels, and a detrusor layer, consisting of multiple sub layers of smooth muscle. The architecture of these layers enables the bladder to expand very easily, which allows filling at a low pressure, and to fully contract during voiding, which allows complete emptying. The overall structure of the guinea pig bladder is quite similar to that in humans [1]. Therefore the guinea pig is one of the most ideal animal models to use in research for dysfunctional voiding syndromes. However, some mayor differences between bladders of upright walking humans and animals that move on four legs such as the guinea pig are the size and overall thickness of the bladder wall and anatomical issues such as environment, the shape of the bladder between neck and dome and length of the urethra.

In our laboratory, the guinea pig was previously used to develop a model that simulates the effects of urethral valves in patients. This model allowed for repeat and longitudinal urodynamic measurements to follow the development of bladder dysfunction [2,3]. In this thesis, bladder tissue obtained from this model was used for structural analysis, both histochemically and by Raman spectroscopy.

To obtain proof of principle, it was first tested in this thesis if Raman spectroscopic analysis can identify the three main layers of the bladder wall. Raman spectra obtained from several hundred different locations in normal bladder tissue from the guinea pig were input into an unguided map-clustering algorithm. The outlines of the clusters that were obtained from a Raman map were compared to an image of the tissue that was histochemically stained after the map measurement. In addition the average cluster spectra were compared with reference spectra of pure components known to be present in the bladder wall. This revealed that the three main clusters of spectra in the Raman map closely correlated with the known bladder wall layers and that the spectral differences between the clusters are linked to clear biochemical and structural differences between the tissues they represent.

Bladder obstruction: guinea pig model

The guinea pig model for partial outlet obstruction of the bladder has been described in the introduction. In this model the partial outlet obstruction was created by placing a silver jeweler's ring around the urethra. The ring caused fibrosis on the outer side of the urethra. This fibrosis, together with the ring, restricted the normal expansion of the urethra as urine is pushed through by bladder contraction, hence causing a partial obstruction. An important difference between the model and the patients it mimics,

besides the type of organism, is that the obstruction in the model is installed postnatally while patients with inborn disease may already develop bladder wall damage prenatally. Only in large animals it is possible to perform pre-natal surgery for placement of an obstruction [4] but such a model is very impractical for a longitudinal follow-up of bladder function. Post-natal installation was done in immature guinea pigs to approach the clinical situation as closely as possible.

As mentioned previously the guinea pig model allowed for the longitudinal monitoring of bladder function with urodynamic measurements both before and after the installation of an obstruction. This individual longitudinal follow-up clearly revealed the individual variations in the rate of changes in function. These variations are obscured when working with single time point data and groups of animals. Moreover, individual variations in the bladder structure that was analyzed at the time of sacrifice could not only be related to the function at that time point, as in other studies, but also to historical functional data obtained during the process of development of bladder wall damage. The advantage of this is apparent in chapter 3. The data presented there show that structural changes measured at the end point, especially the ischemic damage related appearance of glycogen deposits, provide an insight into the severity of bladder function loss that occurred previously. In the clinic such insight is lacking when the obstructive damage has developed prenatally.

To understand what happens when urethral valves are removed in a patient, we also studied the regeneration of the bladder as described in chapter 4. The silver ring was surgically removed, monitoring of function continued and after different time-spans of de-obstruction structural bladder tissue analysis was done. In all animals a significantly lower bladder pressure and a reduced number of unstable contractions were observed and in animals with an obstruction for a short time interval also an increased compliance. In animals with an obstruction for a long time this increase in compliance was less prominent or even absent, whereas bladder pressure still decreased. This proved the efficacy of removal of obstruction and showed that the level of functional changes severely affects the chances for regeneration of function. Correlation of structural analysis, again in particular the scoring of glycogen deposits, and functional analysis revealed that even after removal of obstruction, up to eleven weeks, the bladder glycogen content still reflects the level of functional changes during obstruction. The clinical value of this would be that the outcomes of a glycogen analysis performed even some time after (surgical) removal of obstruction, could still be used for a prognosis of regeneration of function for each patient. This is particularly relevant in newborns with urethral valves where the first urodynamic evaluation is often performed after the valves have been removed.

Medical intervention has been successful in managing bladder overactivity. Oxybutynin and Tolterodine are two well-known examples of clinically applied antimuscarinic drugs that suppress detrusor overactivity and abnormally increased

bladder pressure during voiding. In our model this overactivity is characterized by unstable contractions.

In chapters 5 and 6 we have studied the possibilities of using medical intervention for maintaining good bladder function during partial outlet obstruction. The hypothesis was that keeping the pressure within the normal range would prevent structural damage. The animal model was well suited for applying medical intervention. The intervention was started when the obstructive damage was still developing. In contrast the intervention in patients is applied when bladder functional and structural changes have already occurred. However, the model does mimic the loss of bladder function that continues after birth in children with neurogenic bladder obstruction and enabled a realistic test of the prevention of further bladder deterioration in patients most effectively.

Chapter 5 describes the findings of intervention with oxybutynin. Oxybutynin syrup (Dridase) was given orally to obstructed animals in the same dosage as applied in the clinic. From the clinic it is known that under oxybutynin treatment the duration of voiding is extended whilst bladder pressure remains in the normal range and detrusor overactivity is limited. These events were also found in the data from our model. Bladder pressure and detrusor overactivity indeed were limited and compliance was preserved in the over-all group. However, an increase in flow rate instead of a longer duration of voiding was seen and bladder contractility was increased. In two animals the effectiveness of treatment with oxybutynin temporarily failed for unknown reasons. In these animals the bladder pressure was abnormally high and contractility was increased. After bladder structural analysis also an increase of glycogen storage, a marker for ischemic conditions (explained later on), was witnessed. We concluded that intervention with oxybutynin may have a protective effect on bladder function. However, beneath a normal appearance of function a highly contractile bladder may be developing when for some reason the effectiveness of Oxybutynin is temporarily lost. Caution must be taken during treatment as a high contractile bladder may develop irreversible damage very fast.

The results found in chapters 3 and 4 led to the decision of studying the effects of a medical intervention that aims at maintaining a good blood flow and at reducing the effects of ischemic damage. Therefore we studied the effect of treatment of obstructed animals with acetyl salicylic acid (aspirin). This substance has been well described to maintain blood flow and prevent ischemic damage by reducing the build-up of products from anaerobic metabolism such as prostanoids [5,6]. The findings described in chapter 6 reveal a surprising combination of a bladder pressure during voiding and contractility that were even higher than with obstruction alone, detrusor overactivity but a normal compliance. Most interesting was that this was not accompanied by a significant build-up in glycogen storage. The fact that the contractility was higher than with obstruction alone while the muscle mass was not increased, indicates that the bladder muscle worked more efficiently. Detrusor overactivity still occurred, which

indicates that there are still changes in blood flow causing acute reactions from the bladder nerves. The lack of glycogen build-up indicates that the intervention affects the ischemic cascade that takes place after a period of ischemia. Thus, the bladder could cope with obstruction while maintaining an intact structure. Aspirin seems to protect the bladder from high pressure induced ischemic damage. But as with treatment with Oxybutynin an overall protection of the bladder is not assured.

Structural and molecular changes

It is widely believed that overstretching of the bladder wall triggers the onset of a whole cascade of molecular changes [7]. The reasoning behind this is that the bladder wall is stretched more as pressure increases abnormally due to outlet obstruction. Various authors have used a tissue model, either muscle strips isolated from whole bladder or cell cultures on stretchable carriers, and found a whole range of molecular changes upon stretching [8,9]. A problem with these methods is that they cannot explain how the detrusor layer can produce the extra force that is needed to overcome the resistance. Muscles work less efficient when overstretched. In chapter 7 we therefore postulated that the onset of molecular changes is not necessarily triggered by stretching but by compression of the tissue due to high pressure, in particular the urothelium. This issue is outside the scope of this thesis but would be an interesting area for further research. Either way, an already accepted view is that as a result of this cascade of molecular changes collagen infiltration within muscle fibers occurs. We followed this process during obstruction with Raman spectroscopic mapping analysis of bladder wall tissue (chapter 9). We observed that collagen infiltration was found within muscle fibers. This was shown both by the Raman maps and by elastic Von Gieson staining that was performed on the measured tissues to provide an independent second measure. The added value of the Raman mapping was clear from the discovery of clusters that contained a high number of glycogen deposits. This finding prompted us to further investigate the occurrence of glycogen deposits and of the ischemia that is thought to cause this deposition in the literature. Chapters 3 to 7 all show the direct correlation between glycogen deposition and the degree of functional changes.

Raman maps to study the molecular content of bladder tissue in detail were also applied in another field of urological pathology: bladder cancer. In chapter 10 results of analysis of non-tumor and tumor bladder tissues are presented. Clusters of spectra of non-tumor and tumor classified tissue areas were subjected to molecular analysis using fit procedures with reference spectra of compounds that were either related to tumor bladder tissues, such as various fatty acids, or non-tumor bladder tissues such as collagen. Also a prediction model algorithm was successfully developed. This revealed that spectra from non-tumor tissue contained more collagen while tumor

tissue was characterized by a higher nucleic acid, protein, glycogen and overall lipid content. This exciting approach is also taken by another research group [10,11]. The spectral processing procedures and algorithms used in this study may be used for future analysis of bladder obstruction using Raman spectroscopy.

Ischemia and glycogen scoring

New insights in the metabolism of glycogen under anaerobic conditions of the bladder have been published [12,13]. A clear link was found between the occurrence of (induced) ischemic conditions or hypoxia and an acute decline in glycogen content, emphasizing that the glycogen metabolism pathway, although originally described for skeletal muscle, is the main energy supplier in anaerobic conditions of the bladder too [14]. Upon chronic depletion caused by frequent voiding, a large number of glycogen deposits in the form of granules are stored in muscle cells. In most studies glycogen content was determined by biochemical analysis of solubilised tissue. We have scored the content of glycogen granules in periodic acid Schiff's stained tissue slides. Thus both the location and the number of glycogen granules in the detrusor layer were displayed. We concluded that ischemic conditions started to appear at the serosal side – with blood supply from most peripheral arteries – of the bladder and progressively accumulated over the whole detrusor layer as bladder function further deteriorated (chapter 3). As described above earlier medical intervention had a large effect on prevention of ischemic conditions. In chapter 7 the findings from chapters 5 and 6 were re-evaluated and it was found that compliance and detrusor overactivity correlated best with ischemic conditions. However, it is widely believed that ischemia is caused by either longer voiding or abnormally high increased pressure during voiding. The conclusion of chapter 7 is that the onset and progression of ischemia in the bladder wall is mostly related to the bladder condition between voidings.

The correlation of glycogen scoring to the whole course of bladder functional changes during obstruction, even after periods of de-obstruction was remarkable. Unpublished preliminary data of glycogen scoring in tissue from patients with bladder functional changes upon neurogenic disorders (spina bifida) showed a significant increase compared to tissue from patients without functional changes. However, comparison of glycogen scores to a time course of functional changes in patients is not possible, since in most cases only single point measurements are available and no comparison can be made to former functional changes.

Conclusion

With regard to the aims of this thesis, it can be concluded that after study of the bladder – subjected to partial outlet obstruction – with both functional and structural analysis a relationship was found between the severity of ischemic periods and the level of functional changes. This relationship is the basis of gaining insight in the course of functional changes by measuring the severity of ischemic conditions, determined by scoring the amount of granular glycogen deposits in the detrusor layer. Furthermore, a correlation was found between the occurrence of ischemia and changes in bladder compliance and detrusor overactivity. Histochemistry was a key factor in the glycogen scoring but also revealed collagen infiltration within muscle fibers.

Raman spectroscopic mapping was very successfully used to determine these structural changes in tissue sections in a non-destructive manner and it initiated the study for the scoring of glycogen granules related to bladder function. Additionally, bladder tumor and non-tumor tissue areas were successfully discriminated with Raman mapping. Spectral analysis revealed the compositional basis for this.

Inspiration for much research, including the work in this thesis, was derived from problems in diagnosis and treatment in the clinic. A very convincing new variable in diagnosing bladder functional changes, glycogen scoring, was found. The techniques used and findings presented in this thesis are the basis for further research in order to develop the scoring of glycogen deposits as a measure for historic bladder function into a clinical application.

Prospects

Scoring of ischemia induced glycogen accumulation comprised a major part of this thesis after the value of this was fully recognized. Further study therefore needs to aim at refinement of glycogen scoring and translation of this to non-destructive *in vivo* analysis using fiber optic Raman spectroscopy. To apply Raman spectroscopy for the *in vivo* detection of bladder structural changes, and in particular the accumulation of glycogen, in the clinic, fiber optic probes must be used that can enter the bladder through a working channel of a cystoscope. For this ultimate goal some critical aspects must be resolved. One of these aspects is the maximum depth range of the fiber optic probes in which structural changes inside the bladder wall can still be detected by Raman spectroscopy. It may also be of use to develop fibers that have a specific range of depth, which may be used to detect structural changes only in a specific layer such as glycogen in the muscle layer.

Contemporaneously, studies with techniques that monitor the severity of the ischemia in real-time will also be included. The intention is to use differential pathlength

spectroscopy (DPS) [15,16]. With this technique blood saturation, blood volume and vessel diameter can be determined *in vivo* non-destructively in less than a second. *In vivo* pilot experiments on guinea pig bladders before and four weeks after obstruction show encouraging results. DPS and *in vivo* Raman spectroscopy may simultaneously be applied to measure blood saturation as an acute indication for ischemia and glycogen accumulation that represents the course of development of the ischemia, e.g. present and past. For this approach significant developments in the fields of fiber optic probes and measurement equipment are needed. A grant proposal has been submitted for this purpose.

Ongoing and more specific applied (medical) intervention for prevention of ischemia will also be part of the scope for further research. Combined with the developments described above more insight may be gained for ultimately applying this approach as a clinical treatment.

References

1. Neuhaus J, Dorschner W, Mondry J, Stolzenburg JU. Comparative anatomy of the male guinea-pig and human lower urinary tract: histomorphology and three-dimensional reconstruction. *Anat Histol Embryol* **30**:185-192, 2001.
2. Wolffenbuttel KP, Kok DJ, Minekus JP, van Koevinge GA, van Mastrigt R, Nijman JM. Urodynamic follow-up of experimental urethral obstruction in individual guinea pigs. *Neurourol Urodyn* **20**:699-713, 2001.
3. Kok DJ, Wolffenbuttel KP, Minekus JP, van Mastrigt R, Nijman JM. Changes in bladder contractility and compliance due to urethral obstruction: a longitudinal followup of guinea pigs. *J Urol* **164**:1021-1024, 2000.
4. Peters CA, Carr MC, Lais A, Retik AB, Mandell J. The response of the fetal kidney to obstruction. *J Urol* **148**:503-509, 1992.
5. Cohen SM, Zenser TV, Murasaki G, Fukushima S, Mattammal MB, Rapp NS, Davis BB. Aspirin inhibition of N-[4-(5-nitro-2-furyl)-2-thiazolyl]formamide-induced lesions of the urinary bladder correlated with inhibition of metabolism by bladder prostaglandin endoperoxide synthetase. *Cancer Res* **41**:3355-3359, 1981.
6. Tsukimi Y, Mizuyachi K, Matsumoto H, Sato M, Ng B, Tajimi M. Mechanism of action by which aspirin alleviates detrusor hyperactivity in rats. *J Pharmacol Sci* **95**:101-107, 2004.
7. Mirone V, Imbimbo C, Longo N, Fusco F. The detrusor muscle: an innocent victim of bladder outlet obstruction. *Eur Urol* **51**:57-66, 2007.
8. Chaqour B, Yang R, Sha Q. Mechanical stretch modulates the promoter activity of the profibrotic factor CCN2 through increased actin polymerization and NF-kappaB activation. *J Biol Chem* **281**:20608-20622, 2006.
9. Adam RM, Eaton SH, Estrada C, Nimgaonkar A, Shih SC, Smith LE, Kohane IS, Bagli D, Freeman MR. Mechanical stretch is a highly selective regulator of gene expression in human bladder smooth muscle cells. *Physiol Genomics* **20**:36-44, 2004.
10. Crow P, Uff JS, Farmer JA, Wright MP, Stone N. The use of Raman spectroscopy to identify and characterize transitional cell carcinoma in vitro. *BJU Int* **93**:1232-1236, 2004.
11. Stone N, Hart Prieto MC, Crow P, Uff J, Ritchie AW. The use of Raman spectroscopy to provide an estimation of the gross biochemistry associated with urological pathologies. *Anal Bioanal Chem* **387**:1657-1668, 2007.

12. Uvelius B, Arner A. Metabolism of detrusor smooth muscle in normal and obstructed urinary bladder. *Adv Exp Med Biol* **385**:29-39, 1995.
13. Pessina F, Solito R, Maestrini D, Gerli R, Sgaragli G. Effect of anoxia-glucopenia and re-perfusion on intrinsic nerves of mammalian detrusor smooth muscle: importance of glucose metabolism. *Neurourol Urodyn* **24**:389-396, 2005.
14. DiMauro S, Tsujino S. Nonlysosomal glycogenesis. In: *Myology*, Engel A, Banker B (Eds), McGraw-Hill New York, 1994, p.1554.
15. Amelink A, Sterenborg HJ, Bard MP, Burgers SA. In vivo measurement of the local optical properties of tissue by use of differential path-length spectroscopy. *Opt Lett* **29**:1087-1089, 2004.
16. Bard MP, Amelink A, Hegt VN, Graveland WJ, Sterenborg HJ, Hoogsteden HC, Aerts JG. Measurement of hypoxia-related parameters in bronchial mucosa by use of optical spectroscopy. *Am J Respir Crit Care Med* **171**:1178-1184, 2005.

Summary

Samenvatting

Dankwoord

Curriculum Vitae

List of publications

Chapter

11

Summary

Congenital urethral valves and a dysfunctional sphincter after spina bifida are the two major causes for a partial urethral obstruction in children. Since urine has to be pushed through the obstruction with more force, the bladder has to work harder. This is accompanied by a number of complications such as the strengthening of the bladder, which makes it less compliant. Furthermore, the blood vessels in the bladder wall are (partially) compressed by the abnormally increased pressures during passive bladder filling. This leads to a deficiency in oxygen rich blood supply, also known as ischemia, which is needed for proper muscle function. Due to these processes the bladder has to work harder while the energy supply is decreased. When the cause of the obstruction is removed timely, the bladder can recover and no further consequences occur. However, when the development of bladder wall damage during obstruction progressed for a long time, a recovery of normal bladder function is no longer possible. Even when the obstruction is removed, the bladder is fighting against its own structural changes. The end-stage of this process is called a dripping bladder, or decompensated bladder. In these cases proper contraction of the bladder in order to secrete urine is no longer possible due to damage to the neurological system, severe ischemia and advanced infiltration of a collagen matrix inside the muscle fibres. Eventually the bladder becomes a stiff vesicle for urine storage with continuous high pressure. Urine is secreted by continuous leaking, known as incontinence. The abnormally increased bladder pressure also leads to reflux (a back-flow of urine to the kidneys). The kidneys can poorly withstand this phenomenon and soon after reflux has started kidney damage occurs.

Some of the consequences of an obstructed urethra, widened ureters and a large bladder volume, can already be diagnosed by prenatal ultrasound echography. Soon after birth intervention is performed to prevent proliferation of more damage. However, despite intervention as early as possible, bladder deterioration can still occur. Therefore monitoring of bladder function is essential. After removal of the obstruction bladder function is determined by doing urodynamic measurements several times to determine possible recovery, stagnation or deterioration of the bladder in time. However no insight in the bladder functional history before intervention is available. This makes it impossible to get a good prognosis for ongoing bladder development. At present the monitoring of function may express further deterioration of bladder function but a prognosis at initial intervention would enable better treatment of bladder recovery avoid the ongoing deterioration much sooner.

The aim of this study is to find a solution to get this insight in the development of bladder damage. We also want to gain new and better insights in the course of further bladder functional development during and after intervention. To do this, we have applied an animal model to conscientiously determine the exact course of bladder functional changes during an obstruction and relate this to bladder structure. This

thesis describes two main research lines: the first investigates the correlation between bladder function and bladder structure, paying particular attention to the role of ischemia. This has led to the discovery of the number of glycogen deposits as a marker for ischemic conditions. The number of glycogen deposits strongly correlates with the course of bladder function after partial obstruction. We have used an animal model that allowed us to simulate a partial obstruction of the urethra and monitor changes in bladder function over time. Bladder structure analysis was performed with multiple methods and the structure could be correlated to functional changes in individual animals. To apply determination of glycogen deposits in the clinic it is necessary to be able to perform this in patients in a non-destructive manner, thus without the need for biopsies. For this we studied the possibilities of Raman spectroscopy, which can be applied both *in vitro* and *in vivo*. This forms the second main study outline in this thesis. With *in vitro* Raman spectroscopy changes in bladder structure, including glycogen deposition, are measured without any pre-treatment of tissue. With fibre optic probes glycogen deposition could be measured on multiple locations inside the bladder using *in vivo* Raman spectroscopy. The technical development of these probes, however, is outside the scope of this thesis but remains a goal for future studies.

Chapter 1 is a general introduction in which normal bladder function, dysfunction, the principles behind urodynamic measurements and the animal model for partial outlet obstruction of the bladder are described. Subsequently the bladder structure and also the changes that occur after placement of a partial obstruction, in particular the deposition of glycogen granules are described. Also an explanation of the background and applications of Raman spectroscopy in bladder structure studies and related subjects is included. At the end of this chapter is the scope of this thesis.

In **chapter 2** the relationship between the course of bladder functional changes after partial bladder outlet obstruction and the level of glycogen granule deposition is described. For this the animal model was used. In each animal the glycogen content was scored by visual assessment of a Periodic acid Schiff's (PAS) stain of a histologic tissue slide. Changes in the urodynamic variables bladder pressure, contractility, compliance and detrusor overactivity were compared to the glycogen score in each animal. The glycogen score is a measure for the number of glycogen granules in which a score 0 stands for no glycogen, a score 1 for staining of only a small amount of granules, a score 2 for staining of glycogen throughout larger parts of the detrusor and a score 3 for glycogen throughout the whole detrusor layer. Since this scoring is subjective, three blinded co-workers performed it individually and the results were averaged. More grades in scoring would enhance the mutual variability, thereby making it less accurate. The glycogen content strongly correlated with the time course of functional changes. The more functional changes, the higher were the glycogen scores. With increasing glycogen score the location of granules also changed. A score 1 correlated with granules only apparent at the outer parts of the detrusor layer. A score

2 correlated with granules that emerged from the outer side towards larger part of the detrusor and a score 3 with granules throughout the whole detrusor, up to the lamina propria and urothelium.

Chapter 3 builds on the work presented in chapter 2, the same methodology was used to correlate function with glycogen scores but now with the addition of a period of de-obstruction. The results confirmed those of the previous chapter: even after recovery of bladder function the detrusor still contained glycogen granules and the scoring of content still reflected the course of functional changes during obstruction. This allowed for prognosis on the basis of the glycogen content in the detrusor.

Chapter 4 describes the application of anticholinergics to reduce or even inhibit the formation of bladder damage. Oxybutynin, a bladder overactivity inhibitor, was given orally to animals with a partial obstruction to study if it could inhibit both overactivity and abnormally high pressure during voiding. These variables together with compliance were comparable to values of control animals. However, contractility was increased, which may lead to an even faster rate of bladder deterioration when intervention with oxybutynin is stopped or failed. This happened in two animals in which for unspecified reasons intervention failed and all urodynamic variables showed a decrease in function. The glycogen score showed only a slight increase in all animals except for the two animals with intervention failure, with scores of 2 and 3 respectively.

In **chapter 5** the in vivo effect of acetylsalicylic acid (aspirin) was studied. Aspirin was also given orally to animals with a partial obstruction to study the inhibitory effect of aspirin on the formation of bladder damage. Bladder pressure during voiding and contractility highly increased compared to controls and even obstructed animals. Bladder overactivity was not suppressed but the compliance remained normal. The glycogen scores in all animals were not or barely increased compared to controls. Aspirin therefore does not protect against changes in bladder function after partial obstruction but prevents the formation of ischemic conditions. The bladder can compensate for the increased resistance without damage but it is again not completely protected against increased contractility and overactivity.

In **chapter 6** the results from chapters 2, 4 and 5 are combined to study the effect and the role of ischemia during partial obstruction in more detail. It became clear that ischemia is critically related to a decreased compliance and to a lesser extent to bladder overactivity. Very high pressures during voiding and increased contractility do not have a direct relationship with ischemia, as is clear from the results with aspirin intervention (to a lesser extent with oxybutynin) compared to only obstruction. Changes in function during bladder filling correlated best with ischemic conditions, rather than the functional changes during voiding.

From **chapter 7** onwards the second main research line, Raman spectroscopic mapping of bladder tissues, is described. With these maps a layout of tissue areas is created that have a similar structure and biochemical composition. The bladder wall

layers – urothelium, lamina propria and detrusor – could be mutually distinguished with Raman spectroscopic mapping. A Raman map is a selected area within a tissue section in which spectra are measured. This area is divided in small squares like a grid. In each square one spectrum is measured. By means of a cluster algorithm all spectra from a map measurement are compared to each other. A cluster is formed by spectra with a high level of similar spectral characteristics. The more clusters, the higher the level of similarity. In this work 4 clusters were used, similar to the three main bladder wall layers (serosa excluded) plus one cluster with background signal from only the slide (e.g. holes in the tissue). Then a color is assigned to each cluster, so that the spectra of one cluster are labelled with the same color. In this way a pattern of colors is created that is related to the clusters and therefore to the biochemical composition of the tissue. The measured tissue is histochemically stained after the map measurement. Then a photo image of this stain is compared to the pattern of clusters. The urothelium and the muscle layer were clearly distinguished as separate clusters. The lamina propria mainly consists of a collagen matrix. This matrix also appears in between muscle fibres and was clearly visible in the map. The averaged spectra of the lamina propria and detrusor correlated to spectra measured on pure collagen and actin respectively.

Chapter 8 is a continuation of chapter 7 in which Raman maps are measured on bladder tissue sections from controls and obstructed animals. Again the bladder wall layers could clearly be distinguished. Compared to controls the obstructed bladders showed an increase in collagen matrix within muscle fibres. A more surprising result was obtained by adding an extra cluster to the analysis. After comparison to spectra measured on pure components this cluster correlated with glycogen deposits. This finding actually led us to compare glycogen content with the level of changes in bladder function as described in previous chapters.

Chapter 9 describes how the unique principles of Raman spectroscopic mapping can be used to analyse other forms of bladder pathogenesis: bladder carcinomas. This study aimed at the discrimination between bladder tumor tissue and the surrounding 'healthy' tissue, better referred to as non-tumor tissue. Raman maps were measured on sections from biopsy material of human bladder tissue. After Raman mapping, the measured sections were histochemically stained. In accordance to the evaluation of a pathologist tissue areas in the section were classified as tumor or non-tumor and compared with the pattern of clusters in the maps. Tumor and non-tumor areas were always clustered separately. In total 25 maps from 15 different tissue sections were measured. The averaged spectra of all clusters of all maps were combined in one dataset. A linear discriminant analysis was performed on this dataset to develop criteria for a discrimination model based purely on spectral information of tumor and not-tumor tissue. Validation of these criteria was done by development of discrimination models with spectra of all tissues except those from one patient. The left-out spectra were then classified using this discrimination model. This approach

was repeated for all patients, so that spectral classification was performed 15 times with an overall classification result of 94% sensitivity and 92% specificity. Biochemical differences between tumor and non-tumor areas were characterized by comparison of spectra measured on pure components with the cluster averaged spectra from tumor and non-tumor areas separately. The latter were characterised by an increase in collagen content, tumor areas were characterised by a higher content of lipids, nucleic acids, proteins and glycogen.

The methodology and developed algorithms in this study, although not directly related to bladder obstruction studies, can be applied for further characterisation of structural changes in the bladder after obstruction and for future development of clinical applications.

Chapter 10 is a general discussion and contains the conclusions of this thesis and guidelines and recommendations for future research.

Samenvatting

Aangeboren urethrale kleppen en een dysfunctionele sfincter als gevolg van neurogene schade bij een spina bifida (open rug) zijn bij kinderen de twee grootste oorzaken van een partiële urethrale obstructie, ofwel een vernauwing van de plasbuis. Omdat urine met meer kracht door deze vernauwing moet worden geperst, zal de blaas harder moeten werken. Dit gaat echter gepaard met een aantal complicaties; de blaas versterkt zichzelf waardoor de blaaswand stugger wordt. Tevens worden bloedvaatjes in de blaaswand door de hogere drukken in de blaas al tijdens het passieve vulproces, al dan niet gedeeltelijk, dichtgeknepen. Hierdoor ontstaat een tekort aan zuurstofrijk bloed, ook wel ischemie genoemd, dat nodig is voor een goede spierfunctie. Door deze processen moet de blaas meer werk verrichten terwijl de energievoorziening juist steeds minder wordt. Als de oorzaak, de vernauwing, op tijd wordt opgeheven, kan de blaas weer herstellen en zijn er verder geen gevolgen. Echter, als de ontwikkeling van de blaasschade maar lang genoeg duurt, zal een terugkeer naar een normale blaasfunctie niet meer mogelijk zijn. Ook al wordt de vernauwing opgeheven, de blaas vecht nu een verloren strijd tegen zijn eigen structurele veranderingen. Het eindstadium van dit proces is wat men noemt een druppelblaas, of decompensatieblaas. Door schade aan het neurologisch systeem, ernstige ischemie en vergevorderde ingroei van collageen is het samentrekken van de blaasspiers om urine te kunnen uitdrijven dan niet meer mogelijk. Uiteindelijk is de blaas geworden tot een stugge opslagzak voor urine waarin continu een hoge druk heerst. Urine wordt alleen nog uitgescheiden door continu lekken; incontinentie is een feit. Vanwege de abnormaal hoge drukken in de blaas ontstaat ook reflux, terugstroom van urine naar de nieren. Deze zijn hier zeer slecht tegen bestand en al snel na het ontstaan van reflux treedt dan ook nierschade op.

Het gevolg van een vernauwing in de urethra, verwijde ureters en een groot blaasvolume, kan middels ultrasound echografie al prenataal worden gediagnosticeerd. Zo snel mogelijk na de geboorte kan vervolgens worden ingegrepen om ontwikkeling van verdere schade zo veel mogelijk te voorkomen. Echter, ook al wordt er zo vroeg mogelijk ingegrepen, een verdere verslechtering van de blaasfunctie kan nog steeds optreden. Monitoren van de blaasfunctie is dan ook essentieel. Na verwijdering van de vernauwing wordt nog enkele malen de blaasfunctie bepaald met urodynamische metingen om eventueel herstel, stagnatie of juist verslechtering van de blaas tijdig vast te stellen. Omdat urodynamische metingen slechts een moment opname zijn, wordt er geen duidelijk inzicht in het historisch verloop van schadevorming verkregen. Daardoor is een goede prognose van de verdere ontwikkeling niet mogelijk.

Dit proefschrift richt zich op het vinden en uitwerken van een mogelijkheid om inzicht te krijgen in de voorgeschiedenis van blaasschade en om een nieuw en beter inzicht te verkrijgen in het verloop van verdere ontwikkeling van de functie tijdens en

na interventie. Daarvoor hebben we het verloop van blaasschade achterhaald door in een proefdiermodel nauwgezet de blaasfunctie te volgen tijdens obstructie en deze te relateren aan de structuur. Het doel omvat twee hoofdlijnen: de eerste lijn betreft het correleren van de blaasfunctie aan de blaasstructuur met de rol van ischemie in het bijzonder. Dit heeft ertoe geleid dat we het glycogeengehalte in de spierlaag van de blaas als marker voor ischemie hebben gevonden. Het glycogeengehalte blijkt in hoge mate te correleren met het verloop van de blaasfunctie na een partiële obstructie. We hebben gebruik gemaakt van een diermodel waarin we een partiële obstructie van de urethra kunnen simuleren en in de tijd de veranderingen in blaasfunctie kunnen volgen. Ook werd de structuur van de blaas met verschillende methoden bestudeerd en konden we per individueel dier het tijdpad van functionele veranderingen correleren aan veranderingen in de structuur. Om het scoren van glycogeen ook klinisch te kunnen toepassen, is het noodzakelijk om dit op een niet-destructieve manier – dus zonder het bioteren van de blaas – in patiënten te kunnen doen. Daarvoor hebben we de mogelijkheden van Raman spectroscopie bestudeerd, welke zowel in vitro als in vivo kan worden toegepast. Dit vormt de tweede hoofdlijn in dit proefschrift. Met in vitro Raman spectroscopie zijn veranderingen in blaaswand structuur als gevolg van obstructie, onder andere in glycogeen depositie, zonder enige voorbereiding van weefsel gemeten. Alleen het invriezen van blaasweefsel en het snijden van vriescoupes waren noodzakelijk. Met in vivo Raman spectroscopie zou via fiber optische probes op meerdere plaatsen in de blaas het glycogeen gehalte kunnen worden gemeten. De technische ontwikkelingen voor deze probes vallen buiten dit proefschrift maar zijn wel een doel voor vervolgonderzoek.

Hoofdstuk 1 is een algemene inleiding waarin de normale functie van de blaas, dysfunctie, het principe en het gebruik van urodynamische metingen en het proefdiermodel voor partiële obstructie van de blaas uitgelegd. Vervolgens wordt de opbouw van de blaas en de veranderingen in functie en structuur die optreden als gevolg van partiële obstructie met in het bijzonder de stapeling van glycogeen granules. Ook is er een uitleg over de achtergronden en toepassingen van Raman spectroscopie in blaasstructuur onderzoek en aanverwante toepassingsgebieden toegevoegd. Aan het eind van dit hoofdstuk staat het doel van dit proefschrift.

In **hoofdstuk 2** is de relatie tussen het verloop van de blaasfunctie na een partiële obstructie en de mate van glycogeen granule ophoping in de detrusorlaag beschreven. Hierbij is gebruikt gemaakt van het proefdiermodel. Het glycogeengehalte van elk dier werd gescoord door visuele beoordeling van een Periodic Acid Schiff's (PAS) kleuring van een histologische coupe van het blaasweefsel. De veranderingen in de urodynamische variabelen blaasdruk, contractiliteit, compliantie en detrusor instabiliteit zijn per individueel dier vergeleken met de glycogeenscore. De glycogeenscore is een maat voor de hoeveelheid glycogeen granules waarbij een score 0 staat voor geen aanwezigheid van glycogeen, een score 1 voor kleuring van slechts

enkele glycogeen granules, een score 2 voor glycogeen in gedeeltes van de detrusor en een score 3 voor aanwezigheid van glycogeen in de gehele detrusor van de blaas. Omdat deze scoring subjectief is, werd deze door drie analisten afzonderlijk uitgevoerd en de resultaten gemiddeld. Meerdere gradaties in scores zou de onderlinge variabiliteit alleen maar verhogen en dus onnauwkeuriger maken. Het glycogeengehalte bleek een sterke relatie te hebben met het verloop van functionele veranderingen in de blaas tijdens partiële obstructie. Hoe groter de veranderingen, hoe hoger de glycogeenscore. Naarmate de glycogeenscore hoger werd, werd ook de locatie van de glycogeen granules anders. Een score 1 correleerde met glycogeen granules die alleen aan de buitenste rand van de detrusorlaag verschenen, een score twee correleerde met granules die vanaf de buitenste rand over een groter gedeelte waren verspreid. Pas bij een score 3 reikten de granules, die over de gehele detrusorlaag waren verspreid, tot aan de lamina propria en urotheellaag.

Hoofdstuk 3 is een vervolg op hoofdstuk 2, waarin met dezelfde methodes eveneens het verband tussen glycogeenstapeling en het verloop van blaasfunctie is aangetoond maar met als toegevoegde waarde dat bij deze meetserie een periode van de-obstructie werd toegepast. De resultaten kwamen sterk overeen met de resultaten uit het vorige hoofdstuk; ook na een tijd van herstel na verwijdering van de obstructie bevatte de detrusorlaag nog steeds glycogeen granules waarbij de scoring representatief was voor de mate van functionele veranderingen. Met name voor de kliniek heeft dit als waarde dat ook na het weghalen van de obstructie, nog steeds het historisch verloop van de blaasfunctie kan worden aangetoond waarmee een betere prognose voor verdere blaasfunctie ontwikkeling mogelijk is.

Hoofdstuk 4 beschrijft de toepassing van anticholinergica om de ontwikkeling van blaasschade te remmen, dan wel te voorkomen. Oxybutynine, een remmer voor blaas overactiviteit, is oraal toegediend aan dieren met een partiële obstructie om te bestuderen of hiermee de ontwikkeling van schade in de blaas kon worden geremd door het tegengaan van overactiviteit en het laag houden van de druk tijdens het plassen. Zowel de blaasdruk tijdens plassen, de compliantie en de blaas overactiviteit bij behandeling met oxybutinine tijdens partiële obstructie bleken vergelijkbaar te zijn met de blaasfunctie van controle dieren. Echter, de contractiliteit liet een verhoging zien, welke er toe kan leiden dat als de interventie wordt gestopt bij blijvende obstructie, de blaasfunctie juist sneller zal verslechteren. Dit bleek het geval bij twee dieren waarbij om onduidelijke redenen de interventie niet meer effectief was en waarbij alle urodynamische variabelen een verslechtering lieten zien. De glycogeen scoring was in alle dieren slechts licht verhoogd, behalve weer in de twee dieren met ineffectieve interventie met respectievelijk een glycogeen score van 2 en 3.

In **hoofdstuk 5** wordt het in vivo effect van acetylsalicylzuur (aspirine) onderzocht. Ook aspirine werd oraal toegediend aan dieren met een partiële obstructie, waarbij de remmende werking op de vorming van blaasschade bij partiële obstructie werd vervolgd. Bij aspirine stegen de druk tijdens het plassen en de contractiliteit sterk

vergeleken met controle en zelfs onbehandelde geobstrueerde dieren. De blaas overactiviteit werd niet onderdrukt maar de compliantie bleef normaal. De glycogeen scores van alle dieren bleken niet tot nauwelijks verhoogd te zijn vergeleken met controledieren. Aspirine behoedt de blaas dus niet voor veranderingen in blaasfunctie maar zorgt ervoor dat ischemische condities niet ontstaan. De blaas kan daardoor optimaal compenseren voor een vernauwing terwijl er geen schade optreedt, echter door blaasoveractiviteit en verhoogde contractiliteit is de beschermende rol van aspirine niet compleet.

In **hoofdstuk 6** worden de resultaten uit de hoofdstukken 2, 4 en 5 gecombineerd om dieper op het effect en de rol van ischemie tijdens partiële obstructie in te gaan. Zo is duidelijk geworden dat ischemie vooral verband houdt met een verslechterde compliantie (rekbaarheid van de blaas) en in mindere mate met overactiviteit. Zeer hoge drukken tijdens mictie en verhoogde contractiliteit blijken juist geen direct verband met ischemie te hebben. Dit blijkt uit de bevindingen met aspirine (en in mindere mate met oxybutynine) interventie, vergeleken met de gevolgen van alleen obstructie. Dus niet zozeer functionele veranderingen tijdens plassen maar juist tijdens de vulfase blijken sterk te correleren met ischemische condities.

Vanaf **hoofdstuk 7** wordt de tweede onderzoekslijn, Raman spectroscopische map metingen van blaasweefsel, beschreven. Dit hoofdstuk is de aanzet waarbij gekeken is of met Raman spectroscopische maps de verschillende blaaswand lagen – urotheel, lamina propria en spierweefsel – van elkaar konden worden onderscheiden. Een Raman map is een geselecteerd gebied in een vriesweefsel coupe waarin spectra worden gemeten. Dit gebied wordt als een rooster ingedeeld in kleine vierkantjes, waarin steeds één spectrum wordt gemeten. Door middel van een cluster algoritme worden alle spectra van een map met elkaar vergeleken. Elk cluster wordt gevormd door spectra met onderling sterk vergelijkbare spectrale eigenschappen. Hoe meer clusters, hoe hoger de graad van gelijkenis van spectra in een cluster. In dit werk is ervoor gekozen om vier clusters toe te passen, gelijk aan het aantal lagen (serosa niet meegerekend) in de blaaswand plus één cluster met alleen achtergrond (gaten in weefsel e.d.). Vervolgens wordt aan elk cluster een kleur toegekend. Zo ontstaat een patroon van kleuren, gerelateerd aan de clusters en dus aan de samenstelling van het weefsel. Het weefsel dat gemeten is wordt achteraf histochemisch gekleurd. Een foto van de gekleurde coupe wordt vergeleken met dit patroon. Het urotheel en de spierlaag waren duidelijk als afzonderlijke clusters te zien. De lamina propria bestaat voornamelijk uit een collageen matrix. Deze matrix komt ook voor tussen de spierbundels. Ook dit was duidelijk te onderscheiden. De gemiddelde spectra van de lamina propria en de spierlaag kwamen sterk overeen met spectra gemeten op pure collageen en actine, een hoofdcomponent van spierweefsel.

Hoofdstuk 8 is een vervolg op het voorgaande, waarbij Raman maps zijn gemeten in blaasweefsel coupes van niet-geobstrueerde en geobstrueerde dieren. Ook nu werden de lagen van de blaas afzonderlijk geclusterd. Een duidelijke toename van collageen

in de spierbundels was te zien. Een verrassend resultaat werd verkregen door het toekennen van een extra cluster in de analyse. Na vergelijking van de spectra in dit cluster met spectra van pure stoffen bleek dit cluster te correleren met glycogeen ophopingen. Deze vondst was de aanzet voor de vergelijking van het gehalte aan glycogeen met de veranderingen in blaasfunctie, zoals in de voorgaande hoofdstukken is beschreven.

Hoofdstuk 9 beschrijft hoe de unieke eigenschappen van Raman spectroscopische maps gebruikt kunnen worden voor het bepalen van andere pathogene veranderingen in de blaas: blaastumoren. In deze studie is gekeken of met Raman spectroscopie blaastumorweefsel en het omliggende 'gezonde', beter gezegd het niet-tumor weefsel, kon worden onderscheiden. In ingevroren weefsels van humane blaas bipten werden Raman spectroscopische maps gemeten. Na de metingen werden de coupes histochemisch gekleurd. Aan de hand van de beoordeling van een patholoog werden tumor en niet-tumor gebieden gekarakteriseerd en vergeleken met de patronen van de clusters in de maps. Tumor en niet-tumor gebieden werden pertinent afzonderlijk geclusterd. In totaal werden 25 maps gemeten in 15 weefselcoupes. De gemiddelde spectra van alle clusters van alle maps werden bij elkaar gevoegd in één dataset waarop een lineaire discriminant analyse werd gedaan waarmee criteria werden ontwikkeld om op grond van spectrale informatie tumor en niet-tumor weefsel te onderscheiden. De criteria werden gevalideerd door een discriminant model te ontwikkelen op een dataset bestaande uit alle cluster gemiddelde spectra behalve de cluster gemiddelde spectra van één patient. De weggelaten spectra werden vervolgens met het discriminant model geclassificeerd. Deze aanpak werd herhaald voor alle patiënten, dus in totaal werd 15 keer een spectrale classificatie gedaan. Dit leverde een classificatie op met een sensitiviteit van 94% en een specificiteit van 92%. Biochemische verschillen tussen tumor en niet-tumor gebieden konden worden gekarakteriseerd door het vergelijken van spectra van pure componenten met de cluster gemiddelde spectra van alle maps. Niet-tumor weefsel wordt gekenmerkt door meer collageen en tumor weefsel wordt gekenmerkt door hogere concentraties van lipides, nucleïnezuuren, eiwitten en glycogeen.

De aanpak en de ontwikkelde methodes in deze, niet direct aan blaasobstructie gerelateerde, studie kunnen worden toegepast bij het verder karakteriseren van structurele veranderingen in de blaas na obstructie en voor de toekomstige ontwikkeling van klinische toepassingen.

Hoofdstuk 10 is de algemene discussie met daarin de conclusies van dit proefschrift en de richtlijnen en aanbevelingen voor verder onderzoek.

Dankwoord

Zo, veel van het werk wat ik de afgelopen 8 jaar heb uitgevoerd samengevat in één 'pdf' bestand. Afgedrukt in de vorm zoals deze nu op bladzijde 166 voor u ligt. Het eerste stukje tekst wat de meeste mensen als eerst zullen lezen – na de stellingen – is dit dankwoord dat op het allerlaatst nog aan dit proefschrift is toegevoegd. Maar anders dan alleen de medeauteurs van de artikelen laat dit stukje tekst zien hoeveel mensen er werkelijk al die 8 jaar in grote of kleine vorm, direct of indirect hebben bijgedragen aan de totstandkoming van dit proefschrift.

Dik Kok, aan jou de eer om als eerste te bedanken. Met zo'n naam ben je voorbestemd om in de urologie te gaan werken. Jij was het die met wat papierwerk voor m'n eerste voltijd contract langskwam en de magische woorden sprak: "Oh ja, ik heb je aangesteld als AIO, gaat je wel lukken". Ziehier, na een lange weg met meerdere korte, zeer korte en langere verlengingen is het me gelukt. Toen al had je er alle vertrouwen in en nu nog steeds. Je hebt me de vrijheid gegeven om, met vallen en opstaan, het reilen en zeilen binnen het onderzoekswereldje zelf te ontdekken. Regelmatig liep ik jouw kamer in voor een simpel vraagje of mededeling om vervolgens na lange discussies over een nieuw project of maatschappelijke perikelen weer weg te gaan. Ik hoop dat we ons werk op exact dezelfde lijn en wijze kunnen voortzetten.

Gerwin Puppels, de 'baas' van het Raman spectroscopie lab en wetenschapper pur sang. Geroemd om het gebruik van weinig woorden, berucht om de impact die ze soms kunnen hebben. Maar wel altijd bij het rechte eind. Naast de vrijheid bij Dik zijn jouw geduld in uitleg, inzicht in aanpak en oog voor verbetering in menig manuscript essentieel geweest om dat reilen en zeilen te ontdekken op de juiste manier. Ook heb ik al die jaren gebruik mogen maken van de in de loop der tijd sterk verbeterde faciliteiten in het lab. Van 5 man aan twee bureautjes in een betegeld hok zonder daglicht tot aan een eigen bureau in een statig pand met tapijt en marmeren trappen. Van Raman map metingen tot diep in de nacht met energie verbrassende lasers tot aan het geautomatiseerd multimaps meten op een RiverD HPRM opstelling. Ik zie uit naar een vervolg met een overstap naar *in vivo* Raman toepassingen in de urologie.

Ron van Mastrigt, het is me een genoegen dat ik een van jouw eerste promovendi mag zijn onder jouw aanstelling als professor en promotor. Dankzij mijn verblijf op het urodynamica lab de laatste jaren heb ik kennis kunnen maken met jou als opponent in plezierige en soms felle discussies over alles wat al dan niet lukraak als onderwerp voorbij kwam. Fascinerend is ook jouw analytisch vermogen op vrijwel elk gebied. En je onvermogen om afstand te doen van afgedankte spullen, vooral als er een stekker aan zit.

Tom, voor velen onmisbaar gebleken in hulp met (het opzetten van) metingen en de dataverwerking. Ik ben daar geen uitzondering op. Zonder jouw inbreng was het

Raman spectroscopisch werk in dit proefschrift niet van de grond gekomen. Kees, Peter, Rolf, Diana, Maarten, Jan-Willem, Gilbert, Senada, Luis, Annieke, Sweder, Gunilla en nog vele mensen die ik in de loop der tijd heb mogen ontmoeten in het lab: ook jullie hebben op een aantal vlakken in meer of mindere mate bijgedragen aan metingen, verwerking van data en hulp bij het schrijven van manuscripten. Maar jullie waren ook een inspiratie voor het steeds sneller verlopende 'lunch-in-je-gezicht-proppen', al dan niet gecombineerd met geweldige conversaties over de meest uiteenlopende onderwerpen, met in het bijzonder toch wel de caviaatjes. Dit alles overgoten met een heerlijke saus van schuine, goede en goede schuine humor.

Katja Wolffenbittel en Jeroen Scheepe, beiden kinderuroloog en uitmuntend cavia-chirurg. Het was geweldig om te zien hoe vakkundig de ingrepen werden uitgevoerd. Katja, dankzij jouw voorwerk heb ik op een rijdende trein kunnen stappen. Jeroen, met jou als projectleider voor de laatste 4 jaar hebben we deze trein rijdend gehouden. Dankzij dit proefdiermodel hebben we vrijwel alle studies, die in dit proefschrift staan beschreven, kunnen uitvoeren. Samen met Joop en Fred hebben jullie bijgedragen in de bespreking van ontwikkelingen en uitkomsten van de cavia-urodynamica.

Gedurende de jaren zijn er ook een aantal stagiaires aan de slag geweest, met name op de histologie. Net zoals ik bij de experimentele kinderurologie ben begonnen. Allen hebben zeer goed meegeholpen met de urodynamische metingen bij de cavia's of deze zelfs geheel zelfstandig uitgevoerd. Daarnaast hebben Joanneke en Tessa veel werk verricht met in situ hybridisatie. Brechtje, Bonnie en Marjolein hebben veel immuno's uitgevoerd en met Marloes en Petra heb ik het scoren van de PAS kleuringen opgezet. De mensen van de urodynamica ben ik allereerst veel dank verschuldigd voor de hulp bij het verdoven van de cavia's. Johan, Jan, Tim, Sandra en Els: iedere keer mocht ik jullie tijdens werkzaamheden storen en vragen om een helpende hand. Samen met jullie, Ron, John, Annemoon, Judith en anderen heb ik vele koffie, thee en lunch uurtjes kunnen vullen met gesprekken. Als was het maar over de sterkte van de koffie zelf. Een fijne groep om mee samen te werken en waarbij ik ook graag heb mogen meedenken en helpen bij jullie onderzoeken.

De mensen van de experimentele urologie waren talrijk, veel mensen zijn gekomen en/of vertrokken. Guido, Wytske, Ellen, Astrid, Robert, Delshad, Don, Corrina, Suzanne, Wilma, Sigrun, Natasja, Angelique, Rajesh, Charlie, Joke, Antoine, Flip, Rogier, Dennis en de vele mensen van voorgaande jaren, jullie hebben me in het JNl niet zo vaak gezien. Sommigen hebben nog meegemaakt dat ik mijn stage en afstudeerperiode van het HLO daar heb uitgevoerd. Maar ik ben jullie allen zeker dank verschuldigd voor de vele feedback die ik heb gekregen bij werkbesprekingen maar natuurlijk ook tijdens één op één gesprekken in of rond het lab. Ook hebben velen van jullie de stagiaires meegeholpen in hun werkzaamheden. En natuurlijk dank voor de keren dat ik 'geheel toevallig' kwam binnendruppelen als er weer eens een traktatie stond. Het scheelde weinig of ik had dit dankwoord al eerder en in een geheel andere samenstelling geschreven. Al voordat ik bij Dik in dienst kwam, was ik

één van de kandidaten voor een AIO plaats bij Carl. Tot mijn grote spijt heeft Carl deze promotie niet meer mogen meemaken. Requiescat in Pace.

Net zoals bij de experimentele urologie is vanuit de klinische urologie (Prof. Chris Bangma en collegae) ook vaak belangstelling getoond in mijn werk tijdens presentaties en gesprekken. Ook hier is de feedback juist vanuit de kliniek belangrijk gebleken in het verder ontwikkelen van bestaande en nieuwe projecten.

Naast de reeds bovengenoemde afdelingen wil ik ook graag de mensen van de afdelingen experimentele pathologie, klinische pathologie en het EDC hartelijk danken voor de keren dan ik van de faciliteiten en van de hulp gebruik heb mogen maken.

Naast de vele gesprekken en discussies op het werk, zijn er ook veel vrienden geweest die de verhalen over mijn werk hebben aangehoord. Sommigen zijn al eens op één of meerdere labs wezen rondkijken. De gefronste wenkbrauwen spraken boekdelen: niet de meest alledaagse werkomgeving maar dat maakt het werk juist zo boeiend. Hoewel jullie natuurlijk niet direct met mijn werkzaamheden hebben geholpen, zijn de momenten dat ik even uit de sleur werd getrokken veel meer waard dan jullie beseffen. Goede gesprekken, skate- fiets- en motortrips, etentjes, kroegavonden, feesten en 'velerlei avonturen' (al dan niet in willekeurige vorm gecombineerd) brachten de noodzakelijke afwisseling. Katja, ontzettend fijn dat je samen met mijn zus paranimf wil zijn.

Linda, zus en paranimf, als er iemand is die mijn humor en denkwijze kan begrijpen en aanvullen, dan ben jij het. Je avontuur in Berlijn is voor mij een voorbeeld voor 'niet zeuren: doen!'. Welke beslissing je ook neemt of wending die je doet; ik sta achter je.

The best for last: mijn ouders. Opgegroeid in een fijn nest en met de vrijheid om zoveel mogelijk zelf te ontdekken. Altijd achter mijn beslissingen gestaan en gesteund in materiële vorm maar zeker ook met geestelijke bagage en support. Paps en Mams, de simpele woordjes 'dank je wel' zijn ontoereikend maar laat het een synoniem zijn voor mijn volle waardering voor jullie en wat jullie voor mij betekenen.

Bas

Curriculum vitae

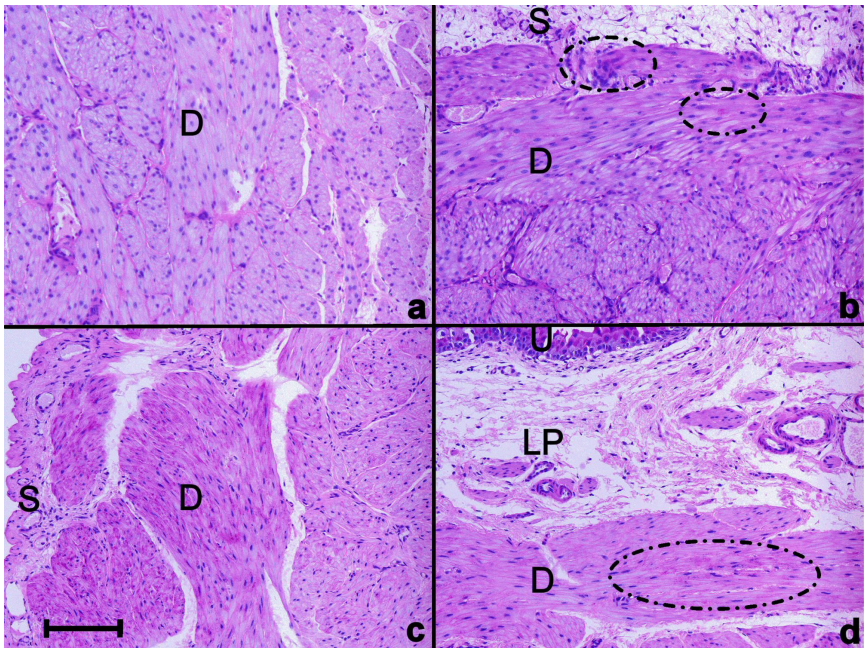
Bas de Jong is geboren te 's Hertogenbosch op 20 oktober 1975. In 1994 is hij geslaagd voor het HAVO diploma waarna hij aansluitend is begonnen aan de opleiding Medische Laboratoriumvaardigheden aan de Hogeschool Brabant, inmiddels Avans Hogescholen genoemd. In 1999 is deze opleiding succesvol afgerond met een afstudeerstudie op de afdeling Kinderurologie van de toenmalige faculteit geneeskunde van de Erasmus Universiteit Rotterdam onder begeleiding van Dr. Dirk Jan Kok. De afstudeerscriptie heeft als titel 'Veranderingen in nieren en blaaswand matrix bij partiële urethrale obstructies'. Na een rondreis van 2 maanden door Australië is hij na een zeer kort sollicitatiegesprek begonnen als analist bij dezelfde afdeling en begeleider. Al snel na de start van de aanstelling is na wederom een zeer kort gesprek besloten om de aanstelling van analist om te zetten in een AIO (nu OIO) functie. Het werk dat voor dit promotietraject is uitgevoerd, staat beschreven in dit proefschrift.

List of publications

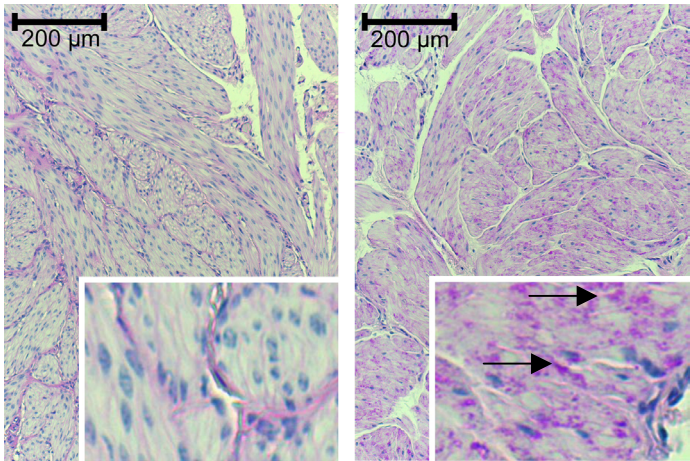
1. **De Jong BWD**, Bakker Schut TC, Wolffenbuttel KP, Nijman JM, Kok DJ, Puppels GJ. Identification of bladder wall layers by Raman spectroscopy. *J Urol* **168**:1771-1778, 2002.
This thesis
2. **de Jong BWD**, Bakker Schut TC, Coppens J, Wolffenbuttel KP, Kok DJ, Puppels GJ. Raman spectroscopic detection of changes in molecular composition of bladder muscle tissue caused by outlet obstruction. *Vibrational Spectroscopy* **32**:57-65, 2003.
This thesis
3. **de Jong BWD**, Brazao CAD, Stoop H, Wolffenbuttel KP, Oosterhuis JW, Puppels GJ, Weber RFA, Looijenga LHJ, Kok DJ. Raman Spectroscopic Analysis Identifies Testicular Microlithiasis as Intratubular Hydroxyapatite. *J Urol* **171**:92-96, 2004.
4. **de Jong BWD**, Bakker Schut TC, Maquelin K, van der Kwast TH, Bangma CH, Kok DJ, Puppels GJ. Discrimination between nontumor bladder tissue and tumor by Raman spectroscopy. *Anal Chem* **78**:7761-7769, 2006.
This thesis
5. **de Jong BWD**, Wolffenbuttel KP, Arentshorst ME, Lodder P, Kok DJ. Detrusor glycogen reflects the functional history of bladders with partial outlet obstruction. *BJU Int* **100**:846-852, 2007.
This thesis
6. **de Jong BWD**, Wolffenbuttel KP, Scheepe JR, Kok DJ. The detrusor glycogen content of a de-obstructed bladder reflects the functional history of that bladder during PBOO. *Neurourol Urodyn*, 2008, accepted for publication.
This thesis
7. **de Jong BWD**, Scheepe JR, Wolffenbuttel KP, Kok DJ. Ischemia in the bladder upon PBOO: the role of voiding pressure, contractility, detrusor overactivity and compliance. Submitted.
This thesis
8. Scheepe JR, **de Jong BWD**, Wolffenbuttel KP, Arentshorst ME, Lodder P, Kok DJ. The effect of Oxybutynin on structural changes of the obstructed guinea pig bladder. *J Urol* **178**:1807-1812, 2007.
This thesis
9. Kok DJ, **de Jong BWD**, Wolffenbuttel KP, Arentshorst ME, Lodder P, Scheepe JR. Prevention of obstruction induced bladder damage by Acetylsalicylic acid. Submitted.
This thesis

10. Wolffenbuttel KP, **de Jong BWD**, Scheepe JR, Kok DJ. Potential for recovery in bladder function after removing a urethral obstruction. *Neurourol Urodyn*, 2008, accepted for publication.
11. Kummeling MTM, **de Jong BWD**, Laffeber C, Kok DJ, Verhagen PCMS, van Leenders GJLH, van Schaik RHN, van Woerden CS, Verhulst A, Verkoelen CF. Tubular and interstitial nephrocalcinosis. *J Urol* **178**:1097-1103, 2007.
12. Koljenovic S, Bakker Schut TC, Wolthuis R, **de Jong BWD**, Santos L, Caspers PJ, Kros JM, Puppels GJ. Tissue characterization using high wave number Raman spectroscopy. *J Biomed Opt* **10**:031116, 2005.
13. Wolffenbuttel KP, Wondergem N, Hoefnagels JJS, Dieleman GC, Pel JJM, Passchier BTWD, **de Jong BWD**, van Dijk W, Kok DJ. Abnormal urine flow in boys with distal hypospadias before and after correction. *J Urol* **176**:1733-1736, 2006.

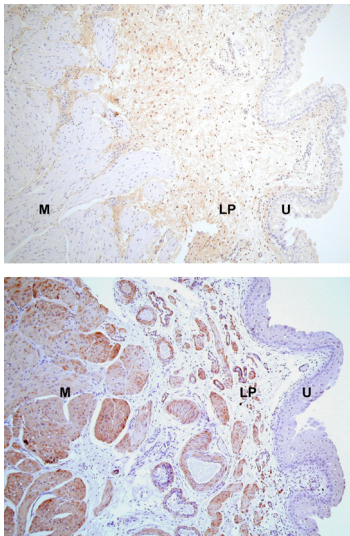
Appendix



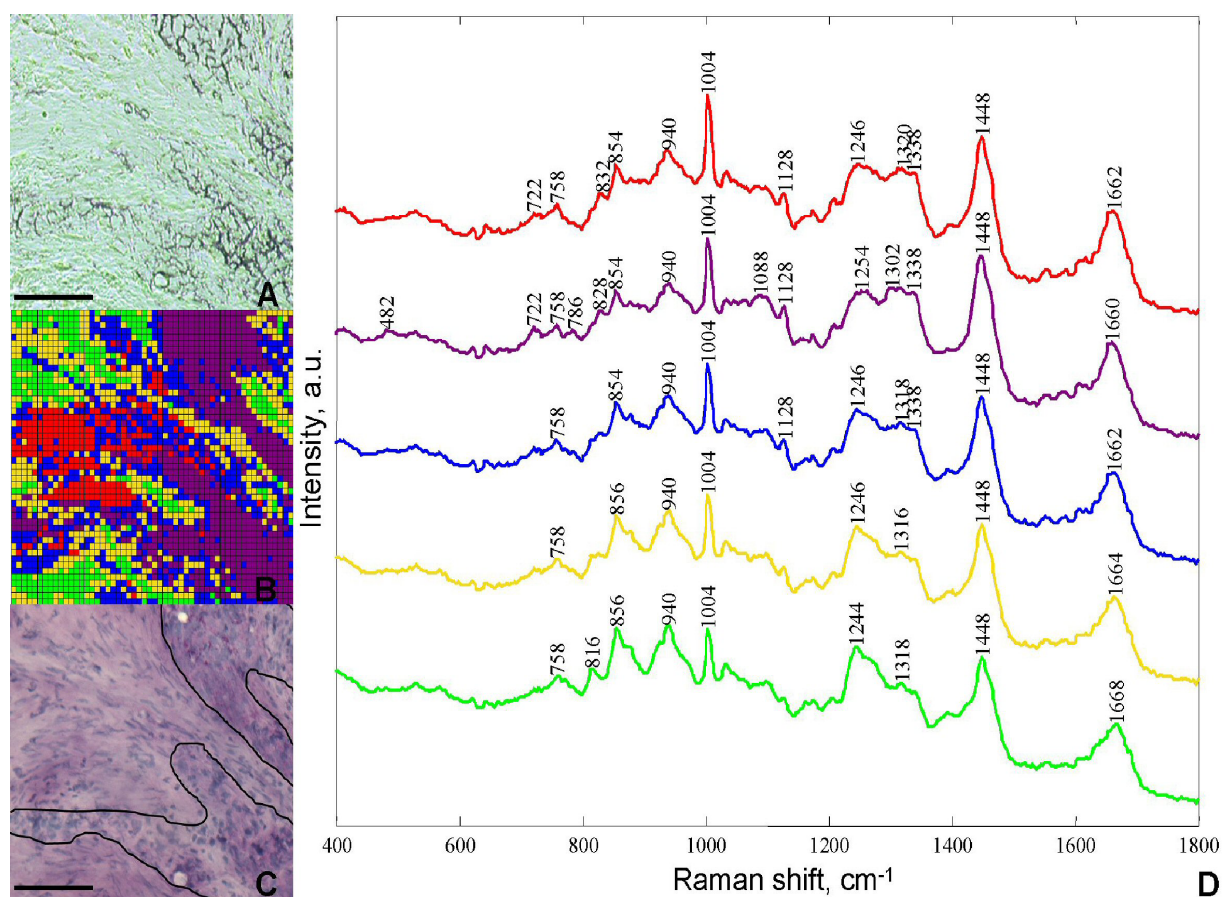
Chapter 2, figure 1
Examples of PAS stains with scores 0 (a), 1 (b), 2 (c) and 3 (d). D, detrusor layer; S, serosa; LP, lamina propria; and U, urothelium. Dotted circles show the small groups of glycogen granules. Bar = 200 μ m.



This figure is representative for:
Chapter 3, figure 1
Chapter 4, figure 2
Chapter 6, figure 1
Example of PAS stains of bladder detrusor layer with scores 0 and 3. Bar = 200 μ m. Inserts are 4x enlargements. Some glycogen granules are denoted with arrows.



Chapter 7, figure 5
Immunohistochemical staining of collagen (a) and smooth muscle actin (b) in bladder wall with diaminobenzidine tetrahydrochloride and Mayer's hematoxylin background staining. Collagen is mainly present in lamina propria (LP) and in smaller amount between muscle fibers (M). Actin is mainly present in the muscle layer and around blood vessels in the lamina propria. U, urothelium.



Chapter 9, figure 2

A: Unstained section of bladder tissue containing both non-tumor and tumor areas, 20 μm in thickness. Scalebar = 100 μm . B: Raman spectroscopic map, each grid element is 6,5 μm by 6,5 μm . Purple area is representative for tumor, red area for muscle tissue, green area for collagen fibers and blue and yellow are areas of transition between two types of tissue. C: Same section as A but HE stained after the measurements. Tissue areas are outlined. D: Averaged spectra of the clusters in B with matching colors, a.u.: arbitrary units.